

Al-Li合金の靱性に及ぼすNaおよびHの影響

(研究課題番号：60750706)

昭和60年度 科学研究費補助金〔奨励研究A〕

研究成果報告書

昭和61年3月

研究代表者 古川 稔
(福岡教育大学)

はしがき

リチウム(Li)は金属元素中もっとも比重が小さいので、Li添加によってAl合金の比重は著しく低下する。また、Al-Li合金においては $L1_2$ 型規則構造をもつ Al_3Li 粒子による析出硬化が期待されるので、現在、Liを含むAl合金は高比強度・高比弾性率を有する航空機用構造材料として、国内外で大きな注目を浴びている。しかし、Al-Li合金は低靱性の欠点を持っており、このことが本系合金の実用化に対する大きな妨げとなっている。低靱性の原因としては、整合な $L1_2$ 型規則析出物を含む合金に特有なすべりの集中と、結晶粒界およびその近傍の脆化などが考えられている。

これまでに著者らは、Al-Li 2元合金の時効組織と室温強度の関係を詳細に調べ、球状規則粒子による硬化理論との対比を行った。さらに、低温(77K)から析出粒子(Al_3Li)が準安定に存在する上限温度付近(523K)までの強度と変形特性を、時効組織や転位組織との関連において明らかにした。

Liを含む多元合金においては言うまでもなく、基本となるAl-Li 2元合金においてもHやNaの靱性に及ぼす影響については不明な点が多い。

本研究では、最初にAl-Li系合金に水素を強制添加することによって、機械的特性、引張破断後の破面および組織にどのような影響があらわれるかを明らかにし、靱性低下を生じる原因を究明する。つぎに、Al-Li 2元合金の強度・靱性に及ぼす溶解雰囲気の影響を明らかにする。

本研究の成果は、新しい高比強度・高比弾性率金属材料開発のための不可欠の基礎資料となることが期待される。

研究組織

研究代表者： 古 川 稔 (福岡教育大学教育学部 助教授)

研究経費

昭和60年度 900千円

研究発表

(1) 学会誌等

M. Furukawa, Y. Miura and M. Nemoto

Arrangement of Deformation Induced Dislocations in Aged Al-Li Alloys

Trans. Japan Inst. Metals, Vol. 26, No. 4, 1985

M. Furukawa, Y. Miura and M. Nemoto

Strengthening Mechanisms in Al-Li Alloys Containing Coherent Ordered Particles

Trans. Japan Inst. Metals, Vol. 26, No. 4, 1985

M. Furukawa, Y. Miura and M. Nemoto

The Effect of Temperature on the Yield Stress of Al-Li Alloy

Trans. Japan Inst. Metals, Vol. 26, No. 6, 1985

K. Yusu, H. Ueda, A. Matsui, M. Furukawa, Y. Miura and M. Nemoto

The Temperature and Orientation Dependence of the Yield Stress of Al-Li Single Crystals

Annual Reports, HVEM LAB., Kyushu Univ., No. 9, 1985

古川 稔, 美浦康宏, 根本 実

δ' -L₁₂ 型規則相を含む Al-Li 2 元合金の降伏応力の歪速度依存性

日本金属学会誌 第49巻 7号, 1985年7月

植田洋史, 松井昭彦, 古川 稔, 美浦康宏, 根本 実

Al-Li 合金の熱処理中の脱 Li

日本金属学会誌 第49巻 7号, 1985年7月

古川 稔, 中村 誠, 美浦康宏, 根本 実

Al-Li 2元合金のヤング率の温度依存性

九州大学工学集報 第58巻 5号, 1985年11月

Y. Miura, A. Matsui, M. Furukawa and M. Nemoto

Plastic Deformation of *Al*-Li Single Crystals

Aluminum-Lithium Alloys III (投稿中)

M. Furukawa, Y. Miura and M. Nemoto

The Strain Rate Dependence of Yield Stress of an *Al*-Li Alloy

Containing δ' -L₁₂ Ordered Particles

Trans. Japan Inst. Metals, Vol. 27, No. 1, 1986

古川 稔, 美浦康宏, 根本 実

Al-Li合金の時効硬化に及ぼすリチウム含有量の影響

九州大学工学集報 (投稿中)

古川 稔, 美浦康宏, 根本 実

Al-Li合金の変形組織のリチウム含有量による変化

九州大学工学集報 (投稿中)

(2) 口頭発表

古川 稔, 美浦康宏, 根本 実

σ 析出相を含む Al-Li 合金の強度のひずみ速度依存性
日本金属学会春期大会 1985年 4月

植田洋史, 松井昭彦, 古川 稔, 美浦康宏, 根本 実

Al-Li 合金の溶体化処理中の Li 損失
軽金属学会春期大会 1985年 5月

松井昭彦, 古川 稔, 美浦康宏, 根本 実

Al-Li 合金単結晶の変形後の転位配列
軽金属学会春期大会 1985年 5月

Y. Miura, A. Matsui, M. Furukawa and M. Nemoto

Plastic Deformation of Al-Li Single Crystals
3rd International Aluminum-Lithium Conference July 1985

柚須圭一郎, 古川 稔, 美浦康宏, 根本 実

析出硬化型 Al-Li 合金単結晶の降伏応力の温度依存性
日本金属学会秋期大会 1985年 10月

研究成果

1. 機械的性質と破面に及ぼす強制水素添加の影響

Al-Li 系合金に水素を電解チャージし、機械的性質を調べ、引張破断後の破面および組織を観察した結果、以下のことが明らかとなった。

- (1) Al-2.78mass % Li 2 元合金, Al-2.6Li-1.2Cu-0.6Mg-0.1Zr 合金, および 7050 合金は、すべての時効状態において、水素を電解添加した場合に、強度は低下し、破断までの伸びも減少した。
- (2) 水素を添加しない場合の引張破断面は、未時効合金では粒内破壊であったものが、時効の進行と共に粒界破壊の傾向をとり、過時効合金では粒界破断面にディンプルが見られた。
- (3) 水素を添加した場合の破面の各時効段階での傾向は、水素を添加しない場合とほぼ同様であるが、大きな違いは粒界に微細なクラックが存在することである。

2. 2 元合金の機械的性質と破面に及ぼす溶解雰囲気の影響

Al-Li 2 元合金の強度・靱性に及ぼすアーク溶解雰囲気 (Ar ガス, Ar + H₂ ガス, Ar + 水素化 Li 添加) の影響を調べた結果、以下のことが明らかとなった。

- (1) 引張試験による破断伸びは、Ar ガス雰囲気 → Ar + H₂ ガス雰囲気 → Ar + 水素化 Li (LiH) の順に減少した。
- (2) 破断面は、Ar ガス雰囲気で溶解した合金では粒界ディンプルであったが、Ar + H₂ ガス雰囲気で溶解した合金には粒界ディンプル中に多数のポイドが見られた。水素化 Li を添加した場合には粒界でのポイドの数がさらに増加した。
- (3) 各雰囲気で溶解したすべての合金において、0.2% 耐力に差は見られなかったが、引張最大強度は水素添加により低下した。
- (4) 定量分析の結果、Al-Li 2 元合金の Li 含有量と H 含有量には正の相関関係が見られた。

さらに、学会誌、研究紀要等に発表した論文の別刷を以下に示し、研究成果とする。

Arrangement of Deformation Induced Dislocations in Aged Al-Li Alloys

By Minoru Furukawa*, Yasuhiro Miura** and Minoru Nemoto**

Deformation induced substructures of aged Al-Li alloys containing coherent δ' -Li₂ ordered particles have been studied by dark field transmission electron microscopy. Dislocations move in pairs when a fine scale precipitation of δ' occurs. The observed shape of dislocations and the separation distance between the dislocations in a pair strongly depend on the size and distribution of δ' . Particles with diameter less than 50 nm are sheared by moving dislocation pairs. Dislocations by-pass the larger particles leaving dislocation loops.

Planar arrangement of deformation induced dislocations, which is generally considered to be responsible for the poor ductility of the present alloys, has not been observed for any aging stage investigated in the alloy with a high Li content.

(Received October 11, 1984)

Keywords: aluminum-lithium alloys, ordered precipitates, precipitation hardening, mechanical properties, superlattice dislocations, transmission electron microscopy, Orowan mechanism

I. Introduction

Aluminum-lithium alloys are attractive especially for aerospace applications, because they offer interesting combinations of high specific strength and high specific modulus. The addition of lithium, however, generally results in decreased ductility. Attempts to improve the ductility of this alloy have been made by alloying, processing and thermo-mechanical treatments⁽¹⁾⁻⁽³⁾.

The precipitation process in Al-Li binary alloys has already been studied by many investigators⁽⁴⁾⁻⁽⁷⁾. Silcock⁽⁴⁾ concluded that the precipitation in Al-Li alloys was a two stage process; solid solution $\rightarrow \delta'$ (Al₃Li) $\rightarrow \delta$ (AlLi). The δ' phase is a quasi-equilibrium phase which is of Li₂ structure and perfectly coherent with the matrix. The δ phase is a coarse equilibrium phase with a B32-type (NaTi) structure.

It is believed that, on plastic deformation, coherent δ' -particles are sheared by moving dislocations leading to a planar dislocation distribution, which may be responsible for low ductility of this material. Transmission electron microscopy actually has revealed sheared

δ' -particles in the deformed alloy⁽⁸⁾⁽⁹⁾. Thus it appears that the strength and ductility of Al-Li alloys are closely related to the characteristic behavior of dislocations. However, only a few papers have been published that describe details of the mode of interactions between dislocations and precipitates. Recently Hosson *et al.*⁽¹⁰⁾ studied the dislocation motion in an Al-2.2 mass%Li (8.0 mol%Li) alloy for typical two aging stages using a pulsed nuclear magnetic resonance technique combined with a TEM technique and proved that the δ' -particles were shearable in the alloy aged for 3.6×10^3 s at 488 K but unsharable after aging for 4.14×10^5 s at 518 K.

The purpose of the present work is to investigate systematically the behavior of deformation induced dislocations in an aged Al-Li alloy with a higher Li content by transmission electron microscopy for the entire stage of aging.

II. Experimental Procedure

Aluminum alloys containing 7.2 and 11.1 mol%Li were prepared by melting Al (99.99%) and Li (99.8%) in an Ar atmosphere. The chemical analysis indicated that the Al-11.1 mol%Li (3.12 mass%Li) alloy, which was extensively investigated in the present work, contained 0.0073 mass%Fe, 0.029 mass%Si and 0.0045 mass%Mg. The alloy ingots were hot

* Faculty of Education, Fukuoka University of Education, Munakata 811-41, Japan.

** Faculty of Engineering, Kyushu University, Fukuoka 812, Japan.

and cold rolled to 3 mm thick strips and cut into compressive specimens of the size $3 \times 3 \times 4.7 \text{ mm}^3$. The specimens were solution treated at 823 K for $1.08 \times 10^4 \text{ s}$ in glass capsules filled with Ar, followed by quenching into iced water and aged at 473 K for various periods. The aged specimens were compression tested at room temperature with an Instron type machine at a nominal strain rate of $3.5 \times 10^{-4} \text{ s}^{-1}$. Slices were taken from the deformed specimens by a rotating wheel fine cutter, and thin foils for transmission electron microscopy (TEM) were prepared using a twin-jet electropolishing apparatus⁽¹¹⁾. The composition of the electrolyte was 20% HClO_4 and 80% $\text{C}_2\text{H}_5\text{OH}$. Microstructures and dislocation configurations were examined by dark field TEM using a JEM-1000D high voltage electron microscope.

III. Experimental Results and Discussion

1. Growth of δ' and age hardening

The yield stress $\sigma_{0.2}$ and the particle size of δ' of the Al-11.1 mol%Li alloy are plotted as a function of aging time at 473 K in Fig. 1. The stress $\sigma_{0.2}$ varies largely with aging time, indicating a strong dependence of $\sigma_{0.2}$ on particle size. A maximum is reached at 10^5 s and the alloy softens by further aging. Observations by TEM reveal fine δ' -particles distributed uniformly in the as-quenched Al-11.1 mol%Li alloy, in agreement with the previous results⁽⁶⁾⁽¹²⁾. The δ' -precipitates are of irregular shape in the as-quenched state and also in the early stage of aging. They tend to spheroidize as the aging proceeds. Noble *et al.*⁽⁵⁾ and Tamura *et al.*⁽¹²⁾ have reported that the coarsening of δ' obeys the Lifshits-Wagner theory⁽¹³⁾⁽¹⁴⁾. Equilibrium δ was observed in the Al-11.1 mol%Li alloy after aging at 548 K for durations longer than $6 \times 10^3 \text{ s}$.

2. Dislocations in deformed Al-Li alloy

It is difficult to observe both δ' and deformation induced dislocations in the same imaging condition. This is due to the fact that the difference in electron scattering efficiency between δ' and the matrix is small and that the

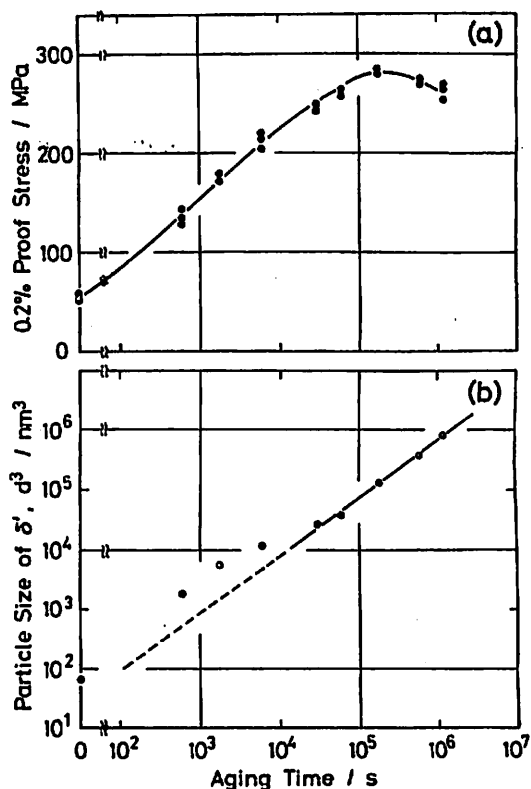


Fig. 1 0.2% proof stress (a) and δ' -particle size (b) vs aging time. Specimens (11.1 mol%Li alloys) were solution-treated at 823 K for $1.08 \times 10^4 \text{ s}$, quenched into iced water and aged at 473 K.

strain field around δ' is extremely small corresponding to the small lattice mismatch between δ' and the matrix. Therefore, δ' -particles were observed in a strong beam dark field image using a superlattice reflection, and the dislocations in the same area were observed in a weak beam dark field image using a matrix reflection. Relative positions of dislocation lines with respect to δ' were known by superimposing the former electron micrograph on the latter.

Figure 2 represents a selected area diffraction pattern, (a), and a 200 dark field image, (b), of a quenched alloy with a lower lithium content (7.8 mol%). Dislocations were introduced by the deformation of 4% in compression at room temperature. Precipitation of δ' is confirmed by referring to the selected area diffraction pattern (Fig. 2a), although the images of δ' were not observed in the micrograph. The 200 weak beam dark field image

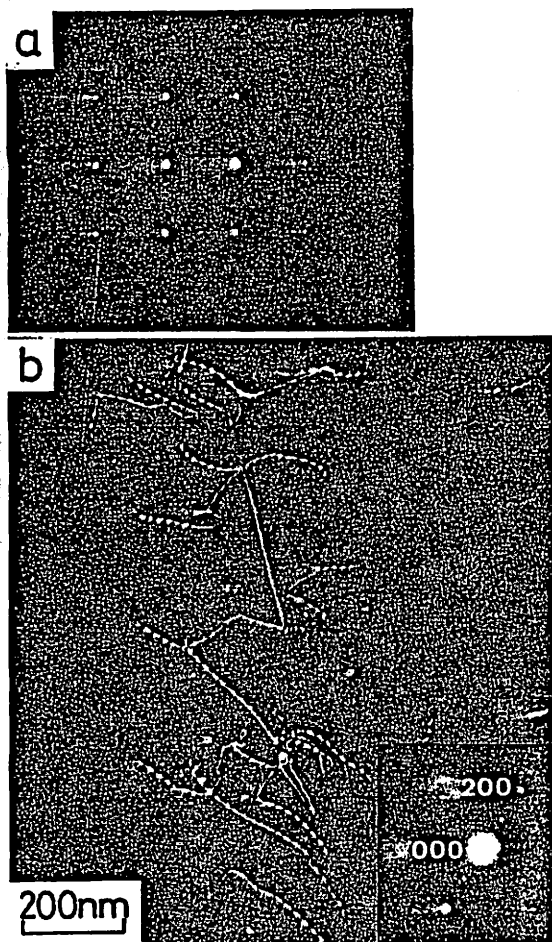


Fig. 2 100 net pattern (a) and 200 dark field image (b) of Al-7.2 mol%Li alloy deformed 4% in compression at room temperature after quenching from 823 K.

(Fig. 2b) shows that the plastic deformation in this alloy proceeds by the motion of single dislocations.

For the alloys with higher lithium contents fine dispersions of δ' were observed in the as-quenched state. Figure 3(a) and (b) show 200 and 100 dark field images taken of the same area of the foil prepared from the not aged Al-11.1 mol%Li alloy deformed 4% in compression. It is clear from the micrographs that the deformation induced dislocations are in pairs. They are rather straight and smooth in spite of the fine dispersion of δ' . The leading dislocation of a pair, moving through an ordered particle, destroys the order along the slip plane and thereby produces an anti-phase boundary (APB) behind it. The second dislocation

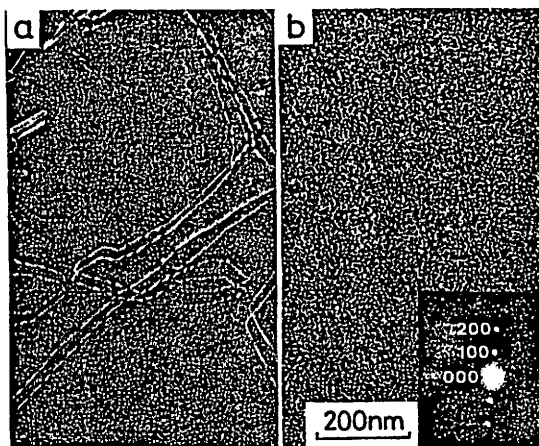


Fig. 3 200 (a) and 100 (b) dark field images of Al-11.1 mol%Li alloy deformed 4% in compression at room temperature after quenching.

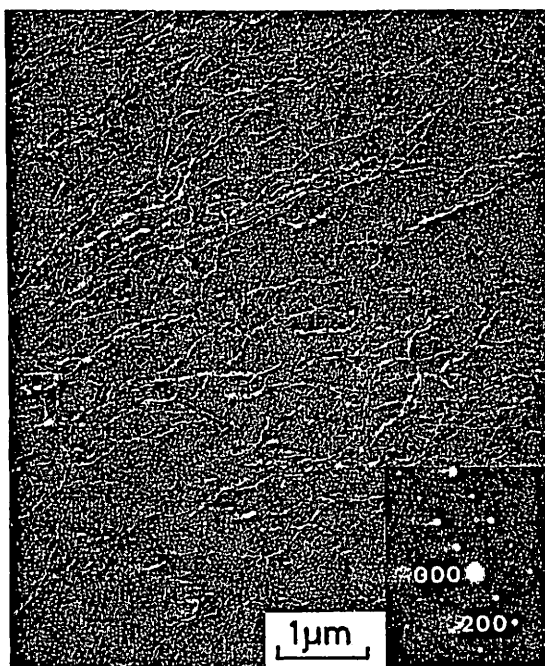


Fig. 4 200 dark field image of Al-11.1 mol%Li alloy aged at 473 K for 1.8×10^3 s and deformed 4% in compression at room temperature.

restores the order eliminating the APB. Paired dislocations have been already observed in deformed Ni-base superalloys⁽¹⁵⁾⁽¹⁶⁾ containing L_2 ordered particles.

Figure 4 shows deformation induced dislocations in an under-aged alloy. The dislocations are distributed uniformly. The following should be mentioned: Pile-ups of dislocations, which imply the occurrence of planar slip and

are considered to be responsible for the low ductility of Al-Li alloy, have been observed only in the as-quenched or under-aged alloys with a lower lithium content in the present study. In Fig. 5 a magnified view of the foil shown in Fig. 4 is represented together with the corresponding 100 dark field image of δ' . It is clear that δ' -particles grow larger on aging and dislocations forming pairs become wavy interacting with the particles. However, unit dislocations forming pairs have different radii of curvature from one another. The observed configuration of superlattice dislocations is strongly dependent on the size and distribution of δ' and analogous to that of dislocations in a Ni-Cr-Al alloy containing L_2 ordered precipitates observed by Gleiter and Hornbogen⁽¹⁵⁾⁽¹⁶⁾.

In the peak-aged alloy, dislocations bow out more vigorously than those in the under-aged alloy as shown in Fig. 6. Superposition of the two dark field images, (a) and (b), shows that the dislocations lie in the matrix avoiding δ' . The distance between the dislocations in a pair is one or two times as large as the particle size, and the distance varies with aging time. In Fig. 7 the distance is plotted against aging time. With the increase of aging time, D decreases first, attains a minimum value of 30 nm at 2×10^3 s and then increases. In the alloy aged for durations more than 2×10^3 s, D nearly equals the size of δ' .

Dislocation pairs, however, are no more

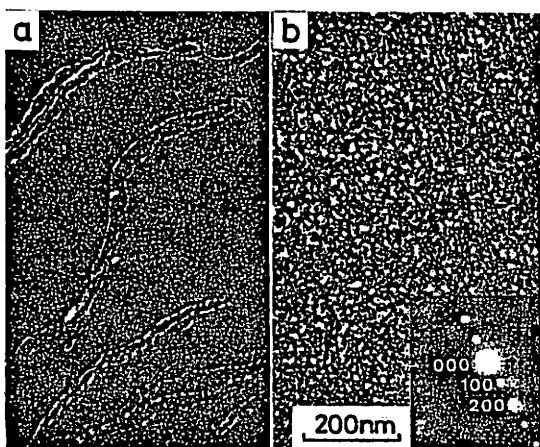


Fig. 5 200 (a) and 100 (b) dark field images of Al-11.1 mol%Li alloy deformed 4% in compression at room temperature after aging at 473 K for 1.8×10^3 s.

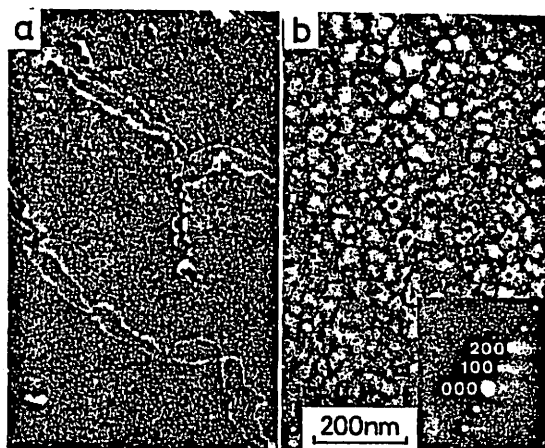


Fig. 6 200 (a) and 100 (b) dark field images of Al-11.1 mol%Li alloy deformed 4% in compression at room temperature after aging at 473 K for 6×10^4 s.

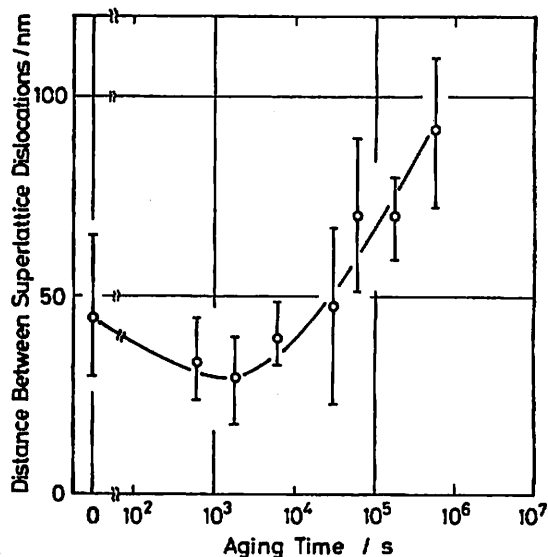


Fig. 7 Variation of distance between superlattice dislocations with aging time at 473 K in Al-11.1 mol%Li alloy deformed in compression at room temperature.

observed in the alloys aged for duration more than 10^6 s, as shown below. Figure 8 shows dark field images of over-aged alloy deformed 4% after aging at 473 K for 6×10^5 s. In Fig. 8(a) single dislocations bow out around spherical particles. Many dislocation loops are also observed. A 100 dark field image of the same area, (b), shows δ' -particles, although their images are not clear enough due to the overlap of them. A clear image of δ' taken of a thin area of the same foil is shown in (c), from which it is clear that the particles are spherical with an average diameter of 80 nm. It is ob-

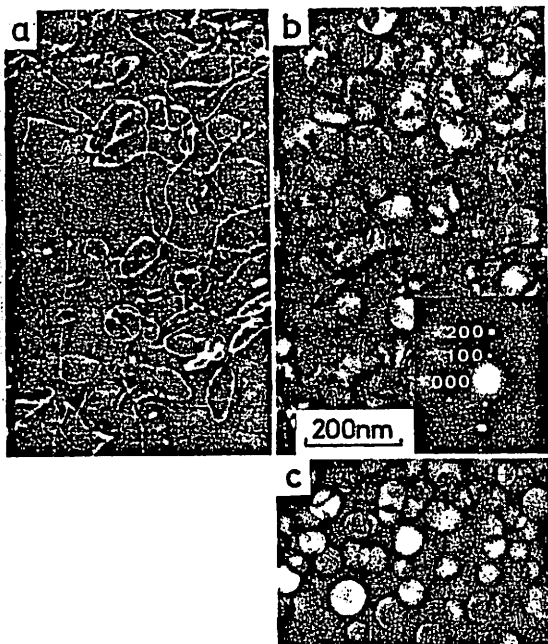


Fig. 8 200 (a) and 100 (b, c) dark field images of Al-11.1 mol%Li alloy deformed 4% in compression at room temperature after aging at 473 K for 6×10^5 s.

vious that the dislocations in the over-aged alloy by-pass the δ' -particles leaving dislocation loops by the Orowan mechanism⁽¹⁷⁾. The average diameter of δ' over which dislocations by-pass the particles is approximately 50 nm.

From the present observations, it is concluded that the Al-Li alloys softened not only by the precipitation of globular equilibrium δ , but also by the coarsening of metastable δ' .

IV. Summary

(1) Room temperature yield stress of the aged Al-11.1 mol%Li alloy increases with aging time in the initial stage of aging at 473 K, attains a maximum at 1.8×10^5 s and decreases by further aging. The diameter of δ' is about 50 nm in the peak-aged alloy which has the maximum 0.2% proof stress of 290 MPa.

(2) In the under-aged and peak-aged alloys, deformation induced dislocations move in pairs. The dislocations are rather straight in lightly aged alloys with very fine δ' , and they increasingly bow out between δ' -particles as the aging proceeds.

(3) In the over-aged alloys, dislocations

by-pass δ' leaving dislocation loops around them.

(4) Dislocations are uniformly distributed in deformed alloys examined except in the under-aged alloys with low Li contents. No indication of severely localized slip, such as dislocation pile-ups or sheared δ' -particles, was observed in the alloys with high Li contents. The formation of planar distribution of dislocations can not be the only reason for the low ductility of high Li content alloy.

Acknowledgments

The authors should like to thank Mr. A. Matsui for his experimental assistance. Thanks are also due to Technical Research Laboratories, Sumitomo Light Metal Industries, LTD., for preparing the Al-Li alloys. This research was supported partly by Grant-in-Aid for Scientific Research from the Ministry of Education, Science and Culture (58550473) and Grant-in Aid from the Light Metal Educational Foundation, Inc.

REFERENCES

- (1) T. H. Sanders, Jr. and E. A. Starke, Jr.: *Aluminum-Lithium Alloys*, Met. Soc. AIME, (1981).
- (2) E. A. Starke, Jr. and T. H. Sanders, Jr.: *Aluminum-Lithium Alloys II*, Met. Soc. AIME, (1984).
- (3) M. Furukawa, Y. Miura and M. Nemoto: *Bul. Japan Inst. Metals*, 23 (1984), 172.
- (4) J. M. Silcock: *J. Inst. Metals*, 88 (1959), 359.
- (5) B. Noble and G. E. Thompson: *Met. Sci. J.*, 5 (1971), 114.
- (6) D. B. Williams and J. W. Edington: *Met. Sci. J.*, 9 (1975), 529.
- (7) H. Suzuki, M. Kanno and N. Hayashi: *J. Japan Inst. Light Metals*, 31 (1981), 122.
- (8) T. H. Sanders, Jr. and E. A. Starke, Jr.: *Acta Met.*, 30 (1982), 927.
- (9) M. Tamura, T. Mori and T. Nakamura: *Trans. JIM*, 14 (1973), 355.
- (10) J. Th. M. De Hosson, A. Huis in't Veld, H. Tamler and O. Kanert: *Acta Met.*, 32 (1984), 1205.
- (11) T. Sano, R. Nishihara, H. Yotsumoto, Y. Miura and M. Nemoto: *Technology Reports of the Kyushu University*, 56 (1983), 491.
- (12) M. Tamura, T. Mori and T. Nakamura: *J. Japan Inst. Metals*, 34 (1970), 919 (in Japanese).
- (13) C. Wagner: *Z. Elektrochem.*, 65 (1961), 581.
- (14) I. M. Lifshitz and V. V. Slyozov: *Phys. Chem. Solids*, 19 (1961), 35.
- (15) H. Gleiter and E. Hornbogen: *Phys. Status Solidi*, 12 (1965), 251.
- (16) H. Gleiter and E. Hornbogen: *Mat. Sci. Eng.*, 2 (1968), 285.
- (17) E. Orowan: *Symposium on Internal Stresses in Metals*, Institute of Metals, London, (1948), p. 451.

Strengthening Mechanisms in Al-Li Alloys Containing Coherent Ordered Particles

By Minoru Furukawa*, Yasuhiro Miura** and Minoru Nemoto**

Strength of Al-Li alloys containing $L1_2$ ordered δ' -particles have been discussed on the basis of observed behavior of dislocations, taking into account various resistances to dislocation motion in the alloys. The measured yield strength and the observed arrangements of deformation induced dislocations are successfully explained in terms of the dislocation-particle interaction theories. Main contributions to the strength of the alloys come from the energy of antiphase boundaries and the friction stresses in the ordered particles and in the matrix.

(Received October 11, 1984)

Keywords: aluminum-lithium alloys, ordered precipitates, precipitation hardening, strengthening mechanism, superlattice dislocations, antiphase boundary, Orowan mechanism

I. Introduction

Strengthening mechanisms of crystals containing ordered particles have been theoretically studied by Gleiter and Hornbogen⁽¹⁾⁽²⁾, and Brown and Ham⁽³⁾⁽⁴⁾. As described in a previous paper⁽⁵⁾, extensive observations of deformation induced substructures of Al-Li alloys containing fine precipitates of coherent, metastable and $L1_2$ ordered δ' -phase have revealed that some of the dislocation configurations are quite similar to those proposed by the above mentioned authors. Dislocations move in pairs when a fine scale precipitation of δ' -particles occurs. They increasingly bow out between δ' -particles with growth of particles. Particles having diameters less than a critical size can be sheared by dislocation pairs. When the particles grow larger, dislocations by-pass the particles and over-age softening occurs.

Recently, Hosson *et al.*⁽⁶⁾ analysed the dislocation motion in an Al-8.0 mol%Li alloy and showed that the δ' -particles formed by aging at 488 K for 3.6×10^3 s are shearable but those formed by aging at 518 K for 4.14×10^5 s are unshearable. Their analysis, however, was only concerned with these two states of aging. The purpose of the present paper is to discuss

the strengthening mechanisms of Al-Li alloys containing fine dispersion of coherent ordered δ' -particles more quantitatively over the whole range of aging on the basis of the observed behavior of deformation induced dislocations.

II. Modes of Interaction between Dislocations and δ'

Figure 1 schematically summarizes the observed modes of interaction between deformation induced dislocations and δ' in an Al-11.1 mol%Li alloy which has been extensively investigated in the previous work⁽⁵⁾. The configuration of dislocations strongly depends on the volume fraction and the size of δ' . In the alloy under-aged or aged nearly to peak strength, dislocations move in pairs. The first dislocation destroys the order and forms antiphase boundaries (APB) in the δ' -particles. The second dislocation can remove the disorder created by the first. They are nearly straight when only very fine dispersion of δ' exists as shown in (a). The dislocations become wavy, as the particles grow as shown in (b) and (c). The wave length, the curvature of the bowed-out dislocations and the separation of dislocations in pairs obviously depend on the distribution of δ' . In the peak-aged state, the dislocations lie in the matrix keeping out of δ' , and the separation distance of the dislocations in pairs is one or two times as large as the particle size, as shown in (c). Particles having

* Faculty of Education, Fukuoka University of Education, Munakata 811-41, Japan.

** Faculty of Engineering, Kyushu University, Fukuoka 812, Japan.

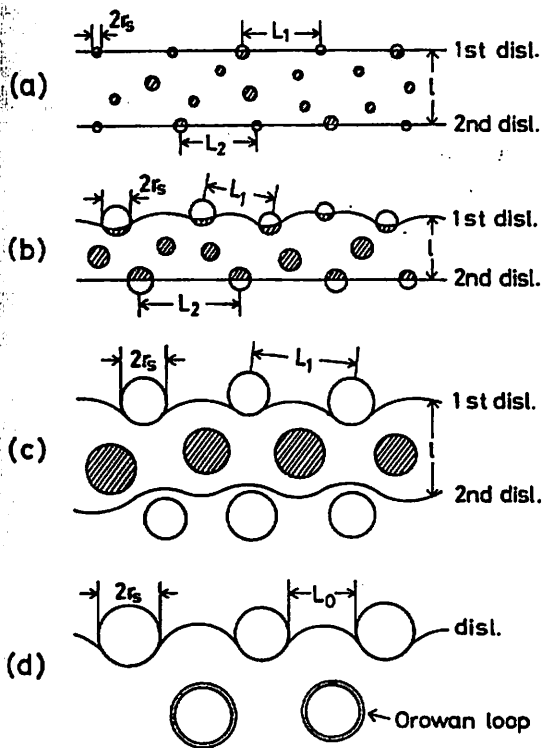


Fig. 1 Schematic representation of the interactions between dislocations and ordered precipitates. Shaded areas represent APB. (a) as-quenched, (b) under-aged, (c) peak-aged and (d) over-aged.

diameters less than about 50 nm can be sheared by dislocation pairs. When the particles grow larger, dislocations by-pass the particles leaving dislocation loops around them, as shown in (d), and the strength of the alloys starts to decrease.

On the basis of these observations, detailed discussion on the strengthening mechanisms in the Al-Li alloys will be made in the following sections taking into account various resistances to the dislocation movements in the alloys.

III. Resistances to the Motion of Dislocations

Some parts of the observed interactions between dislocations and δ' in the present work, for example the mode (c) of Fig. 1, are very similar to those proposed by Gleiter and Hornbogen⁽²⁾. However, the mode (c) in Fig. 1 can not be explained by their model, indicating that some factors other than the APB, only

which Gleiter and Hornbogen⁽¹⁾⁽²⁾, and Hosson *et al.*⁽⁶⁾ have taken into account, contribute as resistances against the motion of the dislocations. Therefore, in the following discussion, various factors will be taken into account.

The nature of a possible resistance to dislocations cutting through coherent ordered δ' -particles can be summarized as follows: (1) Friction stress of the matrix solid solution, τ_0 , (2) resistance due to lattice mismatch between the matrix and δ' , τ_e , (3) resistance due to the difference in shear modulus between the matrix and δ' , τ_{AG} , (4) resistance due to the energy of APB in δ' , γ_0 , (5) resistance due to the energy of the interface created between the cut δ' and the matrix, γ_i , and (6) friction stress in δ' , τ_p .

The first three, (1)-(3), are the resistances in the matrix and the rest, (4)-(6), are those in δ' . Hosson *et al.*⁽⁶⁾ took into account only the energy of APB in their analysis of strength of the Al-Li alloy. For the quantitative discussion of the strengthening mechanisms of Al-Li alloys, each resisting force shown above should be individually evaluated.

1. Friction stress against the dislocation movement in the matrix, τ_0

This stress can be estimated from the magnitude of solid solution hardening of this alloy. Specimens containing 1.6, 3.5, 7.2, 11.1, 15.3 and 21.3 mol% of Li were prepared in the same way as described in the previous paper⁽⁵⁾. Figure 2 shows the 0.2% proof stress $\sigma_{0.2}$ of the as-quenched alloys as a function of Li content. The straight line changes its slope at about 9 mol%Li, which indicates that the precipitation of δ' has occurred in the quenched alloys containing more than 9 mol% of Li as described in the preceding paper. The smaller slope in the region of lower Li content is due to solid solution hardening. Since the Li content of the matrix of the Al-11.1 mol%Li alloy aged at 473 K is about 6.5 mol%, as is known from the δ' -solvus⁽⁷⁾, τ_0 is estimated to be 13 MPa from this smaller slope using the Taylor factor of 2.5. The contribution from the change in Li content during aging is negligibly small.

2. Lattice mismatch of δ' /matrix, ϵ

Hardening due to misfit strain has been

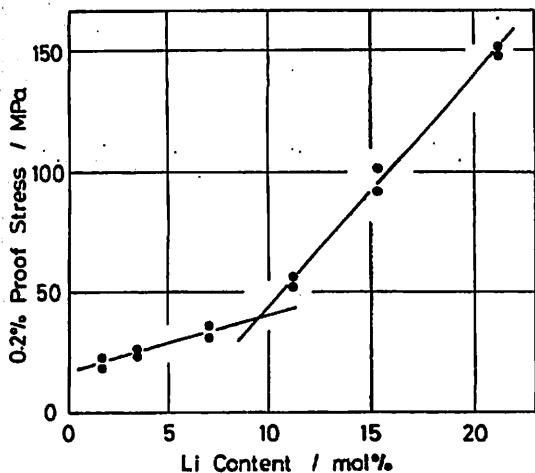


Fig. 2 Change in 0.2% proof stress ($\sigma_{0.2}$) of as-quenched alloys with Li content.

discussed in detail by Gerold and Harberkorn⁽⁸⁾. To estimate the magnitude of strengthening, the lattice mismatch ϵ between δ' and the matrix should be known. Since ϵ of δ' /matrix is small, an accurate measurement is extremely difficult and, therefore reported values⁽⁹⁾⁻⁽¹²⁾ for ϵ are widely scattered, ranging from 0.08 to 0.3%. The misfit strengthening estimated with the model by Gerold and Harberkorn using the most recently reported value of $\epsilon = -0.09\%$ ⁽¹²⁾ can explain only 5% of the strength of the aged Al-Li alloy studied.

3. Difference in shear modulus between δ' and matrix, ΔG

Since δ' is metastable, its shear modulus is not directly measurable. Noble *et al.*⁽¹³⁾ measured the Young's moduli of Al-Li solid solution and of Al-Li alloys containing δ' , and they estimated, using the rule of mixtures, the Young's modulus of δ' to be 96 GPa (corresponding shear modulus is 36.9 GPa). The shear modulus of the matrix (6.5 mol%Li) of the Al-11.1 mol%Li alloy aged at 473 K is estimated to be 30.2 GPa, from the extrapolation of the experimental data of Noble *et al.*

Brown and Ham⁽⁴⁾, and Weeks *et al.*⁽¹⁴⁾ discussed the strengthening due to the difference in shear modulus between the precipitate and the matrix. The value of $\tau_{\Delta G}$ obtained by applying their model to the Al-Li alloy can explain only about 5% of the total

strengthening, which is comparable with τ_c due to lattice mismatch as discussed in the preceding section.

4. APB energy of δ' , γ_0

The energy of APB, created by the slip of $a/2 \cdot \langle 110 \rangle$ dislocation on $\{hkl\}$ planes of a $L1_2$ -ordered phase, is given by Flinn⁽¹⁵⁾ as follows;

$$\gamma_0 = 2vhS^2/a\sqrt{h^2+k^2+l^2}, \quad (1)$$

where S is the degree of long range order, $v = kT_c$ (k is Boltzmann's constant and T_c is the critical temperature for order-disorder transformation) and a is the lattice parameter. Substituting $T_c = 548 \text{ K}$ ⁽⁵⁾⁽¹⁰⁾ for eq. (1), γ_0 of 53 mJ/m^2 is obtained, which is smaller than the value of 195 mJ/m^2 reported by Tamura *et al.*⁽¹¹⁾ The APB energy reported by them, however, seems to be somewhat overestimated, because it was simply assumed that the separation of a superlattice dislocation was governed only by the balance between the APB energy and the repulsive force of dislocations, neglecting all other contributions.

5. Energy of interface created between δ' and matrix, γ_1

The interfacial energy δ_i is indirectly estimated from the rate of Ostwald ripening of δ' . In the present work, γ_1 is estimated to be 190 mJ/m^2 , which well agrees with the reported value of 180⁽¹¹⁾, 240⁽⁹⁾ or 250⁽¹⁶⁾ mJ/m^2 .

6. Friction stress to the motion of dislocations in δ' , τ_p

As the δ' -phase is metastable and τ_p is not directly measurable of the single phase δ' , an alternative estimation of τ_p will be made later in this paper.

IV. Pair Dislocations Cutting δ' -Particles

For a pair of dislocations travelling under an applied shear stress τ , the forces must balance as follows:

(The first dislocation)

$$\tau b - \tau_0 b - \tau_c b - \tau_{\Delta G} b + \Phi G_m b^2 / 2\pi l - \gamma_0 (2r_s / L_1) - \gamma_1 (2b / L_1) - \tau_p b (2r_s / L_1) = 0. \quad (2)$$

(The second dislocation)

$$\begin{aligned} \tau b - \tau_0 b - \tau_e b - \tau_{\Delta G} b - \Phi G_m b^2 / 2\pi l + \gamma_0 (2r_s / L_2) \\ - \gamma_i (2b / L_2) - \tau_p b (2r_s / L_2) = 0. \end{aligned} \quad (3)$$

Here L_1 and L_2 are the particle spacings for the first and the second dislocation, respectively, b is the Burgers vector of $a/2 \cdot \langle 110 \rangle$ dislocation, r_s is the average radius of particles intersected by a slip plane ($=\sqrt{2/3} \cdot r_0$), r_0 is the average radius of particles, l is the separation between the two dislocations, G_m is the shear modulus of matrix, $\Phi G_m b^2 / 2\pi l$ is the repulsive force between the two dislocations, $\Phi = 1/2 \cdot \{1 + (1+\nu)^{-1}\}$ and ν is the Poisson's ratio. From eqs. (2) and (3) we obtain the shear stress necessary for a superlattice dislocation (a pair of $a/2 \cdot \langle 110 \rangle$ dislocations) to cut through the particles:

$$\begin{aligned} \tau = \tau_0 + \tau_e + \tau_{\Delta G} + (\gamma_0 / b)(r_s / L_1 - r_s / L_2) \\ + \gamma_i (1 / L_1 + 1 / L_2) + \tau_p (r_s / L_1 + r_s / L_2), \end{aligned} \quad (4)$$

where, τ_0 , τ_e , $\tau_{\Delta G}$ and γ_i are known as so far discussed. The values of L_1 , L_2 , l , r_s and r_0 in the equation can be determined from the transmission electron micrographs.

When the dispersion of δ' is very fine, both the first and the second dislocation are nearly straight, as shown in Fig. 1(a). In this case, $2r_s / L_1 = 2r_s / L_2 = f$, where f is the volume fraction of δ' . Equation (4), therefore, reduces to

$$\tau = \tau_0 + \tau_e + \tau_{\Delta G} + \gamma_i f / r_s + \tau_p f. \quad (5)$$

Substituting the value of $\sigma_{0.2}$ of as-quenched alloy for eq. (5) and the values of r_0 and f measured by TEM, we obtain the value of τ_p . For $f=0.03$ of the as-quenched alloy, τ_p is 130 MPa, which is appreciably higher than τ_e or $\tau_{\Delta G}$. Now, L_1 and L_2 are left unknown in eq. (4). The particle spacings L_1 and L_2 should depend on the interaction force between dislocations and δ' , and also on f and r_0 .

For the pair of dislocations in the under-aged alloy shown in Fig. 1(b), the effective particle spacing for the first dislocation can be approximated by the Friedel spacing⁽¹⁷⁾ $L_1 = (2TL^2 / \tau b)^{1/3}$, where L is the linear spacing between the particles and T is the line tension of dislocation. The fraction of dislocation line

cutting the particles, $A = 2r_s / L_1$, is given by⁽¹⁸⁾

$$A = 2r_s / L_1 = (4\gamma_0 f r_s / \pi T)^{1/2}. \quad (6)$$

The second dislocation in Fig. 1(b) is nearly straight, because the applied stress acts in the inverse direction to the repulsive force by the first dislocation. Thus, the stress necessary to cut through δ' in the under-aged alloy is given as follows:

$$\begin{aligned} \tau = \tau_0 + \tau_e + \tau_{\Delta G} + \gamma_0 (A - f) / 2b \\ + \gamma_i (A + f) / 2r_s + \tau_p (A + f) / 2. \end{aligned} \quad (7)$$

In the peak-aged alloy, the dislocation pairs lie in the matrix almost touching δ' , as shown in Fig. 1(c). In this case, the particle spacing for both the dislocations, L_1 and L_2 , can be approximated by the Friedel spacing. The applied stress for the dislocation pairs to move cutting through the particles is

$$\tau = \tau_0 + \tau_e + \tau_{\Delta G} + \gamma_0 A / 2b + \gamma_i A / 2r_s + \tau_p A / 2. \quad (8)$$

If the curvature of the bowed out dislocations is smaller than a critical value, the fraction of the dislocation line cutting the particles, $B = 2r_s / L_1$, is given by substituting T / γ_0 for r_s in eq. (6) as follows:

$$B = 2r_s / L_1 = (4f / \pi)^{1/2}. \quad (9)$$

Consequently the critical shear stress of the alloy is given by

$$\tau = \tau_0 + \tau_e + \tau_{\Delta G} + \gamma_0 B / 2b + \gamma_i B / 2r_s + \tau_p B / 2. \quad (10)$$

V. Dislocations By-passing δ'

In the over-aged alloys in which δ' -particles grow over a critical size, approximately 50 nm, dislocations do not move in pairs anymore, but they move as single dislocations by-passing the particles. The particle spacing for the by-passing dislocations can be taken as equal to the square lattice spacing L_0 . For $L_0 < 2r_s$, the following equation for the Orowan stress derived by Kelly and Nicholson⁽¹⁹⁾ can be applicable taking into account Forman-Makin's statistical factor⁽²⁰⁾,

$$\tau = \tau_0 + 0.85(G_m b / 2\pi L_0) \Phi \ln(L_0 / 2b). \quad (11)$$

For $L_0 > 2r_s$, the following equation presented by Ashby⁽²¹⁾ can be used.

$$\tau = \tau_0 + 0.85(G_m b / 2\pi L_0) \Phi \ln(r_s / 2b). \quad (12)$$

VI. Evaluation of Models

As described in the previous sections, a single model or a single theoretical equation can not explain the strengthening mechanisms in the whole range of aging stages of Al-Li alloy. On the basis of the TEM observations of the interactions of dislocations and δ' , we can apply eq. (5) to the very early stage of aging shown in Fig. 1(a), and eq. (7) to the under-aged state shown in Fig. 1(b). To the peak-aged state shown in Fig. 1(c), eqs. (8) and (10) can be applicable, and to the over-aged state eqs. (11) and (12).

The values of L_1 , L_2 , l , r_s and r_0 in these equations can be easily determined on the basis of the TEM observations. However, the measurement of f by TEM was difficult especially in the specimens aged to the intermediate stage because of the combined effects of the irregular shape and the overlapping of the images of δ' . The value of f was able to be obtained only for the as-quenched state and for the over-aged state where the δ' particles were observed separately in the micrographs. The measured values of f for as-quenched and over-aged states of Al-11.1 mol%Li alloy are 0.03 and 0.20, respectively. A good agreement is obtained between the measured value of 0.20 on the fully aged specimen and the estimated value of 0.22 from the solubility limit in the reported phase diagram⁽⁷⁾ of Al-Li alloy.

For the alloys containing precipitates already in the as-quenched state, the volume fraction f , being a function of aging time, can be expressed as⁽²²⁾

$$f = f_\infty [1 - (1 + B(t + t_0))^{-1/3}], \quad (13)$$

where $f_\infty = 0.22$ is the final volume fraction and $B = 2.2 \times 10^{-3} \text{ s}^{-1}$ and $t_0 = 2.52 \times 10^2 \text{ s}$ are constants. These constants, B and t_0 , are determined by solving eq. (13) applying the conditions, $f = 0.03$ for $t = 0 \text{ s}$ and $f = 0.20$ for $t = 6 \times 10^5 \text{ s}$. The solid line in Fig. 3 indicates the calculated values from eq. (13), and the dotted line shows the measurements by Tamura *et al.*⁽¹¹⁾ on an Al-9.5 mol%Li alloy with an X-ray method. The value of $f_\infty = 0.22$ used by Tamura *et al.*

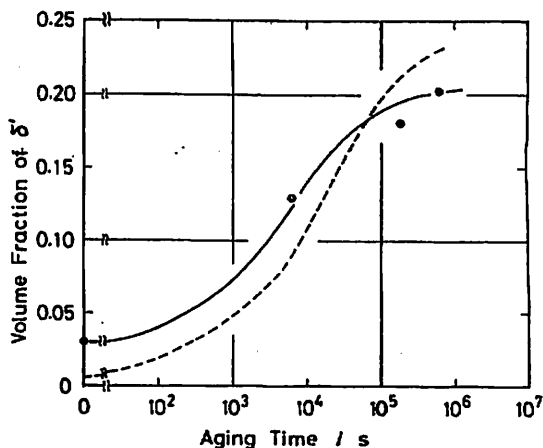


Fig. 3 Volume fraction vs aging time curve of δ' -precipitate in the Al-11.1 mol%Li alloy aged at 473 K. The dotted curve shows the experimental result of Tamura *et al.* for Al-9.5 mol%Li alloy.

for their alloy seems to be too large as compared with $f_\infty = 0.14$ which is estimated from the δ' solvus line of the equilibrium phase diagram recently reported⁽⁷⁾. The similarity between the two curves, however, suggests the validity of eq. (13) for describing the kinetics of precipitation in the Al-Li alloy. Therefore, the values of f for the intermediate stage of aging are estimated using eqs. (13).

Comparison between the strength of the Al-11.1 mol%Li alloy experimentally obtained (thick solid curve) and that estimated from eqs. (5), (7), (8), (10), (11) and (12) (thin solid curves) is shown in Fig. 4. Contributions of σ_0 , ε , ΔG , γ_i , γ_0 and σ_p are also included in the figure where the Taylor factor of 2.5 is used. It will be clear from Fig. 4 that the main contributions to the strength of the alloy come from the energy of APB and the friction stresses in the ordered particles and in the matrix. The contributions from the misfit strain, difference in the shear modulus and the energy of a new interface created on the surface of δ' are insignificant. This is consistent with the observed morphology of paired dislocations in the peak-aged alloy in which the dislocations tend to lie in the matrix keeping out of δ' . If only the APB energy were predominant, the dislocation pairs would partially lie in δ' , as proposed by Gleiter and Hornbogen⁽¹⁾⁽²⁾.

For the over-aged state, the strength is well

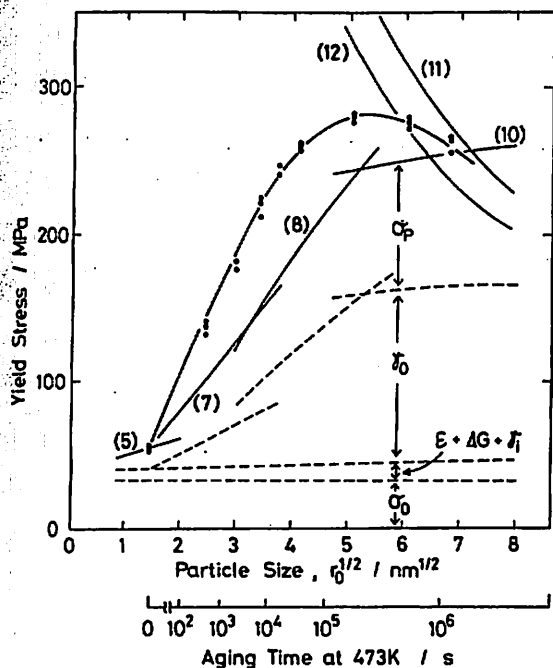


Fig. 4 Variation of yield stress with particle size (thick curve). Thin and dotted curves are based on calculation. The numbers on the curves indicate the equations used to evaluate the yield stress.

explained by the equations based upon the Orowan by-passing model.

VII. Conclusion

Strengthening mechanisms in Al-Li alloys were discussed on the basis of the direct observation of dislocations by TEM, and the following conclusion was obtained.

The strength of the under-aged or peak-aged Al-Li alloys can be explained in terms of a model in which a pair of dislocations cut through the precipitates. Main contributions to the resistance to the moving dislocations come from the APB energy and the friction stresses of δ' -precipitates and of the matrix. The effects of lattice mismatch and of the difference in the shear modulus between δ' and the matrix are relatively insignificant.

In the over-aged alloys, dislocations by-pass the particles leaving Orowan loops. The yield strength of the over-aged alloys can be

estimated by the Orowan by-pass model.

Acknowledgments

This work was supported partly by Grant-in Aid for Scientific Research from the Ministry of Education, Science and Culture (58550473) and Grant-in Aid from the Light Metal Educational Foundation, Inc.

REFERENCES

- (1) H. Gleiter and E. Hornbogen: *Phys. Status Solidi*, **12** (1965), 235.
- (2) H. Gleiter and E. Hornbogen: *Phys. Status Solidi*, **12** (1965), 251.
- (3) R. K. Ham: *Ordered Alloys*, Structural Applications and Physical Metallurgy, Claitors, Baton Rouge, Louisiana, (1970), p. 365.
- (4) L. M. Brown and R. K. Ham: *Strengthening Methods in Crystals*, Elsevier, Amsterdam, (1971), p. 9.
- (5) M. Furukawa, Y. Miura and M. Nemoto: *Trans. JIM*, **26** (1985), 9.
- (6) T. Th M. De Hosson, A. Huis in't Veld, H. Tamler and O. Kanert: *Acta Met.*, **32** (1984), 1205.
- (7) R. Nozato and G. Nakai: *Trans. JIM*, **18** (1977), 679.
- (8) V. Gerold and H. Harberkorn: *Phys. Status Solidi*, **16** (1966), 675.
- (9) B. Noble and G. E. Thompson: *Met. Sci. J.*, **5** (1971), 114.
- (10) D. B. Williams and J. W. Edington: *Met. Sci. J.*, **9** (1975), 529.
- (11) M. Tamura, T. Mori and T. Nakamura: *J. Japan Inst. Metals*, **34** (1970), 919 (in Japanese).
- (12) S. F. Baumann and D. B. Williams: *Aluminum-Lithium Alloys II*, Ed. by E. A. Starke, Jr. and T. H. Sanders, Jr., *Met. Soc. AIME*, (1984), p. 17.
- (13) B. Noble, S. J. Harris and K. Dinsdale: *J. Mat. Sci.*, **17** (1982), 461.
- (14) R. W. Weeks, S. R. Pati, M. F. Ashby and P. Barraud: *Acta Met.*, **17** (1969), 1403.
- (15) P. A. Flinn: *Trans. Met. Soc. AIME*, **218** (1960), 145.
- (16) L. P. Costas and R. P. Marshall: *Trans. Met. Soc. AIME*, **224** (1962), 970.
- (17) J. Friedel: *Dislocations*, Pergamon Press, Oxford, (1964), p. 371.
- (18) N. S. Stoloff: *The Superalloys*, Ed. C. T. Sims and W. C. Hagel, John Wiley and Sons, New York, (1972), p. 79.
- (19) A. Kelly and P. B. Nicholson: *Precipitation Hardening*, *Prog. Mat. Soc.* **10**, No. 3, (1968), p. 151.
- (20) A. J. E. Foreman and M. J. Makin: *Phil. Mag.*, **14** (1966), 911.
- (21) M. F. Ashby: *Physics of Strength and Plasticity*, Ed. by A. S. Argon, Cambridge Mass., (1966), p. 113.
- (22) D. Turnbull: *Solid State Physics*, **3** (1956), 226.

The Effect of Temperature on the Yield Stress of Al-Li Alloy*

By Minoru Furukawa**, Yasuhiro Miura*** and Minoru Nemoto***

Yield stress of aged Al-11.1 mol%Li alloy was measured at temperatures between 77 and 523 K, and the deformation induced dislocation structure was examined by transmission electron microscopy. Strength and dislocation arrangements depend largely both on the aging condition and on the testing temperature. The peak positions in strength vs aging time curves shift to the side of shorter aging time with increasing testing temperature. The mode of interaction between dislocations and δ' -precipitates also varies with the testing temperature. For the specimens aged nearly to the peak strength, the positive temperature dependence of yield stress is observed in the temperature range in which dislocations move in pairs cutting the δ' -precipitates. In the over-aged specimens, dislocations by-pass the precipitates leaving dislocation loops around the precipitates at the beginning of plastic deformation. The shift of peak positions in the aging curves and the variation of the interaction modes between dislocations and precipitates with testing temperature are explained in terms of the positive temperature dependence of cutting stress and the negative temperature dependence of by-passing stress.

(Received February 9, 1985)

Keywords: aluminum-lithium alloy, ordered precipitates, precipitation hardening, mechanical properties, temperature dependence, super-dislocations, transmission electron microscopy, Orowan mechanism

I. Introduction

Precipitation in Al-Li alloys proceeds in two-stages; super-saturated solid solution $\rightarrow \delta'$ (Al₃Li) $\rightarrow \delta$ (AlLi)⁽¹⁾⁻⁽⁴⁾. The Al-Li alloys appreciably harden by precipitation of δ' -phase which is a quasi-equilibrium phase of L₂ ordered structure and is perfectly coherent with the matrix crystal. The δ -phase is a coarse equilibrium phase of B32-type (NaTi) structure. The alloys containing fine precipitation of δ' -phase are especially attractive for aerospace applications, because they offer interesting combination of high specific strength and high specific modulus⁽⁵⁾. Therefore, much work⁽⁶⁾⁻⁽¹²⁾ has been carried out on the room temperature mechanical properties of the alloys. The present authors have investigated the behaviour of deformation induced dislocations at room temperature by transmission elec-

tron microscopy and have discussed the strengthening and deformation mechanisms of an Al-11.1 mol%Li alloy⁽¹⁰⁾⁻⁽¹²⁾.

Recently attention has been paid to the elevated temperature deformation behavior of Al-Li alloys to determine the suitability of the alloys for intermediate-temperature applications⁽¹³⁾⁽¹⁴⁾. It is well known that the strength of the L₂ ordered phase often increases with increasing temperature to a peak value at an elevated temperature⁽¹⁵⁾⁻⁽¹⁷⁾. This behavior is believed to be the main origin of the superior high temperature strength of various γ/γ' nickel base superalloys. The δ' -L₂ ordered phase in the Al-Li alloys is expected to show similar contribution at elevated temperatures.

Although exceptional high temperature strength or apparent positive temperature dependence of the yield strength of binary Al-Li⁽¹³⁾⁽¹⁴⁾, and ternary Al-Li-Mg⁽¹³⁾, Al-Li-Co⁽¹⁴⁾ and Al-Li-Zr⁽¹⁴⁾ alloys have not been found over the temperature range 293-573 K, it has been reported that the modulus normalized yield stresses of Al-Li and Al-Li-Co alloys increase with increasing temperature up to 423 K and then decrease. Tamura *et al.*⁽¹⁸⁾ have found that the yield strength of Al-9.5 mol%Li

* This paper was originally published in Japanese in J. Japan Inst. Metals, 48 (1984), 1068.

** Faculty of Education, Fukuoka University of Education, Munakata 811-41, Japan.

*** Faculty of Engineering, Kyushu University, Fukuoka 812, Japan.

single crystal is higher at room temperature than at 77 K and have explained this phenomenon taking account of the positive temperature dependence of the strength of $L1_2$ ordered phase.

The purpose of the present work is to investigate the temperature dependence of the strength of binary Al-Li alloy having various microstructures more systematically over a wider temperature range and to correlate these mechanical properties with the behavior of deformation induced dislocations.

II. Experimental Procedure

An Al-11.1 mol%Li alloy was prepared by melting 99.99% Al and 99.8% Li in an Ar atmosphere. The alloy contained 0.0032 mol% Fe, 0.026 mol% Si and 0.0046 mol% Mg. The as-cast ingot was hot and cold rolled to a 3 mm thick strip and cut to $3 \times 3 \times 4.7$ mm³. The specimens were solution treated at 823 K for 1.08×10^4 s in glass capsules filled with Ar and then quenched into iced water. The average grain size of the solution treated specimens was approximately 180 μ m. The specimens aged at 423 K-523 K were compressively tested at temperatures between 77 K and 523 K with an Instron-type machine. A compressive strain of 4% was given to the specimens at a normal strain rate of 3.5×10^{-4} s⁻¹. The compressive tests at 77 K and 213 K were performed in liquid nitrogen and in methyl alcohol containing dry ice, respectively. The compressive tests at temperatures above room temperature were performed in a silicon oil bath and the tested specimens were immediately cooled into water. The necessary time for testing was about 400 s. Slices 0.3 mm thick were taken from the deformed specimens by using a fine cutting machine, and thin foils for transmission electron microscopy were prepared using a simple twin-jet electropolishing apparatus⁽¹⁹⁾. The composition of the electrolyte was 20% HClO₄ and 80% C₂H₅OH. Microstructures and dislocation configurations were investigated by dark field transmission microscopy using a JEM-1000 high voltage electron microscope. Young's moduli of the alloy at various aging states were measured at temperatures from

290 K to 443 K by the resonant frequency method using plate specimens (2 mm \times 10 mm \times 80 mm).

III. Experimental Results and Discussion

1. Temperature dependence of yield stress

Figure 1(a) to (c) show the variation of 0.2% proof stress ($\sigma_{0.2}$) of the Al-11.1 mol%Li alloy aged at 423 K, 473 K and 523 K, respectively, as a function of aging time and testing temperature. It should be noted that the values of yield stress of specimens unaged or aged for short periods and tested at high temperatures are strongly affected by aging during testing. A remarkable increase of strength of the alloy aged at 423 K for short periods shown in Fig. 1(a) is due apparently to the age hardening during testing. In the following discussion we will mainly deal with the behavior of the alloy at testing temperatures below the aging temperature and at aging times longer than 400 s within which aging during testing is negligibly small.

From Fig. 1, it is clear that the configurations of the age hardening curves, cross sections cut by planes parallel to the time axis and perpendicular to the temperature axis, are strongly dependent on the testing temperature. The aging time necessary to attain the maximum strength is shortened with increasing testing temperature. For example, the strength of the alloy aged at 473 K attains its maximum value by aging for about 6×10^5 s when tested at 77 K, as shown in Fig. 1(b). On the other hand, the alloy attains a maximum strength by aging for about 6×10^4 s when tested at 473 K. Cross sections cut by planes perpendicular to the time axis and parallel to the temperature axis of Fig. 1 clearly show that the alloy aged nearly to the peak strength have a positive temperature dependence of strength up to about 450 K. The yield stress of the alloy aged at 473 K for 1.8×10^5 s increases from 260 MPa at 77 K to 290 MPa at 423 K with increasing testing temperature. On the other hand, the yield stress of the over-aged alloy decreases monotonically with increasing testing temperature, as shown in Fig. 1(c).

Figure 2 shows the temperature dependence

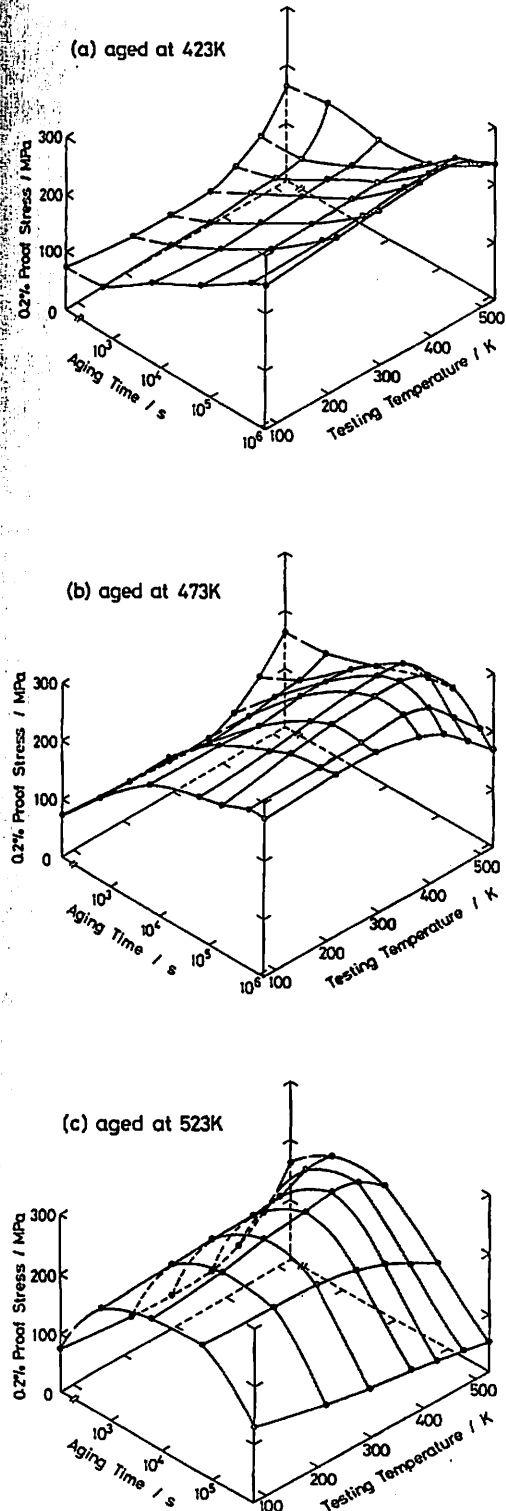


Fig. 1 (a)-(c): 0.2% proof stress-aging time-testing temperature diagram of Al-11.1 mol%Li alloy aged at (a) 423 K, (b) 473 K and (c) 523 K, respectively.

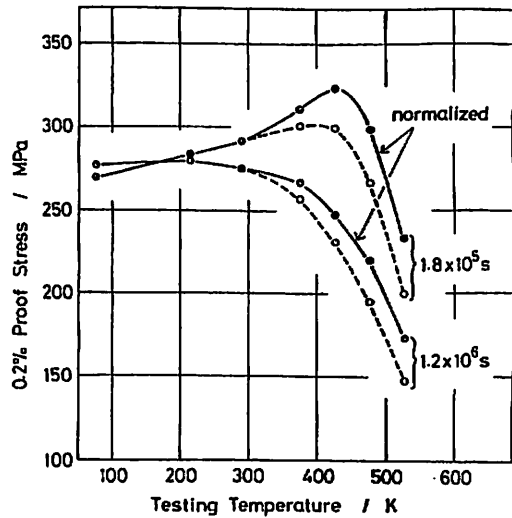


Fig. 2 Temperature dependence of modulus normalized 0.2% proof stress (solid lines) of Al-11.1 mol%Li alloy aged at 473 K for 1.8×10^5 s (peak-aged) and 1.2×10^6 s (over-aged). Dotted lines indicate unnormalized 0.2% proof stress.

of the modulus-normalized yield stress of the alloy aged at 473 K for 1.8×10^5 s (peak-aged) and at 473 K for 1.2×10^6 s (over-aged) in conjunction with the unnormalized yield stress. It is quite clear that the temperature dependence of the yield stress strongly depends on the microstructure, then the mode of the interaction between dislocations and precipitates. In the peak-aged condition, in which the dislocations cut through the δ' -particles during plastic deformation⁽¹⁰⁾⁻⁽¹²⁾, the modulus-normalized yield stress significantly increases with increasing temperature from 77 K up to 423 K and then decreases. In the over-aged state, in which the dislocations by-pass the δ' -particles at the beginning of plastic deformation⁽¹⁰⁾⁻⁽¹²⁾, the modulus-normalized yield stress decreases monotonically with increasing testing temperature. At testing temperatures above 473 K, the yield stress decreases abruptly with increasing testing temperature. Figure 3(a), (b) and (c) show stress-strain curves obtained by temperature change tests for the alloy as quenched, peak-aged or over-aged, respectively. The specimens were first deformed to a strain of about 0.3% in compression at 423 K, then rapidly cooled to room temperature and again compressively tested at room temper-

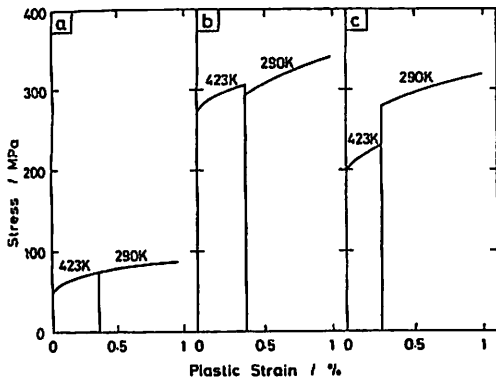


Fig. 3 Variation of stress-strain curves of Al-11.1 mol%Li alloy with temperature change from 423 K to 290 K during testing. (a) As quenched, (b) aged at 473 K for 1.8×10^5 s (peak-aged) and (c) aged at 473 K for 1.2×10^6 s (over-aged).

ature. It is clear that the flow stress decreases with decreasing testing temperature in the peak-aged state but the situation is opposite in the over-aged state.

2. Configurations of deformation induced dislocations

It is difficult to observe both δ' and deformation induced dislocations in the same imaging condition. This is due to the fact that the difference in electron scattering efficiency between the matrix and δ' is small and the strain field around δ' is extremely small corresponding to the small lattice mismatch between the matrix and δ' . Therefore, δ' was observed in a strong beam dark field image using a superlattice reflection, and the dislocations were observed in a weak beam dark field image using a matrix reflection. Figure 4(a), (b) and (c) show the δ' -particles observed using a 100 Ll_2 ordered spot in the as quenched state, after aging at 473 K for 1.8×10^5 s (peak strength at room temperature) and at 473 K for 1.2×10^6 s (over-aged), respectively. Figure 4(a) shows that the quenched alloy contains a uniform dispersion of fine (~ 4 nm dia.) δ' -particles. The δ' -particles are of irregular shape in the as quenched state and tend to spheroidize as the aging proceeds.

Figure 5(a), (b), (c) and (d) show 200 weak beam dark field images of as quenched alloy deformed 4% in compression at 77 K (a), 290

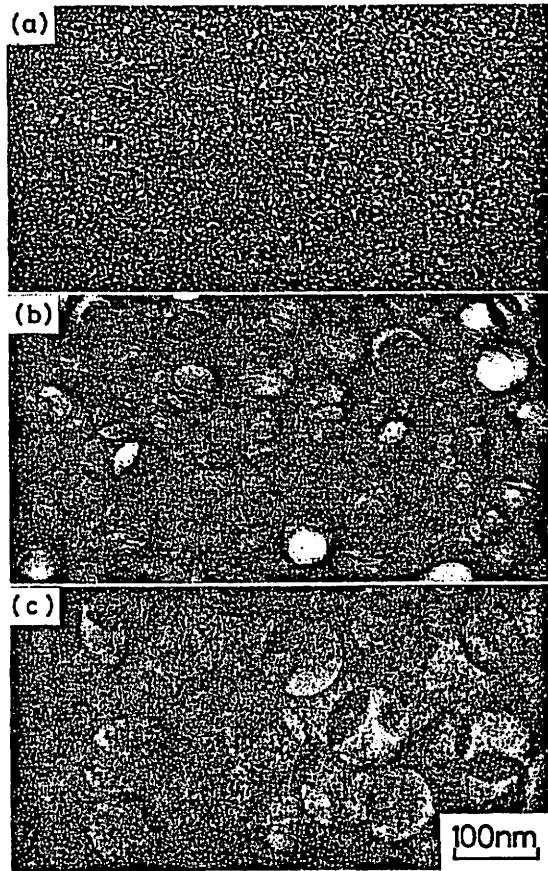


Fig. 4 100 dark field images of Al-11.1 mol%Li alloy. (a) As quenched, (b) aged at 473 K for 1.8×10^5 s (peak-aged) and (c) aged at 473 K for 1.2×10^6 s (over-aged).

K (b), 443 K (c) and 473 K (d), respectively. It is clear from the micrograph that the deformation induced dislocations move in pairs (as superdislocations) when the alloy is deformed at temperatures below 443 K. They are rather straight and smooth at deformation temperatures below 290 K but become wavy, and the separation between two dislocations constituting the superdislocation increases with increasing testing temperature. When the alloy is deformed at 473 K, dislocations move as wavy single dislocations. Since the time necessary for the compression test is not longer than 400 s and the dislocations observed in the alloy deformed at 290 K after aging at 473 K for 600 s are always superdislocations, these morphology changes are not considered to be caused only by the aging during the compression test. This means that the behavior of

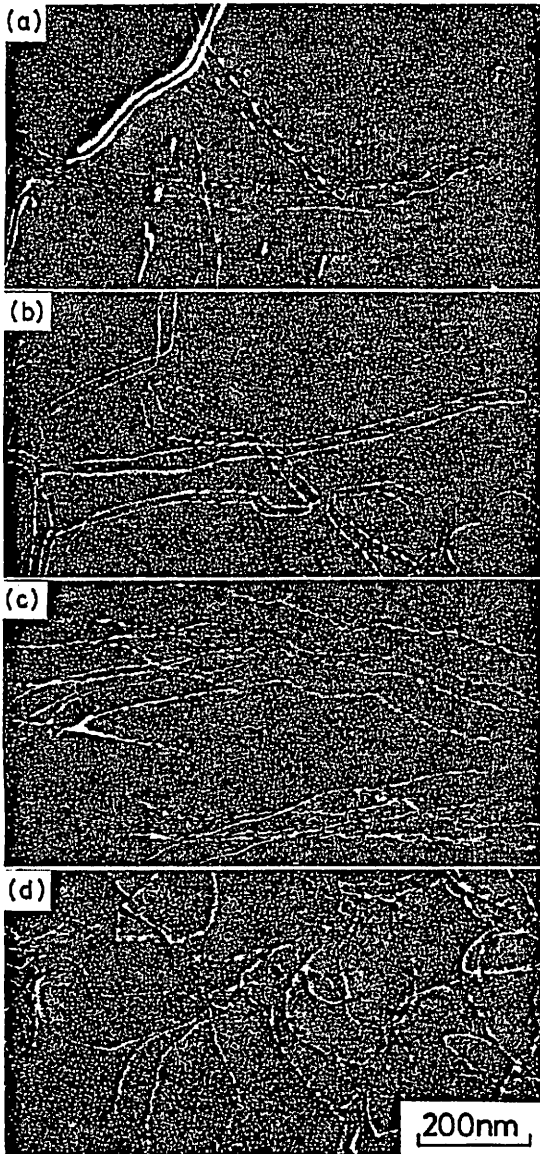


Fig. 5 200 dark field images of Al-11.1 mol%Li alloy quenched from 823 K and deformed 4% in compression at 77 K (a), 290 K (b), 443 K (c) and 473 K (d).

dislocations changes with increasing temperature.

Figure 6(a), (b), (c) and (d) show dark field images of dislocations in the alloy aged at 473 K for 1.8×10^5 s (aged to peak strength measured at room temperature) and then deformed 4% in compression at 77 K (a), 290 K (b), 423 K (c) and 523 K (d), respectively. Dislocations move in pairs, when the alloy is deformed at temperatures below 290 K. They

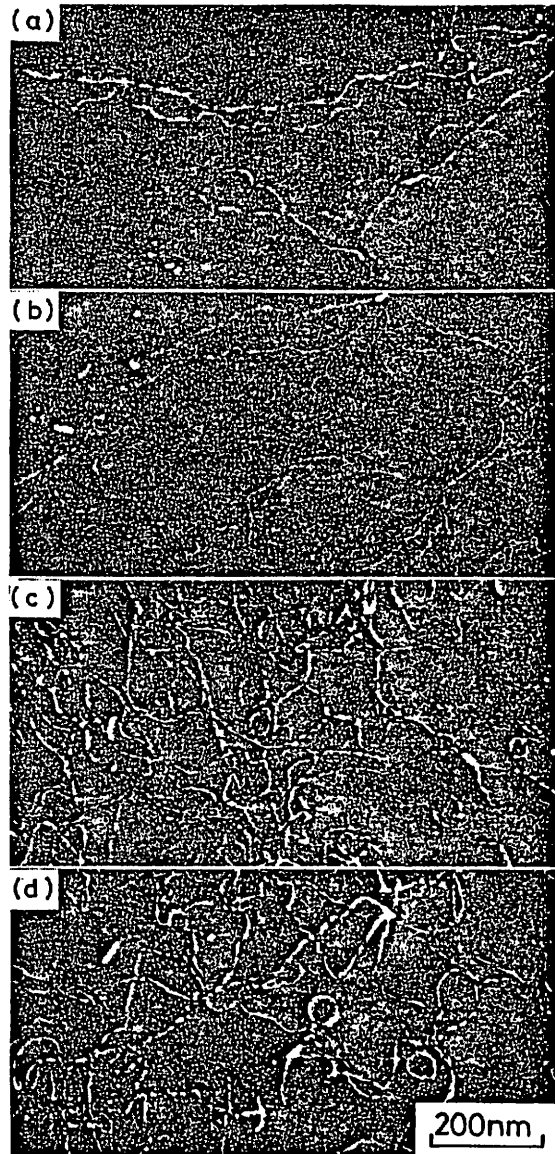


Fig. 6 200 dark field images of Al-11.1 mol%Li alloy aged at 473 K for 1.8×10^5 s and deformed 4% in compression at 77 K (a), 290 K (b), 423 K (c) and 523 K (d).

are wavier than those shown in Fig. 5. The wave length of the bowed-out dislocations is nearly equal to the δ' -particle spacing. Almost all dislocations move as single dislocations at temperatures above 423 K. Furthermore, many dislocation loops are observed in Fig. 6(c) and (d). By the comparison between the 200 dark field image and 100 dark field image of the same area,⁽¹¹⁾ these dislocation loops were known to lie surrounding the δ' -particles. This

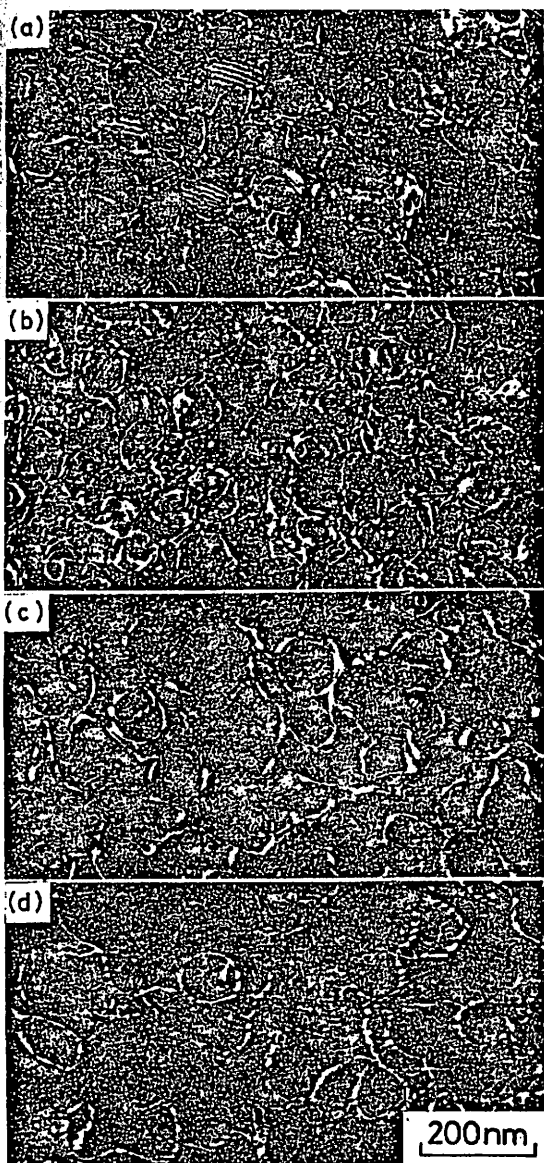


Fig. 7 200 dark field images of Al-11.1 mol%Li alloy aged at 473 K for 1.2×10^6 s and deformed 4% in compression at 77 K (a), 290 K (b), 423 K (c) and 523 K (d).

means that dislocations by-pass the particles leaving the Orowan dislocation loops around them.

Figure 7(a), (b), (c) and (d) show 200 dark field images of the over-aged alloy (aged at 473 K for 1.2×10^6 s) deformed 4% in compression at 77 K (a), 290 K (b), 423 K (c) and 523 K (d), respectively. The deformation induced dislocations in the over-aged alloy are single over the temperature range from 77 K to 523 K. They

bow out between the spherical δ' -particles. Many dislocation loops are also observed. This result indicates that dislocations by-pass the particles by the Orowan mechanism at all temperatures investigated. Figure 7 shows also that the density of the dislocation loops decreases and the average diameter of them increases with increasing deformation temperature. This suggests that the dislocations by-pass the spherical particles by local climb⁽²⁰⁾⁻⁽²²⁾ when the dislocations come into contact with the particles near the edge of them, or that small dislocation loops disappear as a result of shrinkage at elevated temperatures. In the alloy deformed at 77 K, stacking fault contrasts are observed in some of the δ' -precipitates (Fig. 7a). Detailed examination of the mechanism of the formation of stacking fault contrasts will be published elsewhere. Reference should be made to the previous papers⁽¹⁰⁾⁻⁽¹²⁾ for the detailed behavior of dislocations in the Al-Li alloys at room temperature.

Figure 8 shows 200 dark field images of the alloy aged at 473 K for 6×10^5 s and deformed

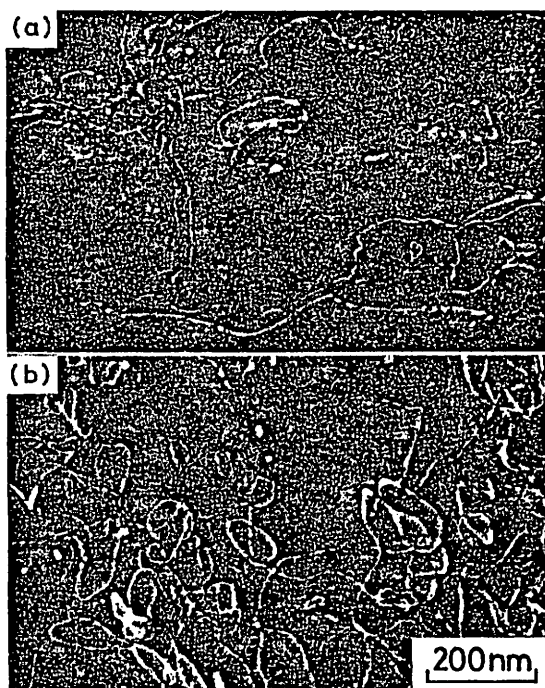


Fig. 8 200 dark field images of Al-11.1 mol%Li alloy aged at 473 K for 6×10^5 s and deformed 4% in compression at 77 K (a) and 290 K (b).

4% in compression at 77 K (a) and 290 K (b). Paired dislocations are observed in (a) but single dislocations and dislocation loops in (b). This result indicates that the mode of interaction between dislocations and δ' -precipitates varies from cutting to by-passing with increasing testing temperature. As known from Fig. 1(b), the alloy shows almost peak strength by aging at 473 K for 6×10^5 s when deformed at 77 K, but attains some over-aged strength when tested at 290 K.

It has been said that the source of characteristic poor ductility of Al-Li alloys is attributed to strain localization when δ' -precipitates are sheared by superlattice dislocations⁽⁹⁾⁽²³⁾. In the full-aged Al-Li single crystal, sheared δ' -precipitates have actually been observed after deformation⁽¹⁸⁾. However, in the present experiment, dislocations were almost always distributed uniformly in the alloy at any aging condition, and pile ups of dislocations or sheared δ' -particles have not been observed at any temperature ranging from 77 K to 523 K.

3. Temperature variation of deformation mechanisms

From the preceding sections, it has been known that the peak positions in strength vs aging time curves shift to the side of shorter aging time with increasing testing temperature. It follows that an alloy having the peak strength at a lower testing temperature is in an over-aged state at a higher testing temperature. The configurations of dislocations observed by TEM have shown that the dislocations move in pairs cutting the δ' -precipitates in the alloy aged before the peak position of the aging curves at any testing temperature. On the other hand, after the peak positions of the curves, dislocations by-pass the precipitates by the Orowan by-passing mechanism at any testing temperature.

Figure 9 represents the projection of the peak points of the aging curves shown in Fig. 1(b) and the regions indicating the morphology of deformation induced dislocations. As seen in Fig. 9, the boundary between the region governed by the cutting mechanism and that by the Orowan by-passing mechanism coin-

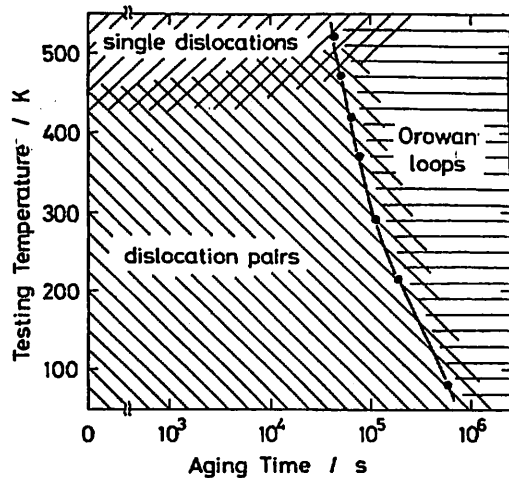


Fig. 9 Projection of the points of peak strength of the aging curves shown in Fig. 1(b) and the regions indicating the morphology of deformation induced dislocations.

cides well with the curve of the projected peak positions. The variation of deformation mechanism with the testing temperature is considered to be closely related to the temperature dependence of cutting stress and of by-passing stress. Figure 10 schematically represents the dependence of the by-passing stress and of the cutting stress on the aging time and testing temperature. Each stress is represented by a curved surface in Fig. 10. The by-passing stress decreases with increasing aging time, since it is

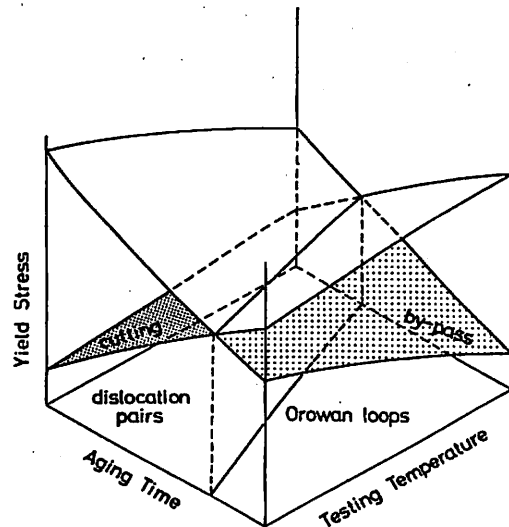


Fig. 10 Schematic representation of the variation of interaction mechanisms between δ' -precipitates and dislocations with aging and testing temperature.

inversely proportional to the δ' -particle spacing⁽¹⁰⁾⁻⁽¹²⁾ and decreases with increasing testing temperature. On the other hand, the cutting stress increases with increasing aging time, since it increases with increasing volume fraction and size of δ' -particles⁽¹⁰⁾⁻⁽¹²⁾, and increases with increasing testing temperature up to some critical temperature as suggested by Fig. 2. The positive temperature dependence of the cutting stress is possibly explained by the increase of the resistance to the motion of superdislocations in the $L1_2$ ordered δ' -particles. For the $L1_2$ ordered phase, the resistance to the motion of dislocations has been successfully explained by the model based on the Kear-Wilsdorf locking⁽²⁴⁾.

Two surfaces showing the by-passing stress and the cutting stress intersect, as shown in Fig. 10. The deformation mechanism of the alloy must be determined by the surfaces lying below. It is evident that the intersection line shifts to the side of shorter aging time with increasing testing temperature, as shown by the projection onto the bottom of the diagram. The experimental results shown in Fig. 9 agree qualitatively well with the behavior shown in Fig. 10 except the high temperature region in which dislocations tend to move as single dislocations at any aging stage. When a leading dislocation of pair cuts through a δ' -particle, disorder is created along the slip plane in the particle. The movement of second dislocation is facilitated because it restores the order. The energy of the antiphase boundary and the repulsive force between two dislocations are main causes which determine the separation distance of the pair.

There are several possibilities to suppress the movement of superdislocations and to increase the separation distance of the paired dislocations at high temperatures. These are (a) decrease of anti-phase boundary energy with increasing temperature, (b) restoration of order after the movement of the first dislocation by diffusion, and (c) climbing of dislocations out of their slip plane by diffusion. Although it is difficult to determine the controlling mechanism to enhance the movement of single dislocations in the Al-Li alloy from the present experimental only, the observations suggest

that the climbing and cross slip of dislocations out of their slip planes must play important roles during plastic deformation at elevated temperatures.

IV. Conclusion

(1) The temperature dependence of yield stress and of dislocation morphology of Al-11.1 mol%Li alloy largely depends on the aging condition. For the alloy aged nearly to its peak strength, the positive temperature dependence of yield stress is observed in the temperature range in which dislocations move in pairs cutting δ' -precipitates.

(2) In the over-aged alloy, dislocations bypass the precipitates leaving dislocation loops around them by the Orowan by-passing mechanism. The yield stress decreases monotonically with increasing deformation temperature.

(3) The separation distance between two dislocations constituting a superdislocation increases with increasing deformation temperature, and finally dislocations move as single ones.

(4) The peak positions in strength vs aging time curves shift to the side of shorter aging time with increasing testing temperature. These peak positions correspond to the critical points at which the operating mechanism changes from cutting to by-passing.

(5) The shift of peak positions in the aging curves can be explained in terms of the positive temperature dependence of cutting stress and the negative temperature dependence of by-passing stress.

Acknowledgments

The authors would like to thank Technical Research Laboratories, Sumitomo Light Metal Industries, LTD., for preparing the Al-Li alloy. Special thanks are also due to Dr. Nakamura of Nagasaki Technical Institute of Mitsubishi Heavy Industries, LTD. for the measurements of temperature dependence of elastic constant of the Al-Li alloy. This research was supported partly by Grant-in Aid for Scientific Research from the Ministry of Education, Science and Culture of Japan

(58550473) and Grant-in Aid from the Light Metal Educational Foundation. Inc.

REFERENCES

- (1) J. M. Silcock: *J. Inst. Metals*, **88** (1959), 359.
- (2) B. Noble and G. E. Thompson: *Met. Sci. J.*, **5** (1971), 114.
- (3) D. B. Williams and J. W. Edington: *Met. Sci. J.*, **9** (1975), 529.
- (4) H. Suzuki, M. Kanno and N. Hayashi: *J. Japan Inst. Light Metals*, **31** (1981), 122 (in Japanese).
- (5) M. Furukawa, Y. Miura and M. Nemoto: *Bul. Japan Inst. Metals*, **23** (1984), 172 (in Japanese).
- (6) H. K. Hardy: *J. Inst. Metals*, **84** (1955-56), 429.
- (7) W. R. D. Jones and P. P. Das: *J. Inst. Metals*, **87** (1958-59), 338.
- (8) W. R. D. Jones and P. P. Das: *J. Inst. Metals*, **88** (1959-60), 435.
- (9) T. H. Sanders, Jr. and E. A. Starke, Jr.: *Acta Met.*, **30** (1982), 927.
- (10) M. Furukawa, A. Matsui, Y. Miura and M. Nemoto: *J. Japan Inst. Light Metals*, **35** (1985), 3.
- (11) M. Furukawa, Y. Miura and M. Nemoto: *Trans. JIM*, **26** (1985), 225.
- (12) M. Furukawa, Y. Miura and M. Nemoto: *Trans. JIM*, **26** (1985), 230.
- (13) B. Noble, S. J. Harris and K. Harlow: *Aluminum-Lithium Alloy II*, Ed. by E. A. Starke, Jr. and T. H. Sanders, Jr., *Met. Soc. AIME*, (1984), p. 293.
- (14) S. H. L. Sastry and J. E. O'Neal: *Aluminum-Lithium Alloy II*, Ed. by E. A. Starke, Jr. and T. H. Sanders, Jr., *Met. Soc. AIME*, (1984) p. 79.
- (15) S. Takeuchi: *Bul. Japan Inst. Metals*, **18** (1979), 249 (in Japanese).
- (16) T. Suzuki: *Bul. Japan Inst. Metals*, **21** (1982), 19 (in Japanese).
- (17) E. Kuramoto: *Bul. Japan Inst. Metals*, **14** (1975), 567 (in Japanese).
- (18) M. Tamura, T. Mori and T. Nakamura: *Trans. JIM*, **14** (1973), 355.
- (19) T. Sano, R. Nishihara, H. Yotsumoto, Y. Miura and M. Nemoto: *Technology Reports of the Kyushu University*, **56** (1983), 491 (in Japanese).
- (20) L. M. Brown and R. K. Ham: *Strengthening Methods in Crystals*, Ed. by A. Kelly and R. B. Nicholson, Elsevier, (1971), p. 9.
- (21) F. J. Humphreys, P. B. Hirsch and G. Gould: *Proc. 2nd. Int. Conf. on Strength of Metal and Alloys*, Cambridge, **1** (1973), p. 31.
- (22) R. S. W. Shewfelt and L. M. Brown: *Phil. Mag.*, **35** (1977), 945.
- (23) D. Webster: *Met. Trans. A.*, **10A** (1979), 1913.
- (24) S. Takeuchi and E. Kuramoto: *Acta Met.*, **21** (1973), 415.

THE TEMPERATURE AND ORIENTATION DEPENDENCE OF THE YIELD STRESS
OF AL-LI SINGLE CRYSTALS

K.Yusu*, H.Ueda*, A.Matsui*, M.Furukawa**, Y.Miura*** and M.Nemoto***.

* Graduate School, Kyushu University.

** Dept. of Tech., Faculty of Education, Fukuoka University of Education.

*** Dept. of Metallurgy, Faculty of Engineering, Kyushu University.

I. Introduction.

Much attention has been paid on the development and application of aluminum alloys containing 2-3mass%Li(1). Mass savings in aircraft frames by the use of the alloys make them attractive to the aluminum and aerospace industries. So far, many basic researches have been made to understand the anomalous mechanical behavior of single crystals with $L1_2$ structure, such as $Ni_3Al(2)$, $Ni_3Ga(3)$, $Pt_3Al(4)$, etc. Our principal interest is to relate those previous results to the case of an age-hardenable Al-Li single crystals which contain $L1_2$ -Al₃Li precipitates. In this paper, experimental results are reported on the dependence of the yield stress of the Al-Li single crystals upon test temperature and crystallographic orientation.

II. Experimental procedures.

Aluminum-lithium alloys with 3-3.5mass%Li were prepared by induction melting 99.99mass%Al and 99.8mass%Li under an argon atmosphere. The as-cast ingots were rolled to sheets, from which rods of rectangular cross section ($3 \times 3 \times 80\text{mm}$ or $5 \times 5 \times 100\text{mm}$) were cut out. Single crystals were grown by the modified Bridgman method in an argon atmosphere with an alumina powder mold. The single crystal rods thus grown were sealed in glass capsules filled with argon and homogenized at 823K for 1.08×10^4 s, followed by quenching into iced water. The crystals were again sealed in glass capsules with argon and aged at 473K to the different aging stages. Compressive specimens ($2 \times 2 \times 3\text{mm}$ or $3 \times 3 \times 5\text{mm}$) of different orientation were cut out and they were deformed to 3 per cent strain in compression at 293-473K. The lithium content of the specimens was around 2mass%. Analysis of slip traces was made on the basis of the observation by an optical microscope, and microstructures (dislocations and precipitates) were examined with a JEM-1000D and/or a JEM-200CX5 electron microscopes.

III. Results.

Marked serrations appeared in the load-elongation curves for the underaged crystals. This is consistent with the observed coarse slip caused by the particle-shearing of super-dislocations (Photo.1).

Figure 1 shows temperature dependence of CRSS on the primary octahedral slip of an underaged crystal (aged for 6×10^4 s). The orientation of the compression axis is shown in the standard stereographic triangle. The CRSS does not change largely up to 423K, but increased by some 20% at 473K, showing a strong positive temperature dependence. In the case of Al-Li alloys, the increase in strength with increasing temperature has been reported for polycrystals(5) and also for single crystals(6), although comprehensive study has not been made.

Orientation dependence of the yield stress is shown in Fig 2, where CRSS of the octahedral slip is plotted as a function of the Schmid factor ratio, N , for cube cross slip. The underaged crystal (aged for 6×10^4 s) shows a higher positive dependence on N than the overaged crystal (aged for 6×10^5 s), in which moving dislocations bypass the $L1_2$ precipitates.

These results are reasonably understood in terms of Kear-Wilsdorf's mechanism(7), where CRSS of octahedral slip on $L1_2$ structure is largely dependent on the tendency for cube cross slip to minimize APB energy. This tendency is determined by the factors, N and Q (the Schmid factor ratio for constriction of Shockley partials). As N increases, in going from $\langle 001 \rangle$ to $\langle 011 \rangle$, the Schmid

factor for the cube slip increases and, in compression, constriction of Shockley partials is more favored on $\langle 011 \rangle$ than on $\langle 001 \rangle$. Thus CRSS of octahedral slip for the $\langle 011 \rangle$ orientation is expected to be larger than that for the $\langle 001 \rangle$ orientation. The present experimental results are consistent with the argument above.

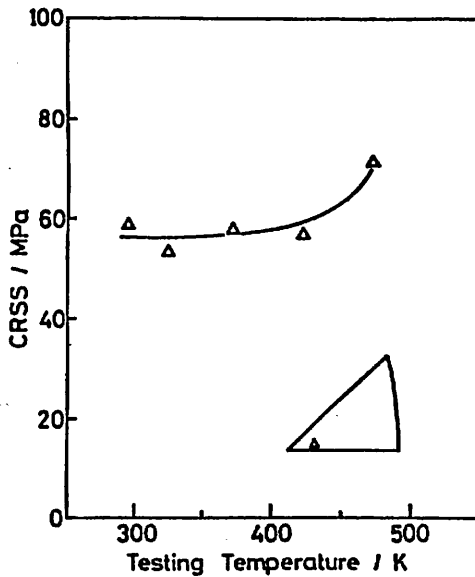


Fig.1. Temperature dependence of CRSS on the primary octahedral slip plane. (aged for 6×10^4 s)

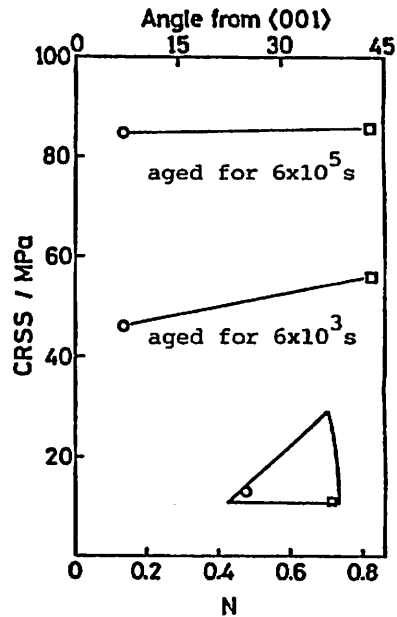


Fig.2. CRSS on the octahedral slip plane as a function of Schmid factor ratio, N .

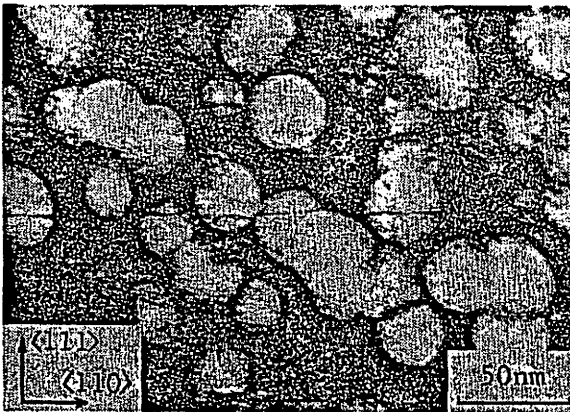


Photo.1. (110) dark field image showing Al_3Li particles sheared by super-dislocations. (aged for 6×10^4 s and deformed 3% in compression at room temperature)

References.

- (1) T.H.Sanders, Jr. and E.A.Starke, Jr. (eds.) : Aluminum-Lithium Alloys, Met. Soc. AIME, 1981.
- (2) C.Lall, S.Chin, and B.Pope : Met. Trans., 10A(1979),1323.
- (3) S.Takeuchi and E.Kuramoto : Acta Met., 21(1973),415.
- (4) D.M.We, D.P.Pope, and V.Vitek : Acta Met., 32(1984),829.
- (5) M.Furukawa, A.Matsui, Y.Miura, and M.Nemoto : J. Japan. Inst. Metals, 48(1984),1068.
- (6) M.Tamura, T.Mori, and T.Nakamura : Trans. JIM, 14(1973),355.
- (7) B.H.Kear and H.G.F.Wilsdorf : Trans. Met. soc. AIME, 224(1962),382.

日本金属学会誌 第 49 巻 第 7 号 (1985) 501-507

 δ' -L₁₂ 型規則相を含む Al-Li 2 元合金の降伏応力の歪速度依存性

古川 稔* 美浦康宏** 根本 実**

J. Japan Inst. Metals, Vol. 49, No. 7 (1985), pp. 501-507

The Strain Rate Dependence of Yield Stress of an Al-Li Alloy Containing δ' -L₁₂ Ordered Particles

Minoru Furukawa*, Yasuhiro Miura** and Minoru Nemoto**

The effect of strain rate on the yield stress of an Al-11.1 mol%Li alloy containing δ' -precipitates has been investigated at temperatures between 77 and 523 K and over the strain rate range from $1.77 \times 10^{-4} \text{ s}^{-1}$ to $1.77 \times 10^{-2} \text{ s}^{-1}$. At testing temperatures below 373 K, the yield stress is almost independent of strain rate at any aging stage. At testing temperatures above 373 K, the yield stress increases linearly with the logarithm of strain rate, and the strain rate dependence increases with increasing testing temperature. The yield stresses of under-aged alloy at temperatures between 373 and 473 K at high strain rates are greater than the yield stress at 77 K. For the alloy under-aged or aged nearly to its peak strength, the temperature range within which the positive temperature dependence of yield stress appears expands to the higher temperature side with increasing strain rate. The strain rate dependence of the yield stress is slightly negative at this aging stage. Within this temperature range, dislocations move in pairs cutting the δ' -L₁₂ ordered particles. The yield stress of the over-aged alloy decreases monotonically with decreasing strain rate and with increasing testing temperature above 373 K. The modulus normalized yield stress is nearly constant at testing temperatures below 373 K at any strain rate investigated. In the over-aged alloy, dislocations by-pass the precipitates at any temperature and strain rate.

(Received March 16, 1985)

Keywords: aluminum-lithium alloy, ordered precipitate, precipitation hardening, mechanical property, temperature dependence, strain-rate dependence, super-dislocation, transmission electron microscopy

I. 緒 言

Al-Li 合金は、高比強度・高比弾性率の航空機材料として実用化が目標されている⁽¹⁾⁽²⁾。航空機材料として用いる場合には、室温以下の温度から約 500 K 付近までの温度範囲にわたり十分な強度を保つことが必要である。Al-Li 合金の強化相である δ' -Al₃Li 相は Ni 基超耐熱合金⁽³⁾⁻⁽⁵⁾中の γ' 相と同じ L₁₂ 型規則相で、温度上昇に伴い強度が増大する。いわゆる強度の正の温度依存性をもつと考えられるため、Al-Li 合金も大きな高温強度が期待できる⁽⁶⁾⁻⁽⁸⁾。この点も本合金が航空機材料として有望視される要因の一つである。

著者らはさきに、種々の時効段階における Al-Li 2 元合金の室温での変形組織を透過電子顕微鏡により観察し、最高強度に達する以前の時効段階では超格子転位が δ' 相を

切って運動し、過時効段階では転位が δ' 相を by-pass することを示し、本合金の析出強化と変形の機構を明らかにした⁽⁹⁾。さらに、77 K から 523 K の温度域での強度の温度依存性を調べ、時効条件によっては降伏応力に正の温度依存性があることを示し、変形機構との関係を検討した⁽⁷⁾。

本論文の目的は、Al-Li 合金の基本的な変形特性を知るために、種々の時効段階にある Al-Li 2 元合金の 77 K から δ' 相が存在する上限温度に近い 523 K までの温度域での、降伏応力および変形機構の歪速度依存性について検討することである。

II. 実験方法

高純度アルミニウム (99.99%) とリチウム (99.8%) をアルゴン気流中でアルミナるつぼを使用して溶解し、金型に鋳込み、リチウム濃度が 11.1 mol% の 2 元合金を作製し

* 福岡教育大学教育学部技術科 (Department of Technology, Faculty of Education, Fukuoka University of Education, Munakata)

** 九州大学工学部冶金学科 (Department of Metallurgy, Faculty of Engineering, Kyushu University, Fukuoka)

た、不純物濃度を分析した結果、鉄 0.0032 mol%, 珪素 0.026 mol%, マグネシウム 0.0046 mol% であった。鋳塊を熱間圧延および冷間圧延により厚さ 3 mm の板とし、これより $3 \times 3 \times 4.7 \text{ mm}^3$ の圧縮試験片を切り出した。試料をパイレックスガラス管にアルゴンガスと共に封入し、823 K で $1.08 \times 10^4 \text{ s}$ 溶体化処理した後、氷水中に焼入れた。つぎに、再びパイレックスガラス管中にアルゴンガスと共に封入し、473 K で時効処理を行った。

時効処理後、77 K から 523 K の範囲の温度で、インストロン型試験機 (TOM/500) を用いて、歪速度 $1.77 \times 10^{-4} \sim 1.77 \times 10^{-2} \text{ s}^{-1}$ の範囲で、歪約 4% まで圧縮試験を行った。77 K および 213 K における圧縮試験は、それぞれ液体窒素中およびドライアイスを混入したメチルアルコール中で行った。室温以上での圧縮試験はシリコンオイルを用いた恒温槽中で行い、変形後はただちに水中に急冷した。

つぎに、時効組織と変形によって導入された転位組織を透過電子顕微鏡 (TEM) により観察するため、圧縮後の試験片から厚さ 0.3 mm の薄板を切り出し、約 0.15 mm 厚さまでエメリー紙で研磨した後、過塩素酸 20%-エチルアルコール 80% 溶液を用い、ツイング法⁽¹⁰⁾により電解研磨して薄膜を作製した。透過電子顕微鏡観察には九州大学超高圧電顕室の JEM 1000D (加速電圧 1000 kV) を用いた。

III. 実験結果

1. 降伏応力の温度および歪速度依存性

Fig. 1 (a) および (b) に、473 K で時効した Al-11.1 mol% Li 合金の降伏応力 (0.2% 耐力: $\sigma_{0.2}$) の時効時間と圧縮試験温度による変化を示す。図中の最短時効時間は $6 \times 10^3 \text{ s}$ である。(a) は歪速度 $\dot{\epsilon} = 1.77 \times 10^{-4} \text{ s}^{-1}$ の場合、(b) は歪速度 $\dot{\epsilon} = 1.77 \times 10^{-2} \text{ s}^{-1}$ の場合である。時効時間による降伏応力の変化 (時効曲線) に注目すると、降伏応力は時効時間の経過と共に上昇し、(a), (b) 両者共に 77 K 試験においては約 $6 \times 10^5 \text{ s}$ 程度で最大となり、その後過時効軟化している。歪速度がもっとも小さい場合には試験に約 500 s を要するので、試験温度が時効温度より高い場合には試験中に組織変化が生じている可能性があるので注意を要する。図中の底面に投影された時効曲線のピークの位置は、試験温度の上昇と共に短時間側へ移行する傾向にある。また (a) と (b) の比較から、そのピークの位置は試験温度が 373 K 以下では歪速度によらずほぼ同じであるが、373 K 以上では歪速度が大きい方が長時間側へ移行していることがわかる。

Fig. 2 (a) ~ (d) に、473 K でそれぞれ (a) $6 \times 10^4 \text{ s}$ (最大強度に達する前の不完全時効段階)、(b) $1.8 \times 10^5 \text{ s}$ 、(c) $6 \times 10^5 \text{ s}$ (b)、(c) はほぼ最大強度付近の完全時効段階)、および (d) $1.2 \times 10^6 \text{ s}$ (過時効段階) 時効した合金の降伏応力の歪速度による変化を示す。いずれの場合も、試験温度が 373 K 以下では降伏応力の歪速度による変化はきわめて小さい

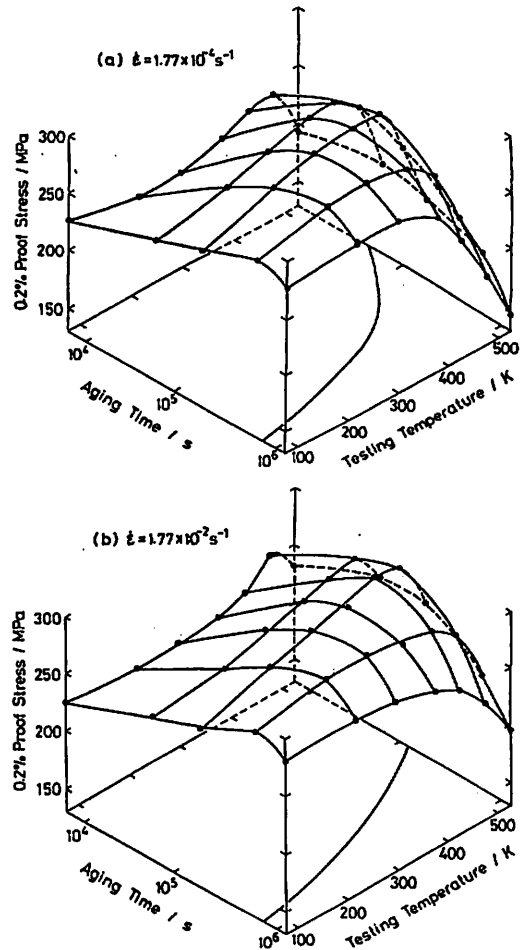


Fig. 1 0.2% proof stress-aging time-temperature diagrams of Al-11.1 mol% Li alloy aged at 473 K and tested in compression at normal strain rates of (a) $1.77 \times 10^{-4} \text{ s}^{-1}$ and (b) $1.77 \times 10^{-2} \text{ s}^{-1}$.

が、423 K 以上では歪速度の増大と共に降伏応力は明らかに上昇している。また、降伏応力と歪速度の対数はほぼ直線関係にあることがわかる。Fig. 3 に、各試験温度における直線の勾配を 473 K での時効時間の関数として示した。降伏応力の歪速度依存性は試験温度により異なり、試験温度が高いほど歪速度依存性が大きい。また、試験温度が 423 K ~ 523 K の範囲では、ピーク強度に達する $1.8 \times 10^5 \text{ s}$ 時効までは時効の進行と共に降伏応力の歪速度依存性が大きくなる傾向が認められる。523 K 試験の場合、時効の進行と共に歪速度依存性は極大値をとった後小さくなる傾向を示す。

Al-Li 合金のきわだった特徴は、Fig. 2 (a), (b) から明らかのように、各温度における降伏応力の歪速度依存性を表わす直線が交差し、高温における強度が低温より高くなることで、これは Li_2 型規則構造の析出相を含む Ni 基超耐熱合金⁽³⁾⁻⁽⁵⁾においても観察されている特異な現象である。この現象は不完全時効段階でかつ歪速度が大きいほど顕著に現われ、過時効段階 (d) では消失する。

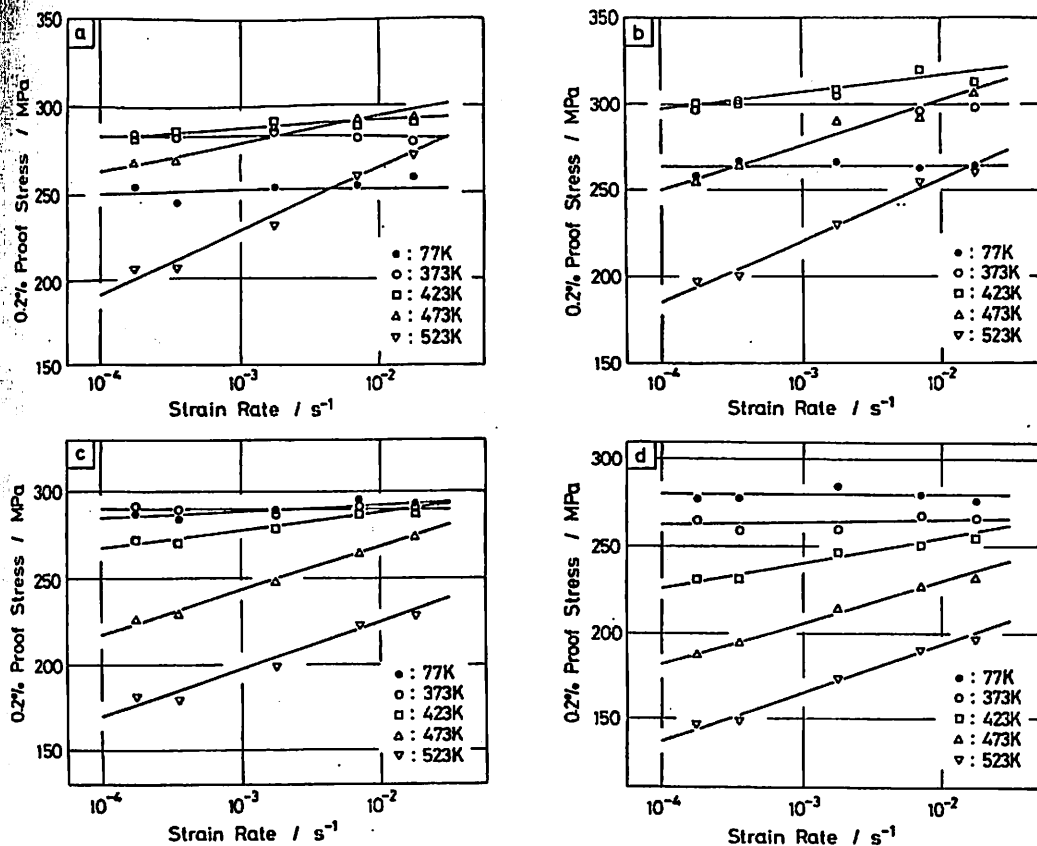


Fig. 2 The effect of strain rate on the 0.2% proof stress of Al-11.1 mol%Li alloy aged at 473 K for (a) 6×10^4 s, (b) 1.8×10^5 s, (c) 6×10^5 s and (d) 1.2×10^6 s.

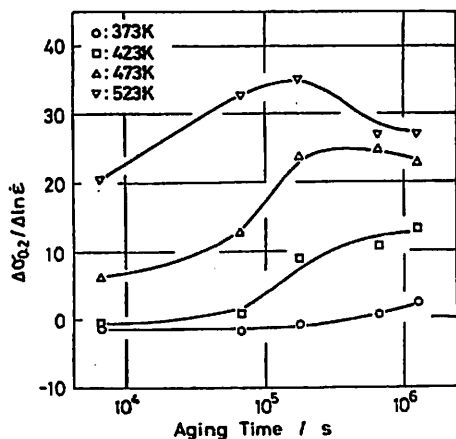


Fig. 3 The effect of aging time at 473 K on the strain rate sensitivity ($\Delta\sigma_{0.2}/\Delta \ln \dot{\epsilon}$).

Fig. 4 (a) ~ (c) は、それぞれ Fig. 2 (a), (b) および (d) 中の 2 つの歪速度について、降伏応力の試験温度による変化を示したものである。破線で示した曲線は Al-Li 合金の剛性率の温度依存性⁽¹¹⁾で補正した降伏応力である。不完全時効段階の試料 (a) では、歪速度が小さい $\dot{\epsilon} = 1.77 \times 10^{-4} \text{ s}^{-1}$ の場合、77 K から 373 K 付近の温度範囲で降伏応力に正の温度依存性が見られる。一方、歪速度が大きい

$\dot{\epsilon} = 1.77 \times 10^{-2} \text{ s}^{-1}$ の場合は、降伏応力の正の温度依存性が存在する温度領域は高温側へ広がり、473 K 付近にまで及んでいる。この傾向は (b) に示す最大強度付近まで時効した試料でも同様である。一方、(c) の過時効段階の試料では剛性率の温度依存性を補正しても降伏応力に正の温度依存性は現われず、通常の Al 合金の強度の温度依存性⁽⁸⁾⁽¹²⁾と同様、降伏応力は温度の上昇と共に単調に低下している。

2. 変形組織の歪速度による変化

Fig. 5 に、473 K で 6×10^4 s 時効した不完全時効段階の試料を 423 K で約 4% 変形した場合の転位組織を示す。(a) は $\dot{\epsilon} = 1.77 \times 10^{-4} \text{ s}^{-1}$ の場合で Fig. 4 (a) から知られるように降伏応力の温度依存性曲線の極大値付近、(b) は $\dot{\epsilon} = 1.77 \times 10^{-2} \text{ s}^{-1}$ の場合で降伏応力の正の温度依存性が強く現われている領域の組織に対応している。写真はいずれも母相の (200) 回折点による弱ビーム暗視野像である。歪速度が小さい場合 (a) は単一転位が支配的であり、多数の転位ループが観察されることから、転位は変形中に δ' 析出物を by-pass するか交差すべりや上昇運動により乗り越えている⁽⁷⁾ことがわかる。また歪速度が大きい場合 (b) には超格子転位が存在しており、 δ' 相粒子の切断機構⁽⁸⁾が働いていることは明らかである。これらの変形組織の観察結果と Fig. 4 (a) の結果は、降伏応力の正の温度依存性が

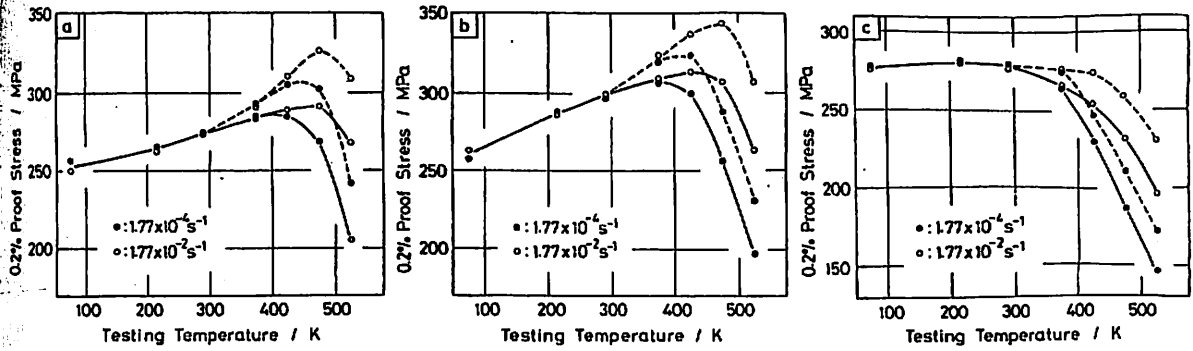


Fig. 4 The effect of strain rate on the temperature dependence of 0.2% proof stress of Al-11.1 mol%Li alloy aged at 473 K for (a) 6×10^4 s, (b) 1.8×10^5 s and (c) 1.2×10^6 s. Dotted lines indicate modulus normalized 0.2% proof stress.

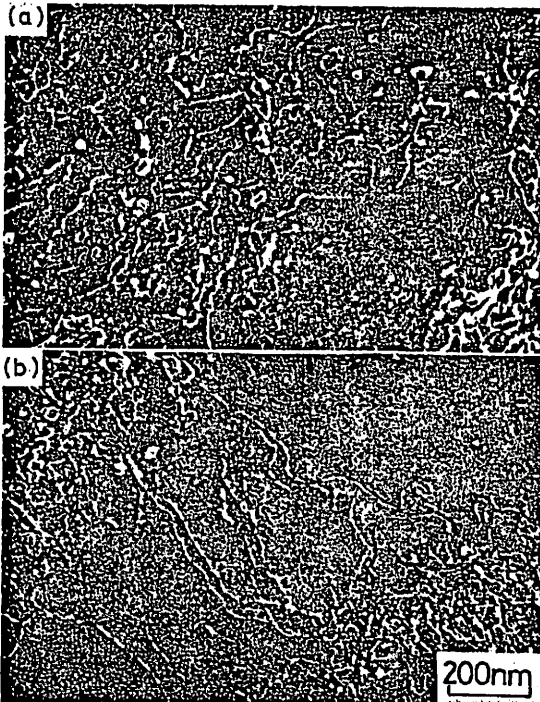


Fig. 5 (200) dark field images of Al-11.1 mol%Li alloy aged at 473 K for 6×10^4 s and deformed 4% in compression at 423 K (a) at a normal strain rate of $1.77 \times 10^{-4} \text{ s}^{-1}$ and (b) at a normal strain rate of $1.77 \times 10^{-2} \text{ s}^{-1}$.

存在する領域では超格子転位による δ' 相粒子の切断機構が働き、それ以上の温度では単一転位による析出粒子の by-pass や乗り越え機構が働いていることを示している。また、同一温度では歪速度が小さいほど粒子の by-pass や乗り越え機構が働き易いことを示している。

Fig. 6 は 473 K で 6×10^6 s 時効し、ほぼ最高強度付近にある合金を、77 K で 2 つの歪速度で変形した場合の TEM 組織である。(a) では単一転位と転位ループ、(b) では超格子転位が観察される。このように、Fig. 5 にみられた傾向が拡散が関与しないと考えられる 77 K においてさえ強く現われることを示している。一方、過時効段階の合金について種々の温度と歪速度で変形した場合の組織を観

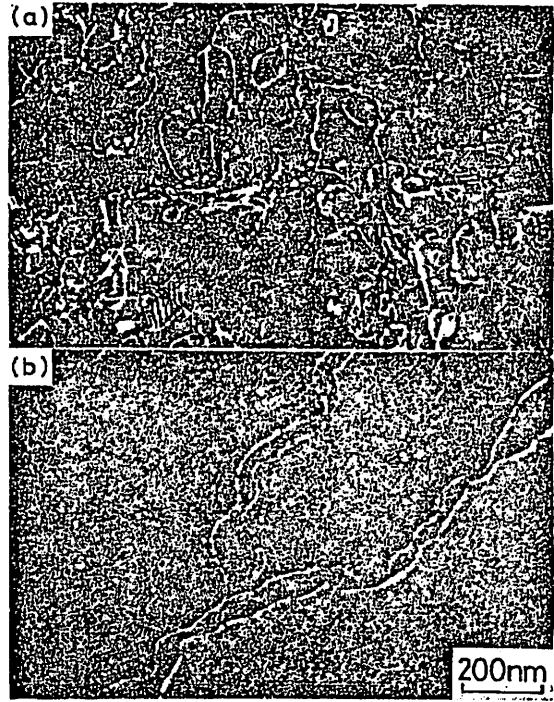


Fig. 6 (200) dark field images of Al-11.1 mol%Li alloy aged at 473 K for 6×10^6 s and deformed 4% in compression at 77 K (a) at a normal strain rate of $1.77 \times 10^{-4} \text{ s}^{-1}$ and (b) at a normal strain rate of $1.77 \times 10^{-2} \text{ s}^{-1}$.

察したが、すべて by-pass 機構が働いており⁽⁷⁾⁽⁹⁾⁽¹³⁾、歪速度による変形組織の差は認められなかった。

IV. 考 察

1. 降伏応力の歪速度依存性

時効した Al-11.1 mol%Li 合金では、切断機構が働く合金においても、Orowan の by-pass 機構⁽¹⁴⁾が働く合金においても、373 K 以下の試験温度では、降伏応力の歪速度依存性は小さい。しかし、373 K より高い温度では、すべての時効状態において降伏応力は歪速度の増大と共に上昇する傾向にあり、降伏応力と歪速度の対数とは直線関係にある。

降伏応力が歪速度にほとんど依存せず一定の値をとる現象は、 δ' 相が析出した Ni 基合金の変形温度が低く (約 0.6 T_m 以下, T_m は合金の融点), 歪速度が大きい場合 ($1.67 \times 10^{-5} \text{ s}^{-1}$ 以上) にも見出されている⁽¹⁵⁾. 本実験の Al-11.1 mol%Li 合金で, 降伏応力の歪速度依存性が小さい温度領域は $0.4 T_m$ 以下である. Ni 基合金を $0.6 T_m$ 以上で変形した場合は, 降伏応力と歪速度の対数との間には Al-Li 合金の場合と同様に直線関係があるが, 直線の傾きは Al-Li 合金の場合と異なり試験温度によらず一定となる. これらの Ni 基合金は, $0.6 T_m$ 以下では δ' 相がバーガース・ベクトル $b = (a/2) \langle 110 \rangle$ の転位対により拡散を伴わずに剪断され, $0.6 T_m$ 以上では $b = (a/2) \langle 110 \rangle$ または $b = (a/3) \langle 112 \rangle$ の転位の拡散を伴う粘性的すべりによって剪断されるものとして説明されている.

一方, Orowan の by-pass 機構が働いている SiO_2 ⁽¹⁶⁾, Al_2O_3 ⁽¹⁷⁾、あるいは BeO ⁽¹⁷⁾ を分散させた Cu 合金では, 約 $0.42 T_m$ 以下の温度においては剛性率で補正した降伏応力は温度によらず一定値をとり, それ以上の温度では温度上昇と共に低下すると報告されている. この分散強化型 Cu 合金の場合も, $0.64 T_m$ 以上では降伏応力と歪速度の対数の間には直線関係があり, その直線の傾きは温度によらず一定である. Cu 合金の $0.64 T_m$ 以上での降伏応力の温度および歪速度依存性は, パイプ拡散支配⁽²⁰⁾, パイプ拡散とダブルジョグ形成支配⁽¹⁷⁾, および体積拡散支配⁽²¹⁾ などによる転位の析出物の乗り越え, すなわち転位の local climb 機構により定量的に説明されている.

by-pass 機構が働く過時効 Al-Li 合金においても, 約 $0.4 T_m$ を境にして, それ以上の温度では剛性率で補正した降伏応力は温度上昇と共に低下する傾向を示すが, 降伏応力と歪速度の対数の間の直線関係の勾配は, Fig. 3 に示されているように温度上昇に伴い大きくなる. その直線の傾きが大きくなる温度範囲は, 373 K から本実験の最高試験温度, つまり $0.4 T_m \sim 0.56 T_m$ の間である. この温度域は, さきの分散強化型 Cu 合金において⁽¹⁶⁾, 剛性率で補正した降伏応力が温度上昇に伴い低下し始める温度 $0.42 T_m$ と, 降伏応力と歪速度の対数を示す直線の傾きが一定となる $0.64 T_m$ の間にある. したがって, 本実験の Al-Li 合金で降伏応力と歪速度の対数の間の直線の傾きが温度上昇と共に大きくなる事実は, 変形の活性化エネルギーが温度により変化することを意味し, 変形機構が過渡的段階にあることを示している. すなわち, 拡散を伴わない転位のすべり運動から拡散支配による転位の析出物の乗り越えがおこる過渡的段階にあることを示している.

2. 変形機構の歪速度による変化

Fig. 1 の底面に投影した各試験温度における時効曲線の最大強度の位置は, 373 K 付近を境として, それ以下の温度では歪速度によらずほぼ同じである. しかし, 373 K 以

上では歪速度が大きい場合の軌跡がより長時間時効側へ移行している. このピークの位置は切断機構と by-pass 機構が働く領域の交線とはほぼ対応する⁽⁷⁾. Fig. 5 に示したように, 歪速度が大きいときには切断機構が働く合金においても, 高温で歪速度が小さくなると, 上昇運動により転位は析出粒子を乗り越えるようになる. しかし, 完全時効段階にある合金についての Fig. 6 が示すように, 77 K においても, 歪速度が小さいときには by-pass 機構が働くが, 歪速度が大きくなると切断機構が働くようになる. このように拡散の関与がないと考えられる低温においても, 歪速度の違いにより変形機構が異なることは, 切断に要する応力と by-pass に要する応力の歪速度依存性が異なることを示唆している.

Fig. 7 に, 切断機構が働いている合金と by-pass 機構が働いている合金の, 室温での降伏応力の歪速度による変化を示す. プロットは同一条件における 10 点の測定値の平均を示している. 図より, by-pass 機構が働いている合金では降伏応力は歪速度の変化によらずほぼ一定値をとるのに対し, 切断機構が働く合金では歪速度の増大と共に降伏応力はわずかに低下する傾向を示す. すなわち, 転位が δ' 相を切断するに要する応力は負の歪速度依存性をもつことがわかる.

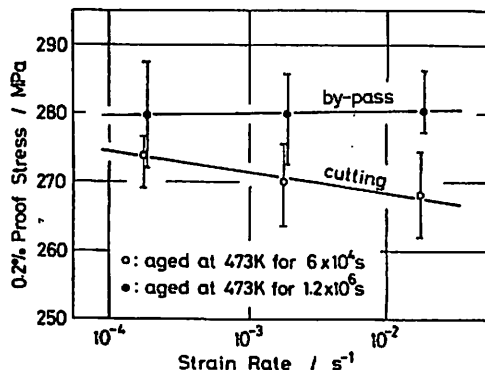


Fig. 7 The effect of strain rate on the 0.2% proof stress at the room temperature of Al-11.1 mol%Li alloy aged at 473 K for $6 \times 10^4 \text{ s}$ (○) and aged at 473 K for $1.2 \times 10^5 \text{ s}$ (●).

Fig. 8 は, 大小 2 つの歪速度に関して, 降伏応力の時効時間および試験温度による変化を模式的にまとめたものである. 図には, 歪速度が小さい場合を太線で, 歪速度が大きい場合を細線で示した. 時効時間の経過に伴い δ' 析出量が増加するため, 転位が δ' 相を切断するに要する応力は時効時間と共に上昇し, また正の温度依存性により試験温度の上昇と共に上昇する. さらに高温になると, 前報⁽⁷⁾ に示したように超格子転位による切断機構は働かず, 単一転位による析出粒子の乗り越え機構が支配的となり軟化する. 正の温度依存性が存在する温度範囲は, 歪速度が大きくなるにつれて高温側へ広がる. 一方, 転位が δ' 相を by-pass するに要する応力は, 時効時間の経過に伴う粒子

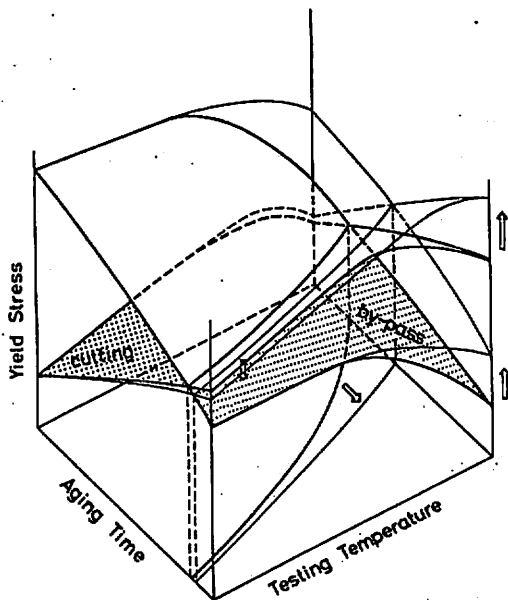


Fig. 8 Schematic representation of the effect of strain rate on the variation of the mechanism of interaction between δ' -precipitates and dislocations with aging and testing temperature.

間隔の増大と共に下降する。その降伏応力は、低温領域では温度変化によらずほぼ一定値を示すのに対し、高温では転位が上昇運動により粒子を乗り越える機構が働き出し、温度上昇と共に単調に減少する。

各時効状態および各試験温度での降伏応力は、切断に要する応力と by-pass に要する応力を示す 2 つの面のうち下方の面により決まる。両者の交線は時効曲線のピークの位置と一致することは前報⁽⁹⁾に示した。 δ' 相の切断に要する応力は Fig. 7 に示されているように負の歪速度依存性をもつので、低温においてもピークの位置は歪速度の増大と共にわずかに長時間時効側へ移行するものと推測される。Fig. 3 から、降伏応力の歪速度依存性は、473 K 付近では時効の進行と共に大きくなるのが明らかである。したがって、Fig. 8 の切断機構による曲面は、高温では長時間時効ほど歪速度の増大と共に上方(高降伏応力側)に移行することになる。その結果、切断機構と by-pass 機構の曲面の交線と与えられる時効曲線のピークの位置は、高温では歪速度の増大と共に長時間時効側へ移行するものと考えられる。

V. 総 括

種々の時効段階の Al-11.1 mol%Li 合金について、77 K ~ 523 K の各温度で、 $1.77 \times 10^{-4} \text{ s}^{-1}$ ~ $1.77 \times 10^{-2} \text{ s}^{-1}$ の歪速度により圧縮試験を行い、変形によって導入された転位組織を透過電子顕微鏡によって観察した結果、以下のことが明らかとなった。

(1) すべての時効段階において、373 K 以下の試験温度では降伏応力の歪速度依存性は小さく、ほぼ一定値とな

る。373 K 以上では、降伏応力は歪速度の増大と共に上昇し、降伏応力と歪速度の対数は直線関係を持つ。その直線の傾きは温度上昇と共に大きくなる。

(2) 焼入れ状態から最高強度に到る時効段階の合金では、降伏応力の正の温度依存性が存在する領域が、歪速度の増大に伴い高温側へ広がる。降伏応力に正の温度依存性が存在するときは、超格子転位対による δ' - Li_2 規則相粒子の切断機構が働いている。それ以上の温度では単一転位による粒子の by-pass および乗り越え機構が働いている。

(3) 過時効合金では、単一転位による析出粒子の by-pass 機構が働いている。373 K 以下では、剛性率で補正した降伏応力は試験温度によらずほぼ一定値を示す。373 K 以上では、歪速度が一定なら降伏応力は温度の上昇と共に単調に低下する。

(4) 拡散の関与がない低温において、超格子転位対の析出粒子切断に要する応力はわずかに負の歪速度依存性をもつ。一方、by-pass に要する応力は、低温では歪速度に依存せず一定である。

(5) 時効曲線のピークの位置は、拡散の関与がない低温では歪速度によらずほぼ同じであるが、高温では歪速度の増大と共に長時間時効側へ移行する。

終りに、本研究を行うにあたり、試料の一部を提供していただいた住友軽金属工業(株)技術研究所、ならびにヤング率測定に協力していただいた三菱重工業(株)長崎研究所に感謝致します。また、本研究の一部は文部省科学研究費補助金(58550473)および軽金属奨学会の助成によることを記し、謝意を表します。

文 献

- (1) E. A. Starke, Jr. and T. H. Sanders, Jr.: *Journal of Metals*, **33**(1981), 24.
- (2) 古川 稔, 美浦康宏, 根本 実: *日本金属学会会報*, **23**(1984), 172.
- (3) 蔵元英一: *日本金属学会会報*, **14**(1975), 567.
- (4) 竹内 伸: *日本金属学会会報*, **18**(1979), 249.
- (5) 鈴木朝夫: *日本金属学会会報*, **21**(1982), 19.
- (6) M. Tamura, T. Mori and T. Nakamura: *Trans. JIM*, **14**(1973), 355.
- (7) 古川 稔, 松井昭彦, 美浦康宏, 根本 実: *日本金属学会誌*, **48**(1984), 1068.
- (8) S. M. L. Sastry and J. E. O'Neal: *Aluminum-Lithium Alloy II*, Ed. by E. A. Starke, Jr. and T. H. Sanders, Jr., *Met. Soc. AIME*, (1983), 79.
- (9) 古川 稔, 松井昭彦, 美浦康宏, 根本 実: *軽金属*, **35**(1985), 3.
- (10) 佐野 毅, 西原良一, 四本晴夫, 美浦康宏, 根本 実: *九州大学工学集報*, **56**(1983), 491.
- (11) 古川 稔, 中村 誠, 美浦康宏, 根本 実: *九州大学工学集報*, 投稿中.
- (12) B. Noble, S. J. Harris and K. Harlow: *Aluminum-Lithium Alloy II*, Ed. by E. A. Starke, Jr. and T. H. Sanders, Jr., *Met. Soc. AIME*, (1983), 65.
- (13) J. Th. M. De Hosson, A. Huis in't Veld, H. Tamler and O. Kamert: *Acta Met.*, **32**(1984), 1205.

- (14) E. Orowan : *Symposium on Internal Stresses in Metals*, Institute of Metals, London, (1948), 451.
 - (15) G. R. Leverant, M. Gell and S. W. Hopkins: *Mater. Sci. Eng.*, **8** (1971), 125.
 - (16) R. S. W. Shewfelt and L. M. Brown : *Phil. Mag.*, **30** (1974), 1135.
 - (17) F. J. Humphreys, P. B. Hirsch and D. Gould : *Proc. 2nd Int. Conf. on Strength of Metals and Alloys*, ASM, (1970), 550.
 - (18) G. Dorey : *Royal Aircraft Establishment*, Tech. Rep. No. 65126, (1965).
 - (19) G. Dorey : *Royal Aircraft Establishment*, Tech. Rep. No. 65126, (1968).
 - (20) L. M. Brown and R. K. Ham: *Strengthening Methods in Crystals*, Ed. by A. Kelly and R. B. Nicholson, Elsevier, (1971), 9.
 - (21) R. S. W. Shewfelt and L. M. Brown : *Phil. Mag.*, **35** (1977), 945.
-

Al-Li合金の熱処理中の脱 Li

植田 洋史* 松井 昭彦* 古川 稔**
美浦 康宏*** 根本 実***

J Japan Inst. Metals, Vol. 49, No. 7 (1985), pp. 562-568

Lithium Loss during Heat Treatment of an Al-Li Alloy

Hiroshi Ueda*, Akihiko Matsui*, Minoru Furukawa**,
Yasuhiro Miura*** and Minoru Nemoto***

Measurements were made of lithium loss in an Al-3.12 mass%Li alloy during the solution treatment at high temperatures under varied atmospheres. The microstructure and the hardness distribution in the surface layer of the alloy were highly sensitive to the temperature, the period and the atmosphere of solution treatment. A considerable amount of lithium was lost in the layer within 0.3 mm from the surface during the solution treatment in this study. Lithium loss during the solution treatment at 823 K for 3.6-36 ks was minimized by Ar gas sealing. The activation energy of diffusion of lithium in aluminum was estimated at 130 kJ/mol from the analysis of the hardness distribution curves. The process of lithium loss during the solution treatment in dynamic vacuum is considered to be controlled by the diffusion of lithium atoms toward the surface from the inside of the crystal.

(Received October 17, 1984)

Keywords: aluminum-lithium alloy, lithium loss, heat treatment, diffusion of lithium, precipitation hardening, ordered precipitates

I. 緒 言

リチウム (Li) は比重が 0.53 であり、金属元素としては最も軽い。Al に Li を添加すると、比重が低下する一方、弾性率および強度が上昇する⁽¹⁾。最近、Li を添加した航空機用高比強度 Al 合金の開発に期待が寄せられている⁽²⁾。また、Al に Li を添加すると比抵抗が増大し誘導電流が少なくなること、および放射化された後の放射能の減衰が速い⁽³⁾ことなどから、Li を含む Al 合金は、核融合炉壁材料としても注目されはじめている⁽⁴⁾。

Al-Li 系合金の基本系である Al-Li 2 元合金は、準安定相 (δ' -Al₃Li 相, L1₂ 型規則格子) の析出による時効硬化性があり、これまでに機械的性質や時効析出挙動に関して多くの研究がなされてきた⁽⁵⁾⁻⁽⁹⁾。しかし、Li は反応性が極めて高く、蒸気圧も高いので、本系合金は実用上つぎのような問題を有していると考えられる。その第一は、合金溶解時の雰囲気およびるつぼとの反応による脱 Li と不純物元素の混入、第二は、熱処理中の脱 Li、第三は、Li 添加による耐食性の劣下などである。このうち溶解時の雰囲気

やるつぼ材との反応および耐食性については、従来から問題とされ、対策が講じられてきているが⁽¹⁰⁾⁽¹¹⁾、熱処理中の脱 Li についてはほとんど注目されていない。Al 合金の熱処理中の溶質元素損失に関する報告は少ないが、いままでに、Al-Mg 合金や Al-Zn 合金などにおいては、大気および真空雰囲気での熱処理中に溶質損失が生じる結果、強度や組織に変化が起こることが知られている⁽¹²⁾⁻⁽¹⁴⁾。

本研究では、Al-Li 2 元合金の熱処理時、とくに高温における溶体化処理時の脱 Li が、この合金の時効組織と強度にどのような影響を及ぼすかを調べ、最適熱処理条件を見出すことを目的とした。

II. 実験方法

1. 試料作製

高純度 Al (99.99 mass%) および高純度 Li (99.2 mass%) を Ar 気流中でアルミなるつぼを用いて溶解し、大気中で金型に鋳込み、熱間および冷間圧延により幅 150 mm、厚さ 3 mm の合金板とした。合金板の平均化学組成を Table

* 九州大学大学院生 (Graduate Student, Kyushu University, Fukuoka)

** 福岡教育大学教育学部技術科 (Department of Technology, Faculty of Education, Fukuoka University of Education, Munakata)

*** 九州大学工学部冶金学科 (Department of Metallurgy, Faculty of Engineering, Kyushu University, Fukuoka)

Table 1 Chemical composition of specimen. (mass%)

Li	Fe	Si	Mg	Al
3.12	0.0073	0.029	0.0045	Bal.

に示す。ここで 3.12 mass% は 11.1 mol% に相当する。マイクロカッターにより塊状試料 (3 mm × 3 mm × 10 mm) および薄板試料 (3 mm × 0.3 mm × 20 mm) を切り出した。また、溶体化処理前にエメリー紙による研摩を行い、さらに電解研摩によって表面を平滑にした。

2. 熱 処 理

Fig. 1 に Al-Li 2 元状態図⁽¹⁾を示す。α-δ 共晶温度は 873 K であり、この温度における Al 中への Li の固溶度は約 14 mol% である。状態図に基づき、本実験では溶体化温度として 823 K を選定した。溶体化時間は 3.6, 10.8, 18, 36 ks とし、溶体化後水中に急冷した。比較した溶体化雰囲気は、(1) バイレックスガラス管への真空封入 (10⁻² Pa 台)、(2) バイレックスガラス管への Ar ガス封入 (約 1 Pa の真空に排気後 Ar ガス置換によって管内を浄

管を挿入し、内部を真空に排気して行い、大気中熱処理および封入試料の熱処理は石英管の両端を開放して行った。脱 Li 機構の検討のために、動的真空中、823, 853, 883 K で、3.6, 10.8, 18, 36 ks 溶体化した。一部の試料については溶体化後ガラス管中に Ar ガス封入し、473 K, 60 ks 時効した。この時効条件下で本 2 元合金はほぼ最大硬さに達することが知られており⁽¹⁵⁾、本研究結果が示すように Ar ガス封入すれば 473 K 時効処理中の脱 Li はほとんど無視できる。

3. 脱 Li 量測定と透過電子顕微鏡 (TEM) 観察

脱 Li 量は、原子吸光分析法による平均濃度測定、斜め切断面についてのマイクロピッカース硬さ測定 (荷重 0.98 N) および TEM 観察により評価した。

TEM 観察用試料作製のために、マイクロカッターにより 0.3 mm 厚の薄板を試料の所定の位置から切り出し、エメリー紙により約 0.2 mm 厚まで研摩し、ツイングジェット電解研摩装置を用いて観察用薄膜とした。電解研摩液は、過塩素酸 + エチルアルコール (1 : 4) である。観察には九州大学超高压電子顕微鏡室の JEM 1000D 電子顕微鏡 (加速電圧 1000 kV) を使用した。

III. 実 験 結 果

1. 脱 Li に及ぼす溶体化条件の影響

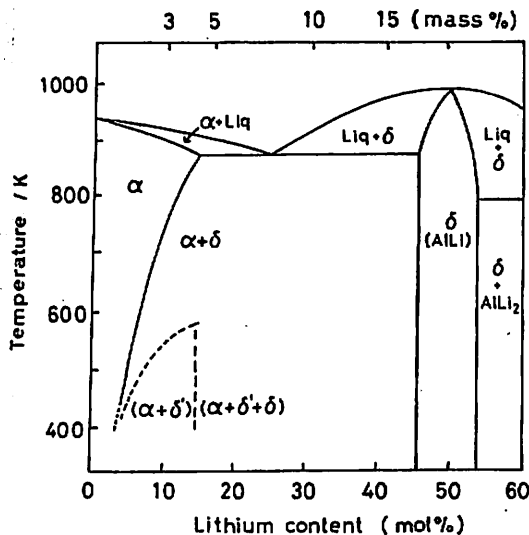
Table 2 に真空封入および Ar ガス封入した試料を 823 K, 10.8 ks, および 36 ks 溶体化後急冷した試料の Li 濃度を原子吸光分析により調べた結果を示す。塊状試料については試料長手方向の中央部で垂直に切り出した約 50 mg

Table 2 Lithium contents of specimens solution treated in different atmospheres. (mass%)

Atmosphere	Specimen shape	Li content	
		t=10.8 ks	t=36 ks
Vacuum sealed	block plate	2.66	2.46
		1.84	0.10
Ar gas sealed	block plate	3.13	3.07
		3.03	2.73

の薄片の平均濃度を示し、薄板試料については全体 (約 50 mg) の平均濃度を示している。溶体化処理後には、塊状試料より薄板試料の方が脱 Li 量は明らかに多く、短時間溶体化した場合より長時間溶体化した場合の方が多。また、この結果から、真空封入より Ar ガス封入した場合の方が脱 Li 量が少ないことがわかる。つぎに真空封入した試料および Ar ガス封入した試料の表面硬度値の溶体化時間による変化を Fig. 2 に示す。図から、真空封入した試料は Ar ガス封入した試料より硬度の低下が著しいことが明らかである。また、真空封入では最初の 3.6 ks 以内での脱 Li 量が多いことがわかる。

Fig. 3 および Fig. 4 に塊状試料と薄板試料を、それぞ

Fig. 1 Al-Li binary phase diagram⁽¹⁾.

化し、さらに溶体化温度ではほぼ 10⁵ Pa になる量の Ar ガスとともに封入、(3) 動的真空 (油拡散ポンプによる 10⁻² Pa 台の連続排気)、および (4) 大気中、の 4 種類である。(1) (2) におけるガラス管の内径は 6 mm、長さは 30 mm である。ガラス管は、焼入れの際、瞬時に割れるため試料は十分に急冷され、かつ試料と大気との接触時間もわずかである。また動的真空中からの急冷に際しては、Ar ガスを炉中に導入した後試料を炉外に引き出して急冷することにより、試料と大気との接触時間が最短となるように注意した。熱処理には、823 K における均熱部が約 50 mm の横型ニクロム巻線炉を使用した。また、動的真空中熱処理は、抵抗炉中に内径 40 mm、長さ 800 mm の不透明石英

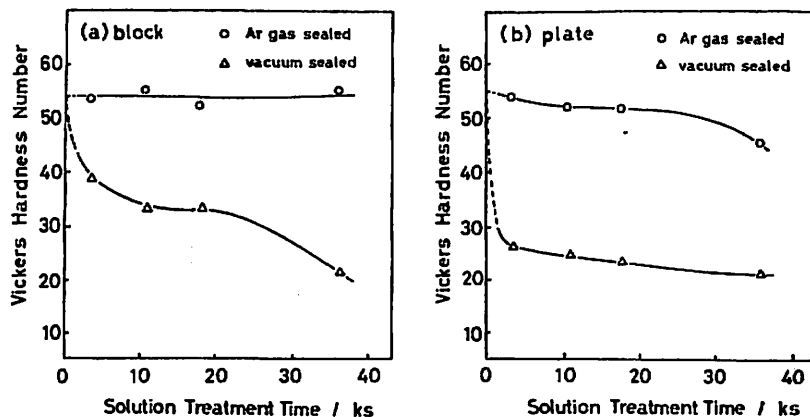


Fig. 2 Vickers hardness as a function of solution treatment time. (a) block and (b) plate.

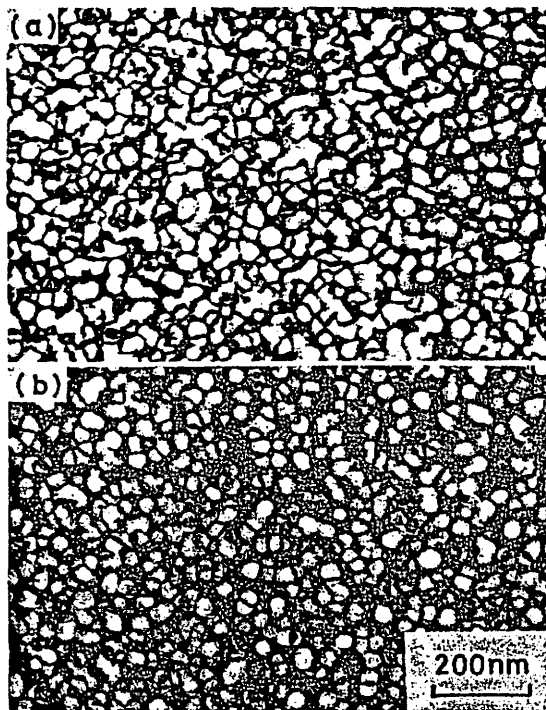


Fig. 3 (100) dark field images showing δ' -precipitates. Specimens were vacuum sealed, solution treated at 823 K for 10.8 ks and aged at 473 K for 60 ks. (a) block and (b) plate.

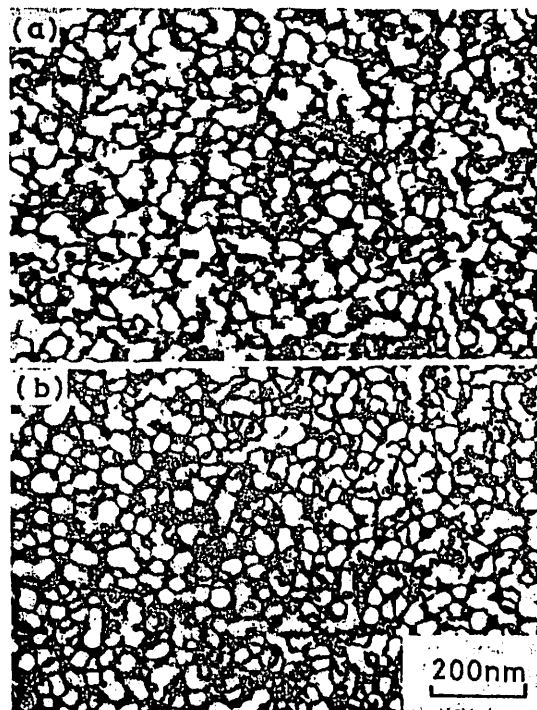


Fig. 4 (100) dark field images showing δ' -precipitates. Specimens were Ar gas sealed, solution treated at 823 K for 10.8 ks and aged at 473 K for 60 ks. (a) block and (b) plate.

れ真空封入および Ar ガス封入状態で溶体化後、さらに 473 K で 60 ks 時効した後の TEM 組織を示す。写真は (100) 規則格子反射を用いた暗視野像で、球状または不定形の白く見える相が δ' -Li₂ 型規則相析出粒子である。いずれも試料の中心部の組織を示す。各写真ともに 100 nm 程度の膜厚を有する部分を撮影したもので、塊状試料の中心部の組織には真空封入と Ar ガス封入とでほとんど差は認められないが薄板試料について比較すると真空封入の方が析出物の密度が明らかに低くなっている。また塊状試料と薄板試料を比較すると、薄板試料中の析出物密度が低く、析出物も球状に近づいていることが明らかである。 δ'

相は Li 濃度が高く母相中での密度が高いほど不規則形状に観察されることが知られており⁽¹⁵⁾、これら TEM 観察結果は、さきの原子吸光分析による測定結果と同様に、薄板試料の脱 Li 量は Ar ガス封入の場合より真空封入の場合の方が大きいことを示している。

2. 試料中の Li 濃度分布

Fig. 5 に塊状試料の溶体化処理後、急冷のまま、および 473 K、60 ks 時効後の表面から深さ方向の硬度分布を溶体化雰囲気別に示す。いずれの場合も試料中心部の硬度は、ほぼ等しく、脱 Li は中心部には逆していないことがわか

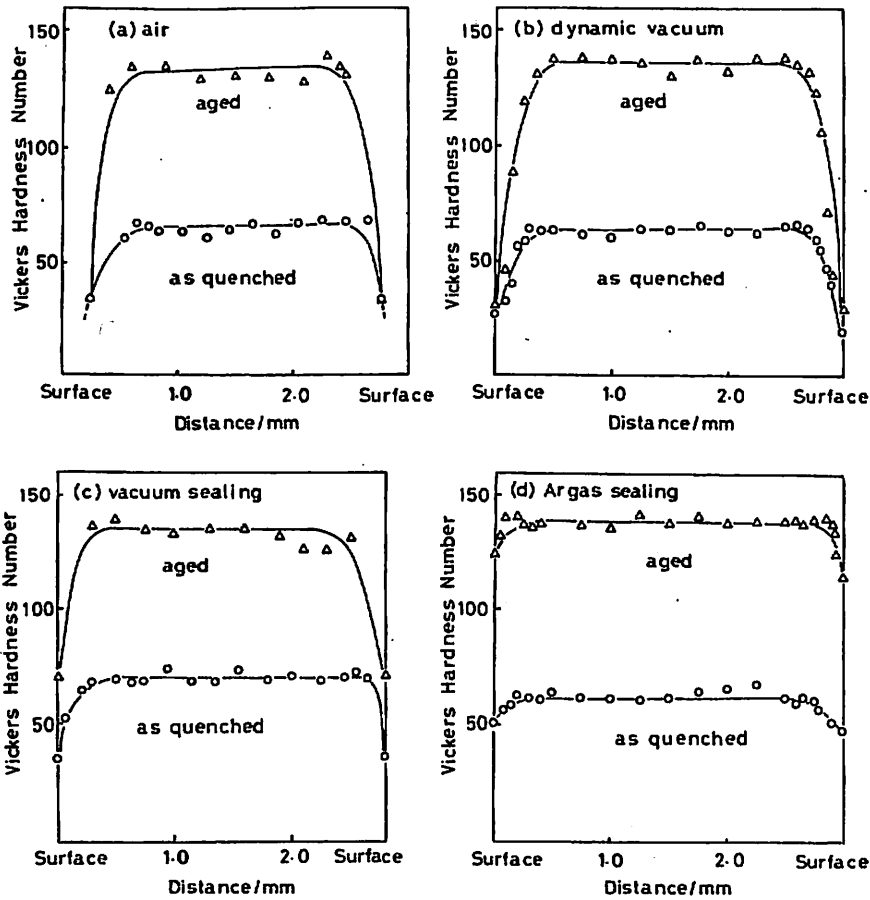


Fig.5 Variation of Vickers hardness with the distance from the surface. Specimens were solution treated at 823 K for 10.8 ks, iced water quenched and aged at 473 K for 60 ks. (a) in air, (b) in dynamic vacuum, (c) vacuum sealing and (d) Ar gas sealing.

るが、試料表面付近の硬度に大きな差が認められる。

大気中で溶体化した試料 (a) は、表面に凹凸が生じ、直接硬さを測定することが不可能であったため、両表面からそれぞれ約 0.2 mm 厚の層をエメリー紙による研磨および電解研磨によって除いた。この試料では、溶体化処理後、急冷のままの状態および時効後においても、表面から約 0.5 mm までの硬度低下が著しく、表面付近での時効硬化性がほとんど失われている。このことは溶体化処理中に表面層での Li 濃度が時効温度 (473 K) における固溶限以下まで低下していることを示している。動的真空中 (b) では、表面付近での時効硬化性はわずかに見られるものの、全般に脱 Li 量が多い。また、真空封入した場合 (c) は、動的真空中に比べて表面付近での時効硬化性がさらに高くなっていることが注目される。Ar ガス封入した場合 (d) は、表面近くでやや硬度が低下しているが、その程度は (a), (b), (c) に比べて小さく脱 Li 量が少ないことが明白である。

Fig.6 および Fig.7 は、それぞれ動的真空中および Ar ガス封入状態で溶体化処理の後、さらに時効した試料の、表面層と中心部から採取した薄膜の端付近 (写真の左側が

端) の TEM 組織を示す。動的真空中で処理した試料では、表面層の析出物の量が明らかに減少している。一方、Ar ガス封入の場合は析出物の分布が表面層と中心部とでほとんど差がなく、全体に高密度である。これらの観察結果は硬度分布測定結果と対応している。

Csanády ら⁽¹²⁾ は、真空中処理した場合に比べて大気中処理した場合の方が、Al-Zn, Al-Mg 合金などの表面近傍に Zn あるいは Mg に著しく富む層が形成されることを XMA による測定により見出している。Al-Li 合金の場合は、上述の結果が示すように、Li 濃度が高い領域の形成は認められない。

IV. 考 察

1. 溶体化処理中の脱 Li

薄板の内部から拡散してきた Li 原子が表面で蒸発する場合、薄板内部の Li 濃度、 $C(x, t)$ は次式⁽¹⁶⁾で与えられる。

$$C(x, t) = \frac{4C_0}{\pi} \sum_{i=0}^{\infty} \frac{1}{2i+1} \sin\left(\frac{2i+1}{h}\pi x\right) \times \exp\left[-\left\{\left(\frac{2i+1}{h}\right)\pi\right\}^2 Dt\right] \quad (1)$$

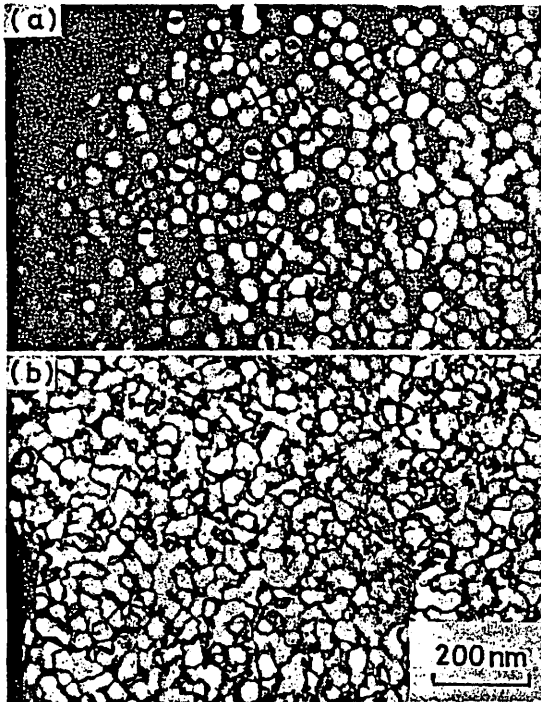


Fig. 6 (100) dark field images showing δ' -precipitates. Specimens were solution treated in dynamic vacuum at 823 K for 10.8 ks and aged at 473 K for 60 ks. (a) surface layer and (b) internal area.

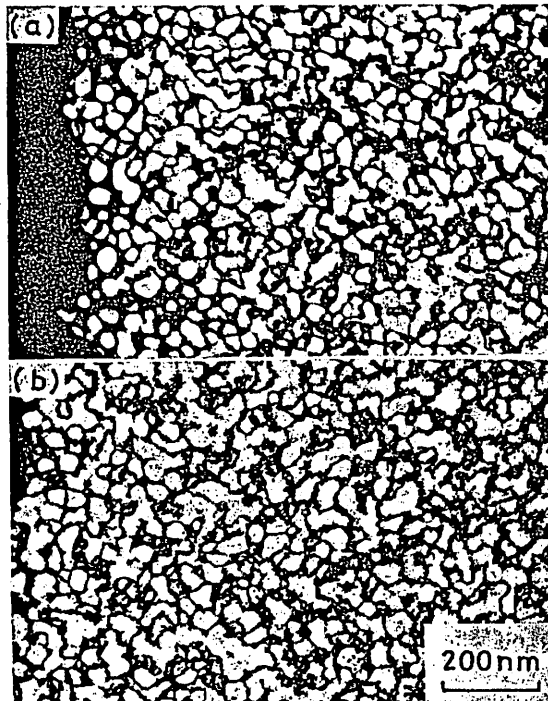


Fig. 7 (100) dark field images showing δ' -precipitates. Specimens were Ar gas sealed, solution treated at 823 K for 10.8 ks and aged at 473 K for 60 ks. (a) surface layer and (b) internal area.

ここで、 x は表面からの深さ、 t は時間、 h は薄板の厚さ、 C_0 は初期濃度、 D は Al 中の Li の拡散係数である。Costas⁽¹⁷⁾によれば、690~870 K において、

$$D = 4.5 \times 10^{-4} \exp\{-139.3 (\text{kJ/mol})/RT\} \text{m}^2 \text{s}^{-1} \quad (2)$$

である。ここで、 R は気体定数、 T は温度である。

式(1)、(2)を用いて薄板試料 ($h=0.3 \text{ mm}$) の溶体化後、表面から深さ方向の濃度、 $C(x, t)$ を計算した結果を Fig. 8(a) に示す。図から薄板の場合は脱 Li が著しく、溶体化時間が 36 ks と長くなると、中心部まで Li は失われることが予測される。

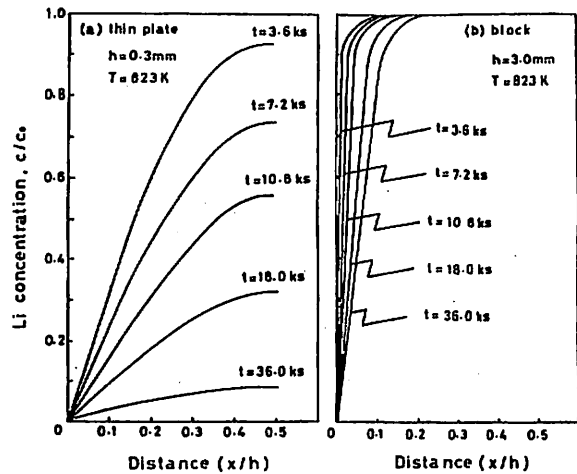


Fig. 8 Calculated lithium concentration as a function of the distance (x/h) from the surface.

(a) plate and (b) block.

塊状試料の場合、すなわち Li の拡散距離に比べて厚さ h が大きい場合、式(1)の級数解では収束が遅い⁽¹⁸⁾。したがって塊状試料の場合は、試料中心部の Li 濃度を不変 ($=C_0$) として得られる単純な次式を用いた。

$$C(x, t) = C_0 \operatorname{erf}(x/\sqrt{2Dt}) \quad (3)$$

この式による計算結果を Fig. 8(b) に示す。この図から塊状試料の場合は、溶体化時間が 36 ks の範囲で、表面から約 0.3 mm の深さまでの領域における脱 Li が著しいことが予測される。

Fig. 9 は動的真空中で溶体化後、473 K、60 ks 時効した塊状試料の表面層における硬度分布を、斜め切断法により測定した結果である。(a)、(b)、(c)は、溶体化温度がそれぞれ 823、853、883 K の場合である。溶体化時間は 3.6、10.8、36 ks の 3 通りである。溶体化温度が一定であれば溶体化時間が長いほど、また溶体化時間が一定であれば溶体化温度が高いほど、表面から深い領域まで硬度の低下が及んでいる。また、これらの硬度分布曲線には表面近くで勾配が急変する点が見られ、その後内部で硬度は急激に上昇している。Fig. 9(a) 中の点線は式(3)による計算値を示すもので、 H/H_0 が C/C_0 に比例するものと仮定した(ただし H は時効後の表面から深さ方向の各位置における硬度、 H_0 は試料中心部の硬度である)。実験で得られた硬度分布

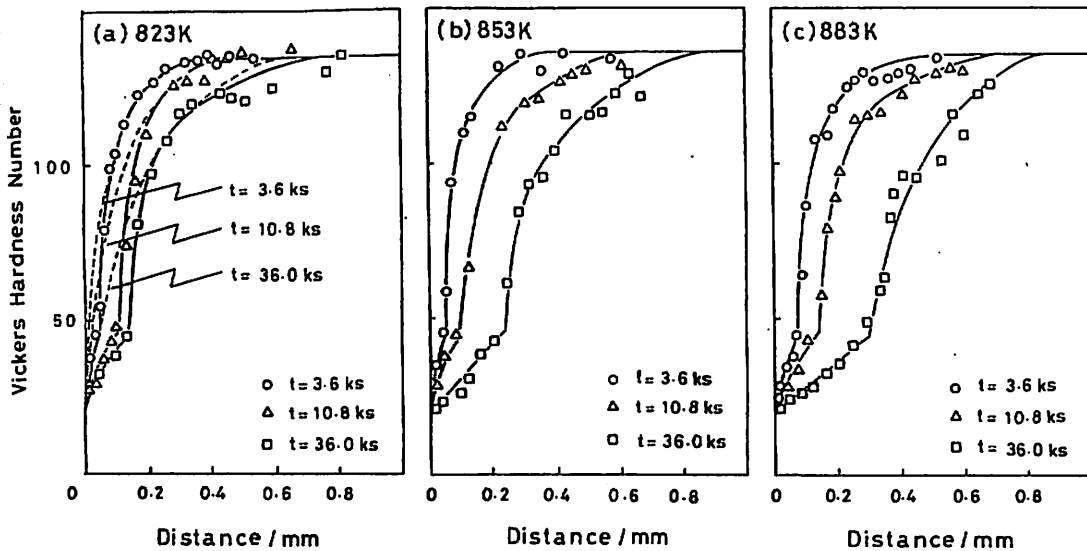


Fig.9 Variation of Vickers hardness with the distance from the surface. Specimens were solution treated in dynamic vacuum at 823 K (a) ,853 K (b) or 883 K (c) for 3.6 ks, 10.8 ks or 36 ks and aged at 473 K for 60 ks.

曲線には勾配が急変する点があるなど細部では計算値と一致しないが、この図は溶体化中の脱 Li 過程が Li の拡散によって律速されることを示唆している。

2. 脱 Li 反応の律速過程

Fig.9 に示したように、動的真空中で溶体化後時効した試料の表面から深さ方向の硬度分布曲線は、2段階に分れている。この事は、固溶硬化のみが働いている層と、さらに析出硬化の働きが加算された層の2層が形成されていると考えると理解できる。すなわち、ごく表面層では、脱 Li が著しく、残存 Li 量が時効温度(473 K)における固溶限以下に低下したため、Li による固溶硬化分のみが硬度に反映されていると考えられる。試料の内部に入るとして、残存 Li 濃度が高くなり δ' 相の析出量が増す。

この領域の硬度は、Li による固溶硬化に δ' 相による析出硬化が加わることになる。Fig.10 は以上のことを模式的に表したものである。したがって Fig.9 における各硬度分布曲線の勾配が急変している点は、Li 濃度が 473 K における Al 中への Li の固溶限 ($C_0=5.6 \text{ mol}\%$) に達している位置に対応すると見なすことができる。 $C_0=11.1 \text{ mol}\%$ 、 $C=5.6 \text{ mol}\%$ とし、式(3)に t =溶体化時間、 x =表面から勾配が急変する点までの距離を代入すれば、各温度における拡散係数、 D が得られる。Fig.11 は得られた D の値を $1/T$ に対してプロットしたものである。最小2乗法によって活性化エネルギーを求めると、約 130 kJ/mol となる。Al 中の Li の拡散の活性化エネルギーの値としては、139.3 kJ/mol⁽¹⁷⁾あるいは 119.2 kJ/mol⁽¹⁹⁾が報告されている。本実験で得られた値は、実験の精度を考慮すれば文献値に近いと判断される。このことと Fig.9 の結果とを考慮すると、溶体化処理中の脱 Li 反応が表面反応ではなく

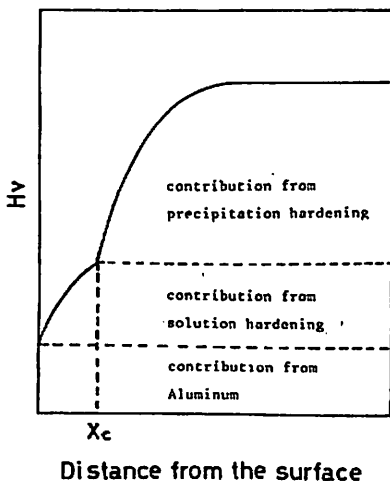


Fig.10 Schematic diagram showing variation of hardness with the distance from the surface.

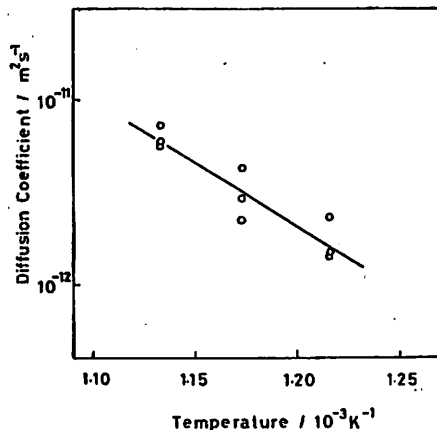


Fig.11 A plot of $\ln D$ against $1/T$.

Al 中の Li の拡散によって支配されていると結論できよう。

最近 Abd El-Salam らは、低濃度 Al-Li 合金 (Al-2.5 mol%Li) を大気中で高温に加熱した際の脱 Li についての実験結果を報告している⁽²⁰⁾。彼らは、熱膨張測定結果から算出した脱 Li 過程の見かけの活性化エネルギーが約 27 kJ/mol (6.44 kcal/mol) であり、この値が Al 中の Li の拡散の活性化エネルギーよりはるかに小さいことから、脱 Li 過程が表面反応に律速されていると結論している。本実験で用いた 11.1 mol%Li 合金を大気中処理すると、表面に凹凸が生じ、表面付近の硬さ分布の精密な測定は不可能であった。したがって律速過程の差異の原因説明は困難であった。しかし両実験共に Al-Li 合金を大気中高温で熱処理した場合には脱 Li がきわめて大きいことを示している。

3. 脱 Li に及ぼす雰囲気の影響

Al-Li 合金を高温に保持している間の脱 Li には、表面での Li の酸化および窒化⁽²¹⁾と表面からの Li の蒸発とが原因として考えられる。いずれの場合も試料内部から表面への Li の拡散がおこる。

本実験における Ar ガス封入と真空封入の場合の差は、単に酸化や窒化のみでは説明できず、表面からの Li の蒸発が主な原因となっていることを示している。Li の蒸気圧⁽²²⁾は、810 K で 1.33 Pa, 900 K で 13.3 Pa とかなり高く、熱処理中に表面層から Li が蒸気として放出される。封入した場合には、Li 蒸気がガラス管内での平衡圧に達すると放出が止まる。しかし、本実験において真空封入した場合、高温長時間溶体化後バイレックスガラス管壁と Li との反応も認められた。このような場合には、Li の放出は止まらず、単純な平衡蒸気圧のみでは脱 Li 量が定められない。一方 Ar ガス封入の場合にはバイレックスガラス管との反応はわずかしき認められなかった。これは、Li の蒸発速度が Ar ガスの存在によって影響され、真空封入の場合より小さくなるためであると考えられる。また、バイレックスガラス管の代りに石英管を用いると、管壁と Li との反応が著しくなる傾向が認められたが、封入管と Li との反応については本研究では詳しい検討は行わなかった。動的真空状態では、真空ポンプによって Li 蒸気は常に吸引されるため、平衡圧に達することなくその放出は続く。一方大気中あるいは低真空度の雰囲気中で高温保持した場合には、蒸発のみではなく酸化などの表面反応が脱 Li の原因となると考えられる。

V. 総 括

Al-3.12 mass%Li 合金の溶体化処理時の表面からの脱 Li に及ぼす溶体化雰囲気、温度、時間の影響を調べた結果、以下の結論が得られた。

(1) Al-Li 合金の表面近傍の組織と強度は、溶体化処理雰囲気、温度および時間により大きく変化する。

(2) 本系合金で用いられる通常の溶体化処理条件下では試料の表面から約 0.3 mm の深さの領域における脱 Li が著しい。したがって薄板試料の熱処理の際には、脱 Li 効果を十分考慮する必要がある。

(3) 823 K, 3.6~36 ks 溶体化処理時の脱 Li 量は Ar ガス封入によって大幅に軽減される。

(4) 本実験によって求められた Al 中の Li の拡散の活性化エネルギーは約 130 kJ/mol であり、文献値にはほぼ一致する。このことは動的真空中での溶体化処理中の脱 Li 過程が、試料内部から表面への Li の拡散によって律速されることを示唆している。

試料分析に際して協力と援助をいただいた上村治男氏に感謝します。なお、本研究の一部は、文部省科学研究費補助金(課題番号 58550473)および軽金属学会研究補助金に依るものである。

文 献

- (1) B. Noble, S. J. Harris and K. Dinsdale : J. Mat. Sci., 17 (1982), 461.
- (2) E. A. Starke, Jr., T. H. Sanders, Jr. and I. G. Palmer : J. Metals, 33 (1981), 24.
- (3) Alcoa Tech. Cent. Rep., AP-220 Res. Project 1045-1, Feb., 1982.
- (4) 核融合材料委員会：核融合材料としてのアルミニウム合金，軽金属協会，(1984)。
- (5) J. M. Silcox : J. Inst. Metals, 88 (1959-60), 357.
- (6) T. Yoshizawa, H. Hasebe and M. Mannami : J. Phys. Soc. Japan, 25 (1968), 908.
- (7) 田村 学，森 勉，中村正久：日本金属学会誌，34 (1970)，919。
- (8) B. Noble and G. E. Thompson : Met. Sci. J., 5 (1971), 114.
- (9) D. B. Williams and J. W. Edington : Met. Sci. J., 9 (1975), 529.
- (10) D. Webster : Aluminum-Lithium Alloys, Ed. by T. H. Sanders and E. A. Starke, Met. Soc. AIME, (1981), p. 228.
- (11) W. R. D. Jones and P. P. Das : J. Inst. Metals, 87 (1958-59), 338.
- (12) Á. Csanády and V. Stefániay : Mat. Sci. Eng., 38 (1979), 55.
- (13) D. K. Chatterjee and K. M. Entwistle : J. Inst. Metals, 101 (1973), 53.
- (14) K. Forsvoll and D. Foss : Phil. Mag., 15 (1967), 329.
- (15) 古川 稔，松井昭彦，美浦康宏，根本 実：軽金属，35 (1985)，1。
- (16) P. G. Shewmon : Diffusion in Solids, McGraw-Hill, (1963), p. 17.
- (17) L. P. Costas : U.S. AEC Rep. TID-16676, 1963.
- (18) 菅野幹宏，鈴木 寿：軽金属，30 (1980)，653。
- (19) C. J. Wen, W. Weppner, B. A. Boukamp and R. A. Huggins : Met. Trans., 11B (1980), 131.
- (20) F. Abd El-Salam, A. I. Eatah and A. Tawfik : Phys. Status Solidi (a), 75 (1983), 379.
- (21) 例えば，小林正夫：日本鉱業会誌，100 (1984)，115。
- (22) R. E. Honig : RCA Rev., 23 (1962), 567.

Al-Li 2 元合金のヤング率の温度依存性

古川 稔*・中村 誠**
美浦 康宏***・根本 実***

Temperature Dependence of Young's Modulus of Al-Li Alloy

Minoru FURUKAWA, Makoto NAKAMURA, Yasuhiro
MIURA and Minoru NEMOTO

(Technology Reports of the Kyushu University Vol. 58, No. 5, October 1985)

Young's modulus of aged Al-11.1 mol% Li alloy was measured at temperatures between 290 and 423 K by a resonant frequency method. Addition of 11.1 mol% lithium to pure aluminum increases the modulus by 17% at room temperature. The modulus of the Al-Li alloy varies with aging time, indicating the dependence on the volume fraction, size and spacing of the δ' -particles, and decreases by 7% with increasing temperature from 290 to 423 K. The temperature dependence of the modulus is nearly equal to those of pure aluminum and commercial aluminum alloys.

1. 緒 言

Al-Li 合金は、高比強度・高比弾性率の航空機材料として注目され、広範な実用化が期待されている¹⁾。Al-Li 2 元合金の析出過程については、過飽和固溶体 $\rightarrow\delta'$ (Al₃Li) $\rightarrow\delta$ (AlLi) の過程を経ることがほぼ確定しており²⁻⁶⁾、 δ' 相の析出により硬化する。 δ' 相は母相と完全に整合な L1₂ 型規則構造をもつ球状の準安定相であり、 δ 相は過時効段階で形成される B32 (NaTl) 型規則構造の粗大な安定相である。

著者らはさきに、Al-Li 2 元合金の析出強化と変形機構をしらべ⁹⁾、さらに 77 K から 523 K の温度域での強度と変形機構の温度依存性⁷⁾ および歪速度依存性⁸⁾ について検討し、Al-Li 合金の強度と変形挙動は、ニッケル基超耐熱合金の場合と同様に L1₂ 型規則相の特性⁹⁻¹¹⁾ に強く依存していることを示した。したがって、Al-Li 合金は高温用アルミニウム合金としても注目され、強度の温度依存性に関してはすでいくつかの報告^{7,9,12)} がある。また、Al-Li 合金の室温におけるヤング率については、すでに比較的詳細な報告がなされている¹³⁾。しかし、その温度依存性については、井上ら¹⁴⁾ による 7.9 mol% Li 合金についての簡

単な報告があるのみである。

本研究の目的は、種々の時効状態の Al-Li 2 元合金について、室温から約 450 K の温度域でのヤング率の温度依存性を調べ、Al-Li 合金の機械的性質に関する基礎資料とし、さらにそれらの結果をこれまでに報告されている実用アルミニウム合金と比較検討することである。

2. 実験方法

高純度アルミニウム (99.99%) とリチウム (99.8%) をアルゴン気流中でアルミナるつぼを使用して溶解し、金型に鋳込み、リチウム濃度が 11.1 mol% の 2 元合金鋳塊を作製した。不純物濃度を分析した結果、鉄 0.0032 mol%、珪素 0.026 mol%、マグネシウム 0.0046 mol% であった。

鋳塊を熱間圧延および冷間圧延により厚さ 3 mm および 2 mm の 2 種類の板とし、これより長手方向が圧延方向と一致するように、それぞれ 3×3×4.7 mm³ の圧縮試験片と 2×10×80 mm³ のヤング率測定用試料を切り出した。試料をパイレックスガラス管中にアルゴンガスと共に封入し、823 K で 1.08×10⁴ s 溶体化処理した後、氷水中に焼入れた。つぎに再びガラス管中にアルゴンガスと共に封入し、473 K で種々の時間時効処理を行った。

時効処理後、77 K から 523 K の範囲でインストロン型試験機 (TOM/500) を用いて、歪約 4% まで圧縮

昭和 60 年 6 月 3 日 受理

* 福岡教育大学教育学部技術科

** 三菱重工(株)長崎研究所

*** 冶金学教室

試験を行った。77 K および 213 K における圧縮試験は、それぞれ液体窒素中およびドライアイスを入れたメチルアルコール中で行った。室温以上の圧縮試験はシリコンオイルを用いた恒温槽中に行い、変形後はただちに水中にて冷却した。1回の試験に要する時間は約 400s であった。

各時効状態の合金についての横振動型静電駆動法¹⁵⁾によるヤング率の測定には、Fig. 1 に示す形状と寸法の試験片を用いた。非磁性材料である Al-Li 合金を磁力で励振させるため、試験片の両端部に厚さ 0.2mm のパーマロイを貼り付け、また試験片を支持するための切り込みを入れた。測定は真空中で昇温しつつ連続的に行った。室温から 423 K までの測定に要した時間は約 5ks であった。また比較のために、99.99%アルミニウムのヤング率も測定した。

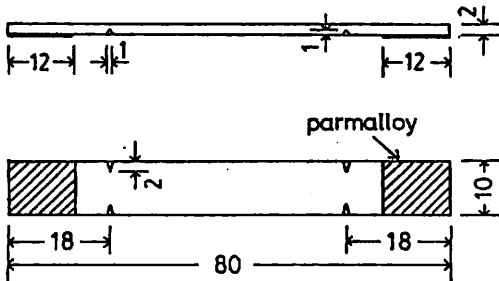


Fig. 1 Specimen shape. Shaded areas represent parmally.

時効析出組織を透過電子顕微鏡 (TEM) により観察するため、各時効処理を施した試料から厚さ 0.3mm の薄膜を切り出し、目視可能なツイーン・ジェット電解研磨装置¹⁶⁾により透過電顕観察用の薄膜を作製した。用いた電解研磨液の組成は、過塩素酸 20%-エチルアルコール 80%である。透過電子顕微鏡観察には、九州大学超高压電顕室の JEM1000D (加速電圧 1000kV) を用いた。

3. 実験結果および考察

3.1. 時効による Al-Li 合金の組織変化

Fig. 2 は、Al-11.1 mol% Li 合金を 823 K から急冷後 473 K で時効した場合に形成される δ' -Li₂ 規則相析出物の透過電子顕微鏡写真で、いずれも (100)Li₂ 規則相反射による暗視野像である。焼入れ状態 (a) ですでに不規則な形状をした Li₂ 規則相 δ' の均一な析出が認められ、時効時間の経過に伴い δ' 相の析出量が增大すると共にその形状も球形となっている。Fig.

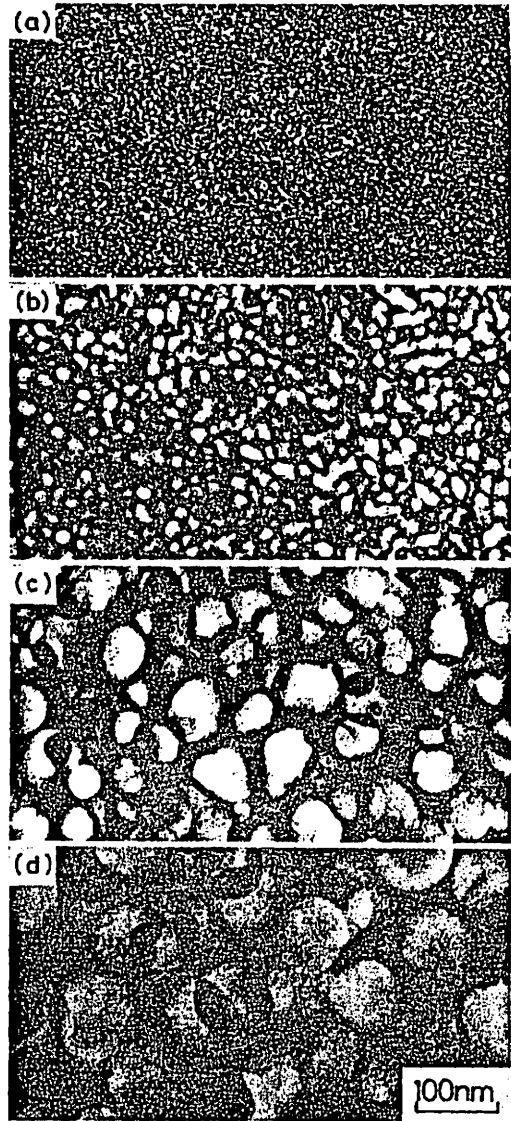


Fig. 2 (100) dark field images of Al-11.1 mol%Li alloy. (a) as-quenched, (b) aged at 473 K for 6×10^3 s, (c) aged at 473 K for 1.8×10^5 s and (d) aged at 473 K for 1.2×10^6 s.

3(a), (b) は、それぞれ重速度 $3.5 \times 10^{-4} \text{ s}^{-1}$ で圧縮試験を行った際の降伏応力 (0.2%耐力: $\sigma_{0.2}$) と電子顕微鏡によって測定した δ' 析出相の体積率の、473 K での時効時間による変化を示す。降伏応力は、時効時間の経過と共に上昇し、約 1.8×10^5 s 時効で最大値約 290 MPa に達した後に、過時効段階に入り下降している。降伏応力が最大値を示す時効段階では、Fig

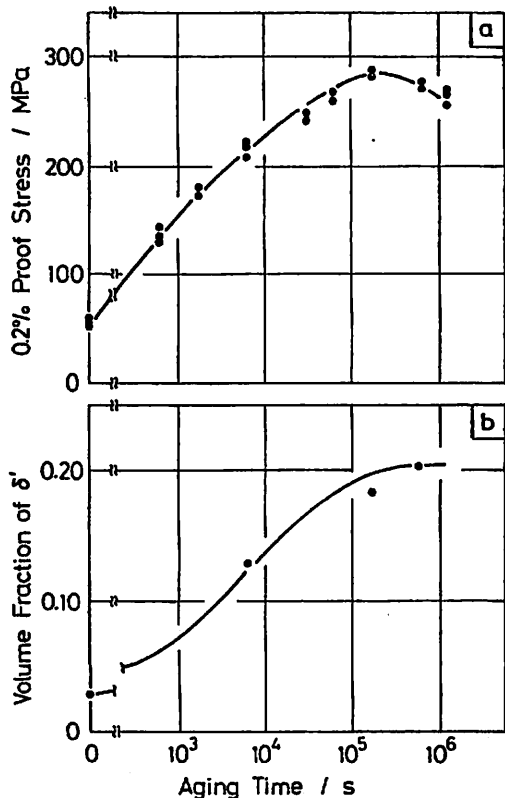


Fig. 3 Aging time dependence of (a) 0.2% proof stress and (b) volume fraction of δ' -precipitate. Specimens (11.1 mol%Li alloys) were solution-treated at 823 K for 1.08×10^4 s, quenched into iced water and aged at 473 K.

3(b) から知られるように δ' 相の析出量はほぼ飽和しており、その時の δ' 粒子の直径は Fig. 2(c) から約 50 nm であることがわかる。過時効段階では、Fig. 2(d) に見られるように、 δ' 相はさらに大きく成長している。しかも、Fig. 4 に示すように粗大な δ 相が析出して来るが、その量はきわめて少ない。

3.2. ヤング率の測定

板状試料の共振周波数 f と試験片の有効質量 m_e およびバネ定数 k との間には次の関係がある¹⁷⁾。

$$f = (k/m_e)^{1/2} / 2\pi \tag{1}$$

横振動型静電駆動法の場合には、ヤング率 E と共振周波数 f との関係は次式で与えられる¹⁷⁾。

$$E \text{ (Pa)} = (48\pi^2 l^3 \rho) / [(8.37)^4 t^2] \cdot f^2 \tag{2}$$

ここで、 l , t および ρ は、それぞれ試験片の長さ、厚さおよび密度である。試料支持のためにつけた切込み

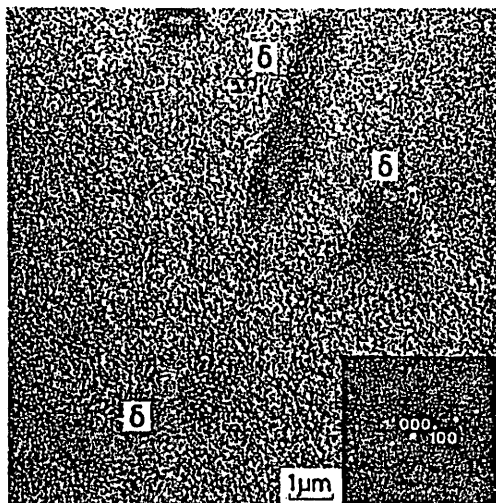


Fig. 4 (100) dark field image of Al-11.1 mol%Li alloy aged at 473 K for 1.2×10^6 s.

の影響は、切込み量が微小であり、モーメントが小さく変位もほぼ 0 の点に位置しているため無視することができる。しかし、パーマロイが貼付された部分は振幅が大きいため、振動数に対するパーマロイ板の質量効果は無視することはできず、補正が必要である。

試料の一部にパーマロイ板を貼付した場合の共振周波数は、近似的に次式で与えられるとする。

$$f' = \{k/(m_e + m_p^*)\}^{1/2} / 2\pi \tag{3}$$

ここで、 m_p^* はパーマロイ板の有効質量である。 m_e および m_p^* は次式により求められる。

$$m_e = \int_0^l \rho A \phi^2(x) dx = \rho A l / 4 \tag{4}$$

$$m_p^* = 2 \times \int_0^{l_p} \rho_p A_p \phi^2(x) dx = 0.1356 \rho_p A_p l \tag{5}$$

ここで、 ρ , ρ_p はそれぞれ試験片およびパーマロイの密度、 A , A_p は試験片とパーマロイ板の断面積、 l , l_p は試験片とパーマロイ板の長さ、さらに $\phi(x)$ は位置 x における変位である。したがって、試料本来の共振周波数は次式により与えられる。

$$f = (k/m_e)^{1/2} / 2\pi = f' \cdot \{(m_e + m_p^*)/m_e\}^{1/2} \tag{6}$$

(6)式によれば、パーマロイ貼付による質量効果はやング率に対して約15%程度となり、無視できない。

密度の実測値は 99.99% アルミニウムで 2.69×10^3 kg/mm³, Al-11.1 mol% Li 合金で $(2.46 \pm 0.01) \times 10^3$ kg/mm³ であった。共振周波数の測定温度域における

実測値は 99.99% アルミニウムで 1.497~1.433 kHz, Al-11.1 mol% Li 合金で 1.786~1.688 kHz であった.

3.3. ヤング率の温度依存性と時効組織依存性

Fig. 5 に, 溶体化焼入れ状態および最高強度まで時効した Al-11.1 mol% Li 合金のヤング率の温度依存性を示す. 図中には, 比較のために 99.99% アルミニウムの測定結果と, これまでに報告されている純アルミニウム^{18,19)}, Al-7.9 mol% Li 合金¹⁴⁾ および 2XXX, 5XXX, 7XXX などの実用アルミニウム合金^{20,21)} についての測定結果も合わせて示した. ヤング率は測定方法の違いによりその値が異なる場合があることが知られている²¹⁾ ので, Fig. 5 中には超音波法で測定された 7075-T6 材²⁰⁾ 以外は, すべて本実験と同じ共振法によるデータを示した.

本実験で示した 99.99% アルミニウムの室温でのヤング率は, 従来の報告^{18,19)} とほぼ同じ値を示している. Al-11.1 mol% Li 合金のヤング率は室温で 80.5~82.5 GPa であり, 純アルミニウムの 70 GPa に対し

て約17%高い値を示しており, 他の実用アルミニウム合金よりも明らかに高い値となっている. 室温での Al-Li 2元合金のヤング率については, これまでに Al-7.9 mol% Li 合金の 77 GPa¹⁴⁾, Al-9 mol% Li 合金の 80 GPa²²⁾ および Al-15.5 mol% Li 合金の 83 GPa²³⁾ などの報告があるが, 本実験結果はこれらの値と矛盾しない. また静的な方法で測定された Al-11 mol% Li 合金の 81.5~83.5 GPa¹¹⁾ とよく一致している.

Fig. 5 に見られるように, Al-11.1 mol% Li 合金のヤング率の温度依存性は, 室温~423 K の範囲ではゆるやかに低下する傾向を示し, 純アルミニウムや他の実用アルミニウム合金とほぼ同じ温度依存性を示す. さらに, 本実験で用いた合金よりリチウム濃度の低い Al-7.9 mol% Li 合金のヤング率の温度依存性ともほぼ一致している. 溶体化焼入れ状態および最高強度に達した時効合金のどちらも, ヤング率は温度上昇と共に平行に低下しており, 熱処理状態の違いによる温度

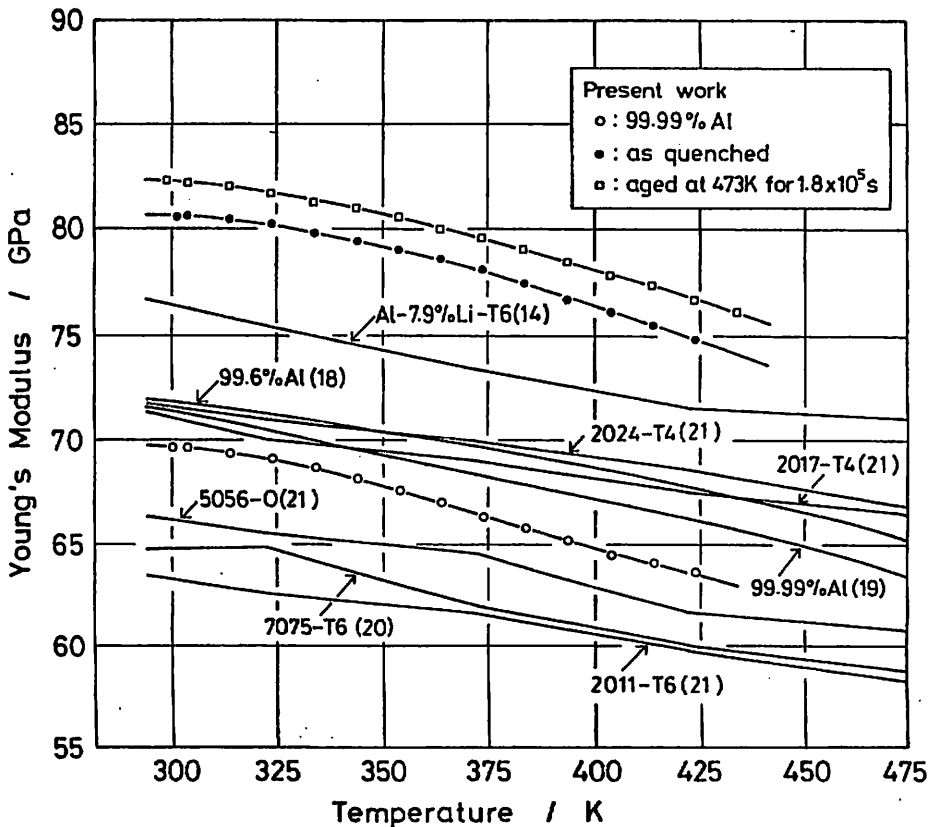


Fig. 5 Temperature dependence of Young's modulus.

依存性の違いはほとんど認められない。423 K におけるヤング率は、室温での値に比べて約 7% 低下しているが、依然として純アルミニウムや他の実用アルミニウム合金より高い値を保っている。

Fig. 6 に、473 K で時効した Al-11.1 mol% Li 合金の各測定温度でのヤング率の時効時間による変化を示す。実用アルミニウム合金においては、焼鈍材や時効材など処理状態によってヤング率が異なるという報告²¹⁾がある。Fig. 6 から、Al-Li 合金のヤング率は時効の進行と共にいったん上昇し、極大値をとった後低下することがわかる。このような時効に伴うヤング率の変化は、Fig. 3 に示した降伏応力の時効時間による変化とほぼ対応している。約 10^5 s 時効後のヤング率は溶体化焼入れ状態に比べて、約 2 GPa 上昇している。この値は、Noble ら¹³⁾が報告している Al-11.1 mol% Li 合金での焼入れ状態での 81.5 GPa と最大時効状態の 83.5 GPa との差に一致する。時効時間が 10^5 s より長くなるとヤング率は低下し始めるが、この時効段階では δ' 相の析出量はほぼ飽和しており、ヤング率が低下する原因としては、 δ' 相の大きさや粒子間隔の粗大化あるいは δ 相の析出が考えられる。しかし電顕観察によれば、 δ 相の析出量は 473 K, 1.2×10^6 s 時効後もきわめて少ない。また、Noble ら¹³⁾によれば δ 相のヤング率は 105 GPa であり、 δ' 相の

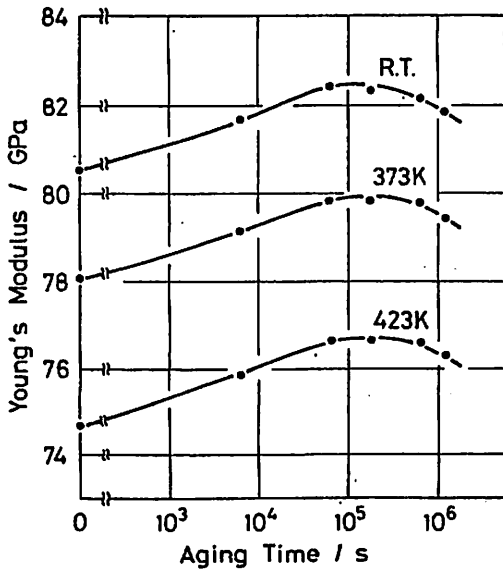


Fig. 6 Young's modulus vs. aging time curves of Al-11.1 mol% Li alloy aged at 473 K.

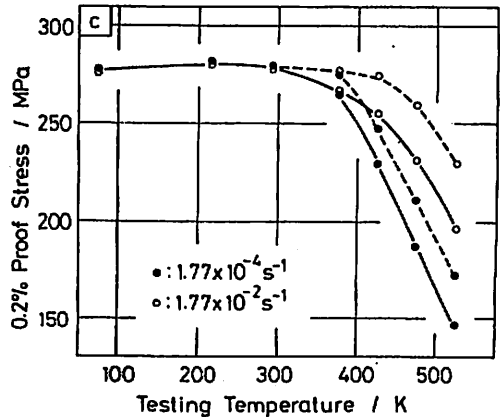
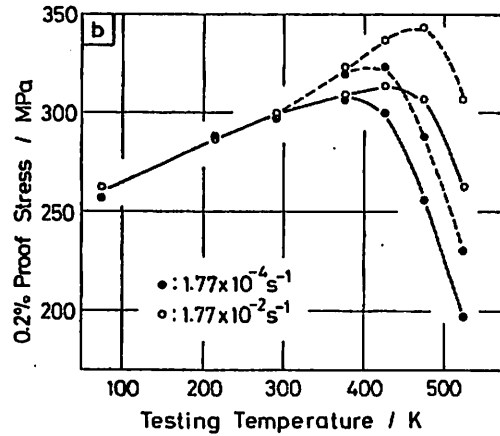
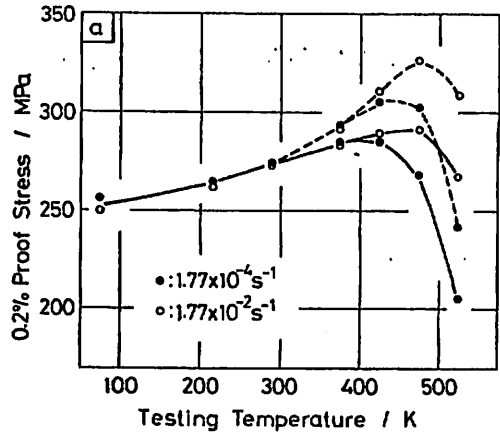


Fig. 7 Temperature dependence of 0.2% proof stress of Al-11.1 mol% Li alloy aged at for (a) 6×10^4 s, (b) 1.8×10^5 s and (c) 1.2×10^6 s. Dotted lines indicate modulus normalized 0.2% proof stress.

ヤング率 96 GPa よりも高く、複合則にしたがえば δ 相の存在はむしろヤング率を上昇させることになる。したがって、長時間時効でのヤング率の減少は、 δ 析出物の粒径と粒子間隔の変化に起因しているものと考えられ、本合金のヤング率に対しては単純な複合則は成り立たないことが知られる。

3.4. 降伏応力の温度依存性

Fig. 7(a)~(c) は、不完全時効、完全時効および過時効の3種の時効段階について、77~523 K の範囲で、2つの歪速度で圧縮試験した場合の降伏応力 (0.2% 耐力) の温度依存性を示す。破線で示した曲線は Al-Li 合金の剛性率の温度依存性で補正した降伏応力である。不完全時効段階の試料 (a) では、歪速度が小さい $\dot{\epsilon}=1.77 \times 10^{-4} \text{ s}^{-1}$ の場合、77 K から 373 K 付近の温度範囲で降伏応力に正の温度依存性が見られる。一方、歪速度が大きい $\dot{\epsilon}=1.77 \times 10^{-2} \text{ s}^{-1}$ の場合は、降伏応力の正の温度依存性が存在する温度領域は高温側へ広がり、473 K 付近にまで及んでいる。この傾向は (b) に示す最大強度付近まで時効した試料でも同様である。一方、(c) の過時効段階の試料では剛性率の温度依存性を補正しても降伏応力に正の温度依存性は現われず、通常のアルミニウム合金の強度の温度依存性^{12,24)} と同様、降伏応力は温度の上昇と共に単調に低下している。

Al-Li 合金のきわだった特徴は、このように高温における強度が低温より高くなることで、これは L₁₂ 型規則構造の析出相を含むニッケル基超耐熱合金²⁻¹¹⁾ において観察されている特異な現象である。この現象は、Fig. 7 に示すように降伏応力の温度依存性を剛性率の温度依存性で補正するとより明確に現われ、不完全時効段階でかつ歪速度が大きいほど顕著であり、過時効段階で転位が δ 相を by-pass するようになると消失し、L₁₂ 型規則相析出の特性が失われることが知られる。

4. 総括

横振動型静電駆動法により、各時効状態における Al-11.1 mol% Li 合金のヤング率を測定し、室温~423 K の範囲でのヤング率の温度依存性を検討した。その結果、以下のことが明らかとなった。

1) Al-11.1 mol% Li 合金の室温でのヤング率は、純アルミニウムの値より約17%高い値を示す。また、Al-Li 合金のヤング率は時効の進行と共に変化し、降伏強度および δ 相の析出量の時効時間に対する曲線

とよく対応する。 δ 相の直径が 50 nm 以上になると、ヤング率は低下しはじめる。

2) Al-Li 2元合金のヤング率は、室温~423 K の範囲において、温度上昇と共にゆるやかに減少する傾向にあり、423 K においては室温より約7%低下する。その温度依存性は、純アルミニウムや 2XXX, 5XXX, 7XXX などの実用アルミニウム合金とほぼ同様であり、高温においても Al-Li 合金のヤング率は純アルミニウムや他の実用アルミニウム合金より高い。

終りに、本研究を行うにあたり試料の一部を提供していただいた住友軽金属工業株式会社技術研究所に感謝致します。また、本研究の一部は文部省科学研究費補助金および軽金属奨学会課題研究助成金の援助によることを記し、謝意を表します。

参考文献

- 1) 古川 稔, 美浦康宏, 根本 実: 日本金属学会会報, 23 (1984), 172.
- 2) J. M. Silcock; J. Inst. Metals, 88 (1959), 357.
- 3) B. Noble and G. E. Thompson; Met. Sci. J., 5 (1971), 114.
- 4) D. B. Williams and J. W. Edington; Met. Sci. J., 9 (1975), 529.
- 5) 鈴木 寿, 菅野幹宏, 林 恒男: 軽金属, 31 (1981), 122.
- 6) 古川 稔, 松井昭彦, 美浦康宏, 根本 実: 軽金属, 35 (1985), 3.
- 7) 古川 稔, 松井昭彦, 美浦康宏, 根本 実: 日本金属学会誌, 48 (1984), 1068.
- 8) 古川 稔, 美浦康宏, 根本 実: 日本金属学会誌, 49 (1985), 501.
- 9) 蔵元英一: 日本金属学会会報, 14 (1975), 567.
- 10) 竹内 伸: 日本金属学会会報, 18 (1979), 249.
- 11) 鈴木朝夫: 日本金属学会会報, 21 (1982), 19.
- 12) B. Noble, S. J. Harris and K. Harlow; *Aluminum-Lithium Alloys II*, Ed. by E. A. Starke, Jr. and T. H. Sanders, Jr., Met. Soc. AIME, (1984), p. 65.
- 13) B. Noble, S. J. Harris and K. Dinsdale; J. Mat. Sci., 17 (1982), 461.
- 14) 井上武司, 武蔵一浩, K. S. Harlow, 福沢 康, 小島 陽, 中村正久: 日本金属学会講演概要, 1985年4月, 254.
- 15) Y. Shirakawa and I. Oguma; Sci. Rep. RITU, A-18 Suppl. (1966), 523.
- 16) 佐野 毅, 西原良一, 四本晴夫, 美浦康宏, 根本 実: 九州大学工学集報, 56 (1983), 491.
- 17) R. E. D. Bishop and D. C. Johnson; *The Mechanics of Vibration*, Cambridge University Press (1960).
- 18) W. Köster; Z. Metallkde., 32 (1940), 282.
- 19) 阿部勝憲, 丹治雅典, 吉永日出男, 猪住正太郎: 軽金属, 27 (1977), 279.

- 20) 財満鎮雄, 竹内洋一郎, 入交 裕: 軽金属, 21 (1971), 803.
- 21) 入交 裕, 財満鎮雄, 竹内洋一郎, 田丸一男: 軽金属, 22 (1972), 710.
- 22) T. H. Sanders, Jr. and E. A. Starke, Jr.; Acta Met., 30 (1982), 927.
- 23) W. R. D. Jones and P. P. Das; J. Inst. Metals, 88 (1959-60), 435.
- 24) S. M. L. Sastry and J. E. O'Neal; Aluminum-Lithium Alloy II, Ed. by E. A. Starke, Jr. and T. H. Sanders, Jr., Met. Soc. AIME, (1984), 79.
-

The Strain Rate Dependence of Yield Stress of an Al-Li Alloy Containing δ' -Li₂ Ordered Particles*

By Minoru Furukawa**, Yasuhiro Miura*** and Minoru Nemoto***

The effect of strain rate on the yield stress of an Al-11.1 mol%Li alloy containing δ' -precipitates has been investigated at temperatures between 77 and 523 K and over the strain rate range from $1.77 \times 10^{-4} \text{ s}^{-1}$ to $1.77 \times 10^{-2} \text{ s}^{-1}$. At testing temperatures below 373 K, the yield stress is almost independent of strain rate at any aging stage. At testing temperatures above 373 K, the yield stress increases linearly with the logarithm of strain rate, and its strain rate dependence increases with increasing testing temperature. The yield stresses of under-aged alloy at temperatures between 373 and 473 K at high strain rates are greater than the yield stress at 77 K. For the alloy under-aged or aged nearly to its peak strength, the temperature range within which the positive temperature dependence of yield stress appears expands to the higher temperature side with increasing strain rate. The strain rate dependence of the yield stress is slightly negative at this aging stage. Within this temperature range, dislocations move in pairs cutting δ' -Li₂ ordered particles. The yield stress of the over-aged alloy decreases monotonically with decreasing strain rate and with increasing testing temperature above 373 K. The modulus normalized yield stress is nearly constant at testing temperatures below 373 K at any strain rate investigated. In the over-aged alloy, dislocations by-pass the precipitates at any temperature and strain rate.

(Received September 4, 1985)

Keywords: aluminum-lithium alloy, ordered precipitate, precipitation hardening, mechanical property, temperature dependence, strain-rate dependence, super-dislocation, transmission electron microscopy

I. Introduction

Aluminum alloys containing lithium are attractive for aerospace applications because of their high elastic modulus and high strength⁽¹⁾⁽²⁾. The alloys are appreciably hardened by precipitation of δ' -phase which is a quasi-equilibrium phase of the Li₂ ordered structure. It is well known that the strength of the Li₂ ordered phase often increases with increasing temperature to a peak value at an elevated temperature. This behavior is believed to be the main origin of the superior high temperature strength of various γ/γ' nickel-base superalloys⁽³⁾⁻⁽⁵⁾. The Al-Li alloys containing the γ' -Li₂ ordered phase are expected to show high strength at elevated temperatures⁽⁶⁾⁻⁽⁸⁾ because of this structural similarity to

the nickel-base superalloys. This aspect also makes the Al-Li alloys attractive for aerospace applications, since materials for aerospace structures are required to keep adequate strength over a wide range of temperature.

The present authors have investigated the behavior of deformation induced dislocations at room temperature by transmission electron microscopy and have discussed the precipitation strengthening and deformation mechanisms of an Al-11.1 mol%Li alloy⁽⁹⁾⁽¹⁰⁾. Furthermore, the authors have reported the characteristic temperature dependence of the strength of the alloy at various aging stages in a temperature range between 77 and 523 K and have correlated these mechanical properties with the behavior of deformation induced dislocations⁽⁷⁾.

The purpose of the present work is to investigate the strain rate dependence of the strength and deformation mechanism of binary Al-Li alloy having various microstructures in a temperature range between 77 and 523 K.

* This paper was originally published in Japanese in J. Japan Inst. Metals, 49 (1985), 501.

** Department of Technology, Faculty of Education, Fukuoka University of Education, Munakata 811-41, Japan.

*** Department of Metallurgy, Faculty of Engineering, Kyushu University, Fukuoka 812, Japan.

II. Experimental Procedures

An Al-11.1 mol%Li alloy was prepared by melting 99.99%Al and 99.8%Li in an argon atmosphere. The alloy contained 0.0032 mol% Fe, 0.026 mol%Si and 0.0046 mol%Mg. The as-cast ingot was hot and cold rolled to a 3 mm thick strip and cut to 3 mm × 3 mm × 4.7 mm specimens. The specimens were solution treated at 823 K for 1.08×10^4 s in glass capsules filled with argon, followed by quenching into iced water and aged at 473 K for various periods.

The aged specimens were tested in compression at temperatures between 77 and 523 K with an Instron-type machine over a nominal strain rate range from $1.77 \times 10^{-4} \text{ s}^{-1}$ to $1.77 \times 10^{-2} \text{ s}^{-1}$. The compressive testes at 77 and 213 K were performed in liquid nitrogen and in methyl alcohol containing dry ice, respectively. The compressive tests at temperatures above room temperature were performed in a silicon oil bath, and the tested specimens were immediately cooled into water.

Slices 0.3 mm thick were taken from the specimens deformed approximately 4% by using a fine cutting machine, followed by polishing down to 0.15 mm in thickness on emery paper. Thin foils for transmission electron microscopy (TEM) were prepared using a modified twin-jet electropolishing apparatus⁽¹¹⁾. The composition of the electrolyte was 20% HClO₄ and 80% C₂H₅OH. Microstructures and dislocation configurations were investigated by dark field transmission electron microscopy using a JEM-1000D high voltage electron microscope in HVEM Laboratory of Kyushu University.

Young's moduli of the alloy at various aging stages were measured at temperatures from 290 K to 443 K by a resonant frequency method using plate specimens (2 mm × 10 mm × 80 mm)⁽¹²⁾.

III. Experimental Results

1. Temperature and strain rate dependence of yield stress

Figures 1(a) and (b) show the variation of

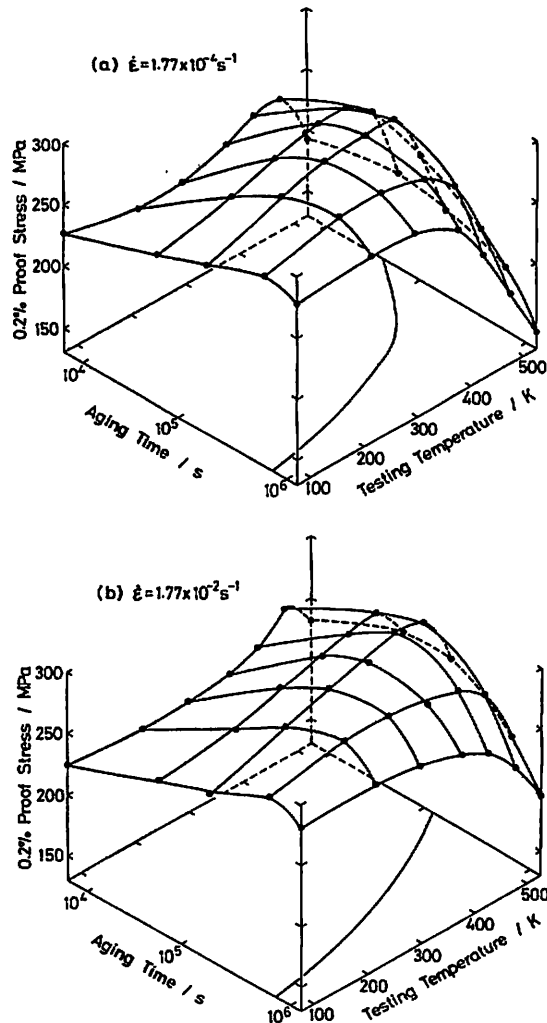


Fig. 1 0.2% proof stress-aging time-testing temperature diagrams of Al-11.1 mol%Li alloy aged at 473 K and tested in compression at normal strain rates of (a) $1.77 \times 10^{-4} \text{ s}^{-1}$ and (b) $1.77 \times 10^{-2} \text{ s}^{-1}$.

yield stress (0.2% proof stress: $\sigma_{0.2}$) of the Al-11.1 mol%Li alloy at nominal strain rates of $1.77 \times 10^{-4} \text{ s}^{-1}$ and $1.77 \times 10^{-2} \text{ s}^{-1}$, respectively, as a function of aging time at 473 K and testing temperature. The shortest aging time shown in Fig. 1 is 6×10^3 s. It is found that the yield stress strongly depends on the aging time and testing temperature. In both (a) and (b), the yield stress of the alloy tested at 77 K attains a maximum value by aging for about 6×10^5 s and decreases by further aging. In the case of the minimum strain rate $1.77 \times 10^{-4} \text{ s}^{-1}$, the necessary time for testing is 500 s.

Therefore, the values of yield stress of specimens tested at temperatures above the aging temperature are strongly affected by the aging during testing. As shown by the projection onto the bottom of the figures, the peak positions of the aging curves shift to the side of shorter aging time with increasing testing temperature. It is evident that the projected peak positions in (a) and (b) almost overlap each other at testing temperatures below 373 K in spite of different strain rates. On the other hand, the peak positions shift to the side of longer aging time with increasing strain rate at temperatures above 373 K.

Figures 2(a)-(d) show the variation of yield stress of the alloy aged at 473 K for (a) 6×10^4 s (under-aged), (b) 1.8×10^5 s (peak-aged), (c) 6×10^5 s (peak-aged) and (d) 1.2×10^6 s (over-

aged), respectively. At testing temperatures below 373 K, the yield stress is almost independent of strain rate at any aging stage. At temperatures above 423 K, however, the yield stress increases linearly with the logarithm of strain rate, and its strain rate dependence increases with increasing testing temperature. Figure 3 shows the gradient of these lines in Fig. 2 as a function of aging time at 473 K. The strain rate sensitivity ($\Delta\sigma_{0.2}/\Delta \ln \dot{\epsilon}$) increases with increasing testing temperature. Furthermore, at testing temperatures between 423 and 523 K, the strain rate sensitivity increases with increasing aging time, until the alloy attains a maximum strength. At 523 K of testing temperature, the strain rate sensitivity attains its maximum value by aging for 1.8×10^5 s and decreases by further aging.

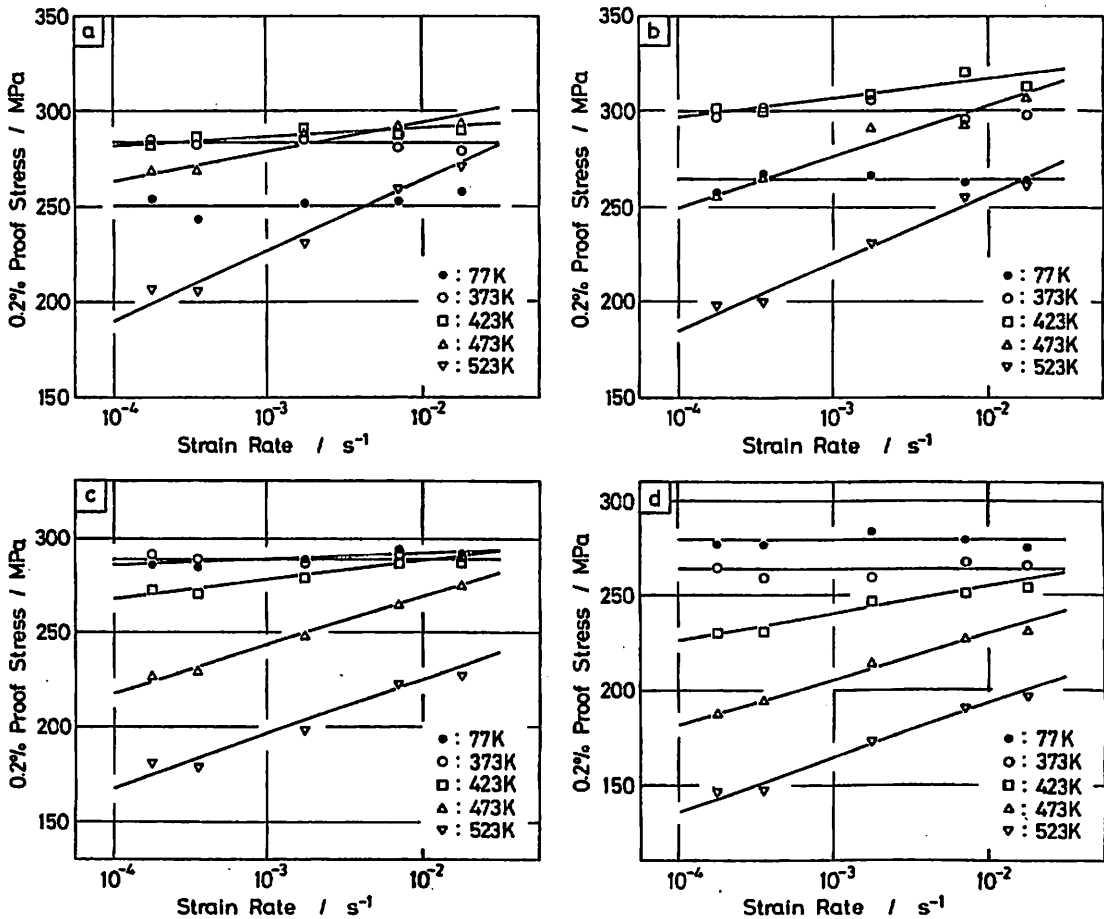


Fig. 2 The effect of strain rate on the 0.2% proof stress of Al-11.1 mol%Li alloy aged at 473 K for (a) 6×10^4 s, (b) 1.8×10^5 s, (c) 6×10^5 s and (d) 1.2×10^6 s.

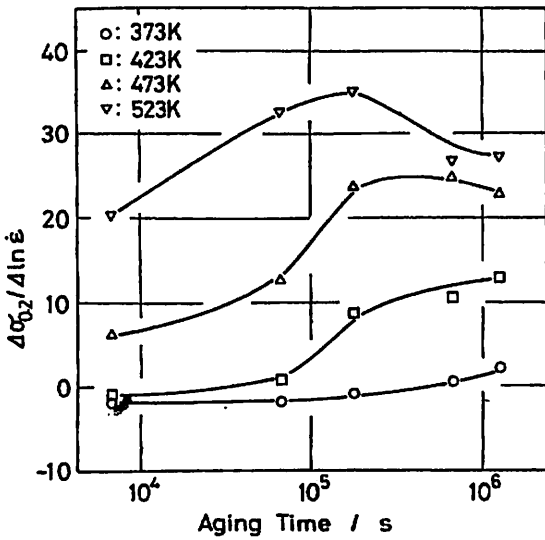


Fig. 3 The effect of aging time at 473 K on the strain rate sensitivity ($\Delta\sigma_{0.2}/\Delta \ln \dot{\epsilon}$).

In Figs. 2(a) and (b), the cross-over in the yield stresses at various testing temperatures occurs. Above this cross-over point, the yield stress is higher at higher temperatures. The similar anomalous phenomenon was observed in the nickel-base superalloys⁽⁹⁾⁻⁽⁵⁾ containing the Li₂ ordered precipitates. For the Al-Li alloy, however, the magnitude of this phenomenon is known to be dependent on the aging stage. A more distinguished phenomenon is observed when the under-aged alloy is tested at higher strain rates. On the other hand, in the over-aged state (d), the cross-over in the yield stress is not observed.

Figures 4(a)-(c) show the effect of strain rate on the temperature dependence of yield stress of the alloy aged at 473 K for (a) 6×10^4 s, (b) 1.8×10^5 s and (c) 1.2×10^6 s, respectively. Dotted lines in these figures indicate the modulus normalized yield stress⁽¹²⁾. In the under-aged (a) and peak-aged (b) conditions, the yield stress increases with increasing temperature from 77 K up to about 373 K, when the alloy is tested at a lower strain rate. On the other hand, at a higher strain rate the temperature range within which the positive temperature dependence of yield stress appears expands to the higher temperature side up to about 473 K. In the over-aged state (c), even the modulus normalized yield stress decreases monotonical-

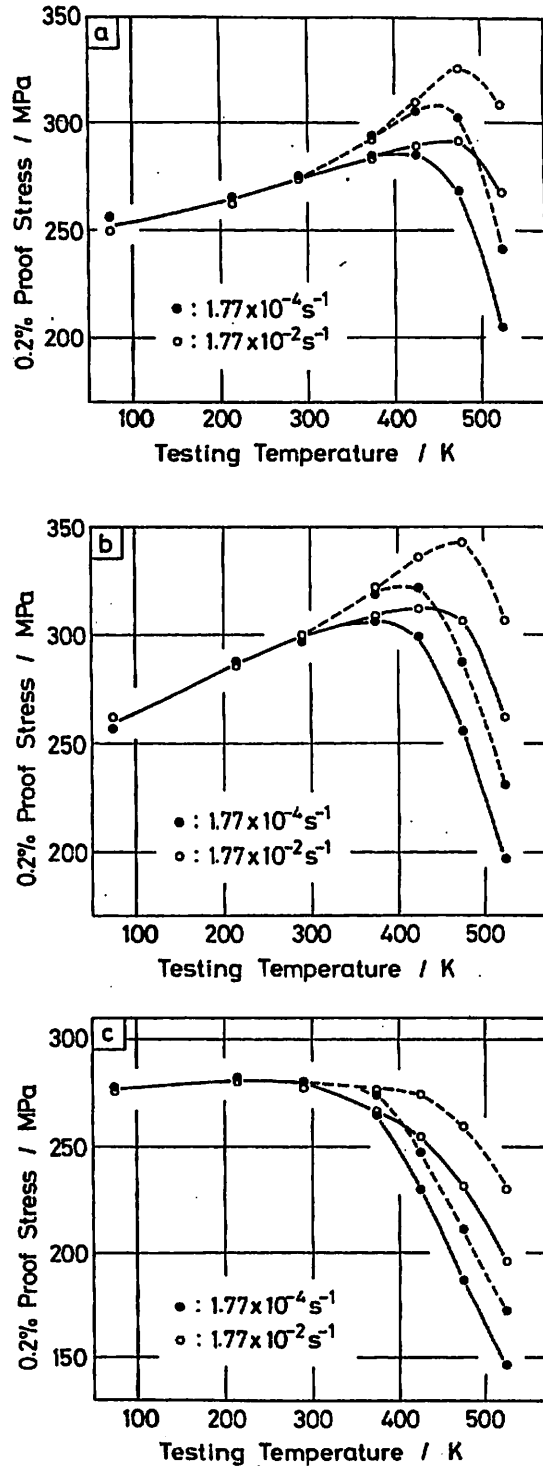


Fig. 4 The effect of strain rate on the temperature dependence of 0.2% proof stress of Al-11.1 mol%Li alloy aged at 473 K for (a) 6×10^4 s, (b) 1.8×10^5 s and (c) 1.2×10^6 s. Dotted lines indicate modulus normalized 0.2% proof stress.

ly with increasing testing temperature similarly to those of ordinary aluminum alloys⁽⁸⁾⁽¹³⁾. It should be noted that δ' particles are completely dissolved in solid solution at temperature above the solvus of the Al-11.1 mol%Li alloy, 548 K.

2. Configurations of deformation induced dislocations

Figures 5(a) and (b) show 200 weak beam dark field images of the alloy aged at 473 K for 6×10^4 s (under-aged) deformed 4% in compression at 423 K at a normal strain rate of (a) $1.77 \times 10^{-4} \text{ s}^{-1}$ and (b) $1.77 \times 10^{-2} \text{ s}^{-1}$, respectively. Referring to Fig. 4(a), it can be known that the micrographs show the structures of the deformed alloys near the peaks in Fig. 4(a). When the alloy is deformed at a lower strain rate, Fig. 5(a), the deformation induced dislocations are single and wavy. Many dislocation loops can also be observed. This micrograph indicates that the deformation induced dislocations climb over the δ' -particles

by cross-slip and/or climbing motion⁽⁷⁾, or bypass the particles leaving the Orowan dislocation loops around them⁽⁷⁾⁽⁹⁾. At a higher strain rate, Fig. 5(b), it is clear that dislocations cut through the δ' -particles during plastic deformation⁽⁷⁾⁽⁹⁾, since they are observed as pairs. By the comparison between these configurations of deformation induced dislocations and Fig. 4(a), it should be clear that dislocations move in pairs cutting the δ' - Li_2 ordered particles in the temperature range within which the positive temperature dependence of yield stress appears. At temperatures above this range, dislocations move as single dislocations bypassing or climbing the particles. Furthermore, it is known that the dislocations tend to bypass or climb the particles with decreasing strain rate when the deformation temperature is almost the same.

Figures 6(a) and (b) show 200 weak beam dark field images of the alloy aged at 473 K for 6×10^5 s (peak-aged) and deformed 4% in compression at 77 K at a normal strain rate of (a)

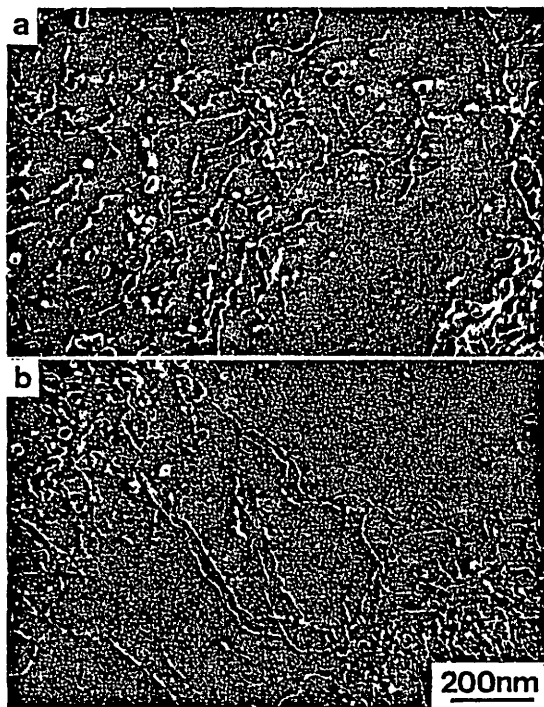


Fig. 5 (200) dark field images of Al-11.1 mol%Li alloy aged at 473 K for 6×10^4 s and deformed 4% in compression at 423 K (a) at a normal strain rate of $1.77 \times 10^{-4} \text{ s}^{-1}$ and (b) at a normal strain rate of $1.77 \times 10^{-2} \text{ s}^{-1}$.

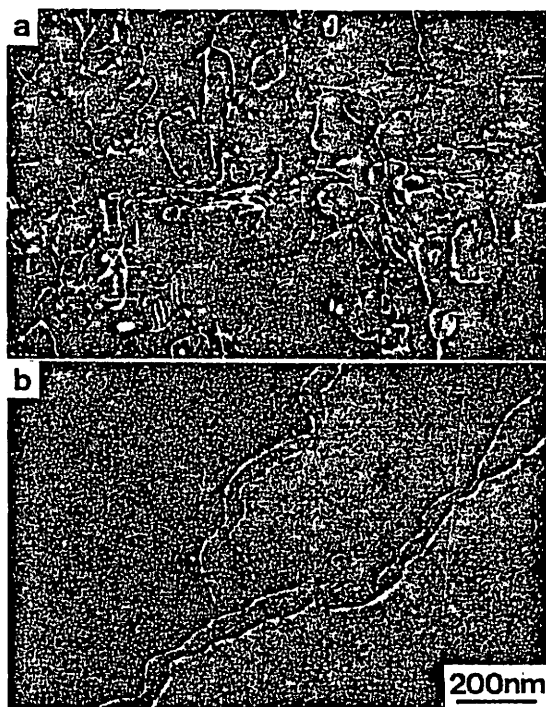


Fig. 6 (200) dark field images of Al-11.1 mol%Li alloy aged at 473 K for 6×10^5 s and deformed 4% in compression at 77 K (a) at a normal strain rate of $1.77 \times 10^{-4} \text{ s}^{-1}$ and (b) at a normal strain rate of $1.77 \times 10^{-2} \text{ s}^{-1}$.

$1.77 \times 10^{-4} \text{ s}^{-1}$ and (b) $1.77 \times 10^{-2} \text{ s}^{-1}$, respectively. Single dislocations and dislocation loops are observed in (a) and super-dislocations in (b). Therefore, even at a low temperature of 77 K, at which the atom diffusion rarely plays a part in the motion of dislocations, the same tendency as that observed in Fig. 5 appears. On the other hand, in the over-aged alloy, dislocations by-pass⁽⁷⁾⁽⁹⁾⁽¹⁴⁾ the particles at any testing temperature and strain rate.

IV. Discussion

1. Strain rate dependence of yield stress

At testing temperatures below 373 K ($0.4T_m$, T_m : melting point of the alloy), the yield stress of Al-11.1 mol%Li alloy is almost independent of strain rate at any aging stage. At temperatures above 373 K, however, the yield stress increases linearly with the logarithm of strain rate at all aging stages, and its strain rate dependence increases with increasing temperature.

In a nickel-base superalloy containing γ' -Li₂ ordered precipitates, the yield stress is almost independent of strain rate, when the alloy is deformed at lower temperatures ($< 0.6T_m$) and at higher strain rates ($> 1.67 \times 10^{-5} \text{ s}^{-1}$)⁽¹⁵⁾. When the nickel-base superalloy is deformed at temperatures above $0.6T_m$, the yield stress increases linearly with the logarithm of strain rate⁽¹⁵⁾, while the strain rate dependence of the yield stress of the superalloy is nearly constant regardless of the testing temperature. The strain rate independent yield stress of the nickel-base superalloy at temperatures below $0.6T_m$ has been explained in terms of the diffusionless shear of γ' phase by $(a/2)\langle 110 \rangle$ dislocation pairs in coarse, planar bands, and the strain rate dependent yield stress at temperatures above $0.6T_m$ has been explained by the viscous glide of $(a/2)\langle 110 \rangle$ or $(a/3)\langle 112 \rangle$ dislocations in the γ' -particles. The strain rate independent yield stress of the Al-Li alloy can be also explained by the diffusionless shear of the δ' particles by the moving dislocation pairs.

The modulus normalized yield stress of cop-

per strengthened by dispersion of oxide particles (SiO_2 ⁽¹⁶⁾, Al_2O_3 ⁽¹⁷⁾⁻⁽¹⁹⁾ or BeO ⁽¹⁷⁾) has been known to be almost independent of the testing temperature below about $0.4T_m$ and to decrease with increasing testing temperature above $0.4T_m$. Also for these dispersion strengthened copper alloys, the yield stress increases linearly with the logarithm of strain rate at temperatures above $0.64T_m$, and the strain rate dependence of the yield stress is almost constant regardless of the testing temperatures. The temperature and strain rate dependence of the yield stress of these copper alloys at temperatures above $0.64T_m$ has been quantitatively explained in terms of the local climbing mechanisms in which the motion of dislocations is governed by pipe diffusion⁽²⁰⁾ and/or double-jog formation⁽¹⁷⁾, or bulk diffusion⁽²¹⁾. Between 0.4 and $0.64T_m$, the deformation mechanism is considered to vary with changing temperature.

In the over-aged Al-Li alloy in which the dislocations by-pass the δ' -particles, the modulus normalized yield stress decreases monotonically with increasing temperature above $0.4T_m$. As seen in Fig. 3, however, the strain rate dependence of the yield stress increases with increasing temperature from $0.4T_m$ to $0.56T_m$. This temperature range is involved in the range between $0.4T_m$, below which the yield stress of the dispersion strengthened copper alloys⁽¹⁶⁾ is almost independent of temperature and strain rate, and $0.64T_m$, above which the strain rate dependence of the yield stress becomes constant. Therefore, in the over-aged Al-Li alloy the activation energy of deformation is considered to vary with temperature. That is to say, the deformation mechanism varies gradually from that governed by the diffusionless motion of dislocations to that governed by the diffusion controlled motion of dislocations with increasing deformation temperature from $0.4T_m$ up to $0.56T_m$.

2. Variation of deformation mechanisms with strain rate

As shown in Fig. 1, the peak positions of the aging curves are almost independent of the strain rate at temperatures below 373 K .

However, at temperatures above 373 K, the peak positions shift to the side of longer aging time with increasing testing temperature. As already reported⁽⁷⁾, the transition from the cutting mechanism to the Orowan by-passing mechanism occurs always nearly at the peak positions. When the under-aged alloy is deformed at 423 K (Fig. 5), the motion of dislocations is governed by the by-passing mechanism at a lower strain rate (a), and by the cutting mechanism at a higher strain rate (b). On the other hand, when the peak-aged Al-Li alloy is deformed at 77 K (Fig. 6), the motion of dislocations is governed by the by-passing mechanism at a lower strain rate (a) and by the cutting mechanism at a higher strain rate (b). Namely, the deformation mechanism varies with strain rate even at lower temperatures, where the motion of dislocations is almost unaffected by the atom diffusion. This means that the strain rate dependence of the cutting stress should be different from that of the by-passing stress.

Figure 7 shows the strain rate dependence of yield stress in two different aging stages; cutting and by-passing stages. Each point in the figure is the average of ten measurements at room temperature. From Fig. 7, it is clear that the by-passing stress is nearly constant at any strain rate investigated and the cutting stress slightly decreases with increasing strain rate. The cutting stress in the Al-Li alloy, therefore, seems to have a characteristic negative strain

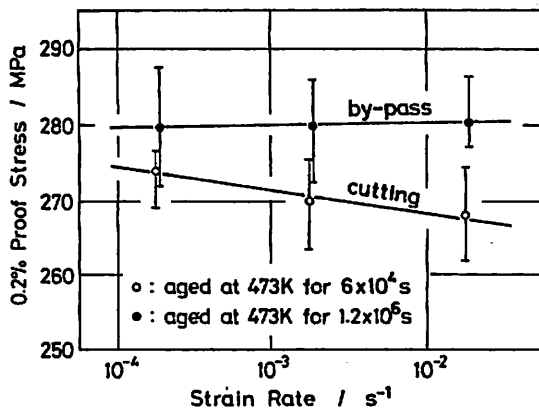


Fig. 7 The effect of strain rate on the 0.2% proof stress at room temperature of Al-11.1 mol%Li alloy aged at 473 K for 6×10^4 s (○) and aged at 473 K for 1.2×10^6 s (●).

rate dependence.

Figure 8 represents schematically the dependence of the yield stress on the aging time and testing temperature. Thick lines and thin lines indicate the yield stress tested at a lower strain rate and that tested at a higher strain rate, respectively. The cutting stress increases with increasing aging time, since it increases with increasing volume fraction of δ' -precipitates, and increases with increasing testing temperature up to some critical temperature possibly because of the characteristic positive temperature dependence of the strength of the $L1_2$ ordered δ' phase, as reported in the previous report⁽⁷⁾. At temperatures above the critical temperature, dislocations tend to move as single dislocations and climb over the particles, and then the yield stress decreases with increasing temperature. The temperature range within which the positive temperature dependence of yield stress appears expands to the higher temperature side with increasing strain rate. On the other hand, the by-passing stress decreases with increasing aging time, since it is inversely proportional to the δ' -particle spacing. The by-passing stress is

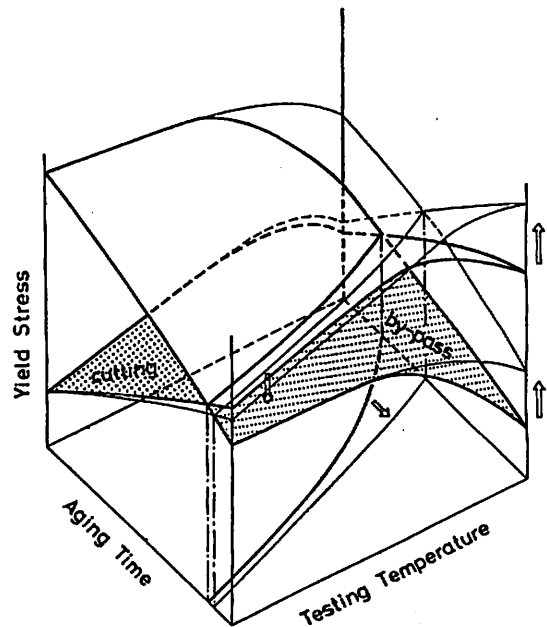


Fig. 8 Schematic representation of the effect of strain rate on the variation of the mechanism of interaction between δ' -precipitates and dislocations with aging and testing temperature.

almost independent of temperature below the critical temperature and decreases with increasing temperature above the critical temperature, since dislocations climb over the δ' -particles at elevated temperatures.

Two surfaces showing the cutting stress and the by-passing stress intersect, and the yield stress at each aging time and each testing temperature is determined by the surfaces lying below. As shown in the previous report⁽⁷⁾, the intersection line of two surfaces separates the two regions, the cutting stress prevailing in one of them and the by-passing stress doing in the other. The intersection line coincides well with the peak positions in yield stress vs aging time curves. The peak positions must shift to the side of longer aging time with increasing strain rate even at lower temperatures, since the cutting stress decreases with increasing strain rate as shown in Fig. 7. It is clear from Fig. 3 that the strain rate sensitivity increases with increasing aging time at testing temperatures near 473 K. Therefore, the surface showing the cutting stress in Fig. 8 shifts to the side of higher stress with increasing strain rate and aging time at elevated deformation temperatures. The peak positions showing the boundary between the region governed by the cutting mechanism and that by the by-passing mechanism consequently shift to the side of longer aging time with increasing strain rate at elevated temperatures.

V. Conclusion

(1) At testing temperatures below 373 K, the yield stress of Al-11.1 mol%Li alloy is almost independent of strain rate at any aging stage. At testing temperatures above 373 K, the yield stress increases linearly with the logarithm of strain rate, and its strain rate dependence increases with increasing testing temperature.

(2) For the alloy under-aged or aged nearly to its peak strength, the temperature range, within which the positive temperature dependence of yield stress appears, expands to the higher temperature side with increasing strain rate. Within this temperature range, dislocations move in pairs cutting δ' -Li₂ ordered particles. Above this temperature

range, dislocations move in single dislocations by-passing and climbing the particles.

(3) In the over-aged alloy, dislocations by-pass the particles at any temperature and strain rate. The modulus normalized yield stress is nearly constant at testing temperatures below 373 K, and decreases monotonically with decreasing strain rate and with increasing testing temperature above 373 K.

(4) The strain rate dependence of the cutting stress is slightly negative at low temperatures at which diffusion has almost no influence on the motion of dislocations, while the by-passing stress is nearly constant at lower temperatures at any strain rate.

(5) The peak positions of aging curves are almost independent of strain rate at temperatures below 373 K but shift to the side of longer aging time with increasing strain rate at temperatures above 373 K.

Acknowledgments

The authors would like to thank Technical Research Laboratories, Sumitomo Light Metal Industries, LTD. for preparing the Al-Li alloy. Special thanks are also due to Nagasaki Technical Institute of Mitsubishi Heavy Industries, LTD. for the measurements of temperature dependence of elastic constants of Al-Li alloy. This research was supported partly by Grant-in Aid for Scientific Research from the Ministry of Education, Science and Culture of Japan and Grant-in Aid from the Light Metal Educational Foundation, Inc.

REFERENCES

- (1) E. A. Starke, Jr. and T. H. Sanders, Jr.: *Journal of Metals*, **33** (1981), 24.
- (2) M. Furukawa, Y. Miura and M. Nemoto: *Bul. Japan Inst. Metals*, **23** (1984), 172 (in Japanese).
- (3) E. Kuramoto: *Bul. Japan Inst. Metals*, **14** (1975), 567 (in Japanese).
- (4) S. Takeuchi: *Bul. Japan Inst. Metals*, **18** (1979), 249 (in Japanese).
- (5) T. Suzuki: *Bul. Japan Inst. Metals*, **21** (1982), 19 (in Japanese).
- (6) M. Tamura, T. Mori and T. Nakamura: *Trans. JIM*, **14** (1973), 355.
- (7) M. Furukawa, Y. Miura and M. Nemoto: *Trans. JIM*, **26** (1985), 414.
- (8) S. M. L. Sastry and J. E. O'Neal: *Aluminum-Lithium Alloy II*, Ed. by E. A. Starke, Jr. and T. H. Sanders, Jr., *Met. Soc. AIME*, (1983), p. 79.

- (9) M. Furukawa, Y. Miura and M. Nemoto: *Trans. JIM*, **26** (1985), 225.
- (10) M. Furukawa, Y. Miura and M. Nemoto: *Trans. JIM*, **26** (1985), 230.
- (11) T. Sano, R. Nishihara, H. Yotsumoto, Y. Miura and M. Nemoto: *Technology Reports of the Kyushu University*, **56** (1983), 491 (in Japanese).
- (12) M. Furukawa, M. Nakamura, Y. Miura and M. Nemoto: *Technology Reports of the Kyushu University*, **58** (1985), 795 (in Japanese).
- (13) B. Noble, S. J. Harris and K. Harlow: *Aluminum-Lithium Alloy II*, Ed. by E. A. Starke, Jr. and T. H. Sanders, Jr., *Met. Soc. AIME*, (1983), p. 65.
- (14) J. Th M. De Hosson, A. Huis in't Veld, H. Tamler and O. Kamert: *Acta Met.*, **32** (1984), 1205.
- (15) G. R. Leverant, M. Gell and S. W. Hopkins: *Mater. Sci. Eng.*, **8** (1971), 125.
- (16) R. S. W. Shewfelt and L. M. Brown: *Phil. Mag.*, **30** (1974), 1135.
- (17) F. J. Humphreys, P. B. Hirsch and D. Gould: *Proc. 2nd Int. Conf. on Strength of Metals and Alloys*, ASM, (1970), p.550.
- (18) G. Dorey: *Royal Aircraft Establishment*, Tech. Rep. No. 65126, (1965).
- (19) G. Dorey: *Royal Aircraft Establishment*, Tech. Rep. No. 65126, (1968).
- (20) L. M. Brown and R. K. Ham: *Strengthening Methods in Crystals*, Ed. by A. Kelly and R. B. Nicholson, Elsevier, (1971), 9.
- (21) R. S. W. Shewfelt and L. M. Brown: *Phil. Mag.*, **35** (1977), 945.
-